PHYSICAL REVIEW D **94,** 035002 (2016)

Study of Majorana fermionic dark matter

Chun-Khiang Chua and Gwo-Guang Wong

Department of Physics and Chung Yuan Center for High Energy Physics, Chung Yuan Christian University, Taoyuan, Taiwan 32023, Republic of China

(Received 10 December 2015; published 9 August 2016)

We construct a generic model of Majorana fermionic dark matter (DM). Starting with two Weyl spinor multiplets $\eta_{1,2} \sim (I, \mp Y)$ coupled to the Standard Model Higgs, six additional Weyl spinor multiplets with $(I \pm 1/2, \pm(Y \pm 1/2))$ are needed in general. It has 13 parameters in total, five mass parameters and eight Yukawa couplings. The DM sector of the minimal supersymmetric Standard Model is a special case of the model with $(I, Y) = (1/2, 1/2)$. Therefore, this model can be viewed as an extension of the neutralino DM sector. We consider three typical cases: the neutralinolike, the reduced, and the extended cases. For each case, we survey the DM mass m_χ in the range of (1,2500) GeV by random sampling from the model parameter space and study the constraints from the observed DM relic density; the direct search of LUX, XENON100, and PICO experiments; and the indirect search of Fermi-LAT data. We investigate the interplay of these constraints and the differences among these cases. It is found that the direct detection of spin-independent DM scattering off nuclei and the indirect detection of DM annihilation to the W^+W^- channel will be more sensitive to the DM searches in the near future. The allowed mass for finding $\tilde{H}$-, $\tilde{B}$-, $\tilde{W}$-, and non-neutralino-like DM particles and the predictions on $\langle \sigma(\chi\chi \to ZZ, ZH, t\bar{t})v \rangle$ in the indirect search are given.

DOI: 10.1103/PhysRevD.94.035002

I. INTRODUCTION

It has been more than 80 years since the first evidence of dark matter (DM) was observed by Fritz Zwicky [1]. So far, all the astrophysical and cosmological observations of DM evidence show that DM exists everywhere no matter whether it is from the galactic scale [2–4], the scale of galaxy clusters [5,6], or the cosmological scale [7,8]. Even though DM makes up about 85% of the total mass in the Universe [9,10], we still do not know much about its nature. A leading class of DM candidates is the so-called weakly interacting massive particles (WIMPs) [11,12], which are nonluminous and nonbaryonic cold DM (CDM) matter. The WIMPs are assumed to have been created thermally during the big bang and frozen out of thermal equilibrium escaping the Boltzmann suppression in the early Universe. The DM relic density is approximately related to the velocity averaged DM annihilation cross section by a simple relation [13],

$$\Omega_\chi h^2 \approx \frac{0.1 \text{ pb} \times c}{\langle \sigma v \rangle}. \tag{1}$$

On the other hand, the recent measured value of the CDM relic density is [14]

$$\Omega_\chi^{\text{obs}} h^2 = 0.1198 \pm 0.0026. \tag{2}$$

It suggests the case of DM with mass in the range of 100 GeV to few TeV and an electroweak size interaction. That is the so-called WIMP miracle.

The searches of DM particles in experiments have made much progress in recent years. Several complementary searching strategies have been continuously executed, including the direct detection of DM-nucleus scattering in underground laboratories, the indirect detection of DM annihilation processes in astrophysical observation (see Ref. [15] for a brief review), and the DM direct production at colliders [16–18]. The null results of finding the DM from LUX [19], XENON100 [20], PICO [21,22], and Fermi-LAT [23] experiments put the related upper limits on spin-independent (SI) [24,25], spin-dependent (SD) [26,27], DM-nucleus scattering cross sections, and the velocity averaged DM annihilation cross sections, respectively. Except working on the well-known models such as the minimal supersymmetric Standard Model (MSSM) directly [13,28–30], analyzing in the model-independent research with the effective operators of dark matter coupled to Standard Model (SM) particles [31–33] is a way to search the properties of DM due to the little-known nature of DM. Some authors also constructed models in which the DM couples to the SM particles via a mediator; see, for example, Higgs portal models [34–38], two-Higgs-doublet portal models [39,40], fermion portal models [41], the dark Z' portal [42], the left-right model [43,44], and so on.

In the DM-nucleus elastic scattering, the DM is highly nonrelativistic. Basically, only the scalar-scalar (SS), vector-vector (VV), axial vector-axial vector (AA), and tensor-tensor (TT) DM-quark interactions are nonvanishing [31].[1]

[1]We will return to this point and take a closer look in Sec. II C.

 © 2016 American Physical Society

In Ref. [45], one of the authors (C. K. C.) studied pure weak eigenstate Dirac fermionic dark matter with renormalizable interaction. It is well known that a Dirac fermionic DM particle, without a special choice of quantum number, usually gives an oversized SI DM-nucleus cross section through VV interaction from the Z-exchange diagram. To accommodate the bounds from direct searches, the quantum number of DM is determined to be $I_3 = Y = 0$. There are only two possible cases: either the DM has nonvanishing weak isospin ($I \neq 0$) but with $I_3 = Y = 0$ or it is an isosinglet ($I = 0$) with $Y = 0$. In the first case, it is possible to have a sizable $\chi\bar{\chi} \to W^+W^-$ cross section, which is comparable to the latest bounds from indirect searches. There is no tree-level diagram in DM-nucleus elastic scattering. It successfully evades the SI bounds, but it pays the price of detectability in a direct search. In the second case, to couple DM to the SM particles, a SM-singlet vector mediator X is required from the renormalizability and the SM gauge quantum numbers. The allowed parameter space and the consequences were studied. To satisfy the latest bounds of direct searches and to reproduce the DM relic density at the same time, resonant enhancement via the X pole in the DM annihilation diagram is needed. Thus, the masses of DM and the mediator are related. It is arguable that the phenomenology of Dirac fermionic DM is not very rich.

The Majorana DM can naturally evade the dangerous Z-exchange diagram from the VV interaction and can have rich phenomenology. A well-known example is the lightest neutralino in the MSSM [13,28]. In this work, we construct a generic class of Majorana fermionic DM models having an arbitrary weak isospin quantum number. As we shall see, the MSSM DM sector is a special case in this model, and therefore, this model can be viewed as an extension of the neutralino DM sector. We consider three typical cases: the neutralinolike, the reduced, and the extended cases. Note that a somewhat related study to the reduced case has been given in Ref. [46].

This paper is organized as follows. In Sec. II, we construct a generic model of Majorana fermionic DM and give the formulas for the DM annihilation to the SM particles as well as DM-nucleus elastic scattering. We give the results of the neutralinolike, the reduced, and the extended cases in Sec. III. We discuss the coannihilation and give the conclusions in Sec. IV. We present explicitly the relevant Lagrangian of the WIMP mass term in Appendix A. The four-component Majorana and Dirac mass eigenstates for neutral and single charged WIMPs are constructed, respectively, in Appendix B. We present the Lagrangian of WIMPs interacting with the SM particles in Appendix C, give the matrix elements of DM annihilation to the SM particles in Appendix D, and show that the Lagrangian is CP conserved in Appendix E. The formulas used in DM-nucleus elastic scattering are derived in Appendix F. The formulation and the corresponding matrix elements for WIMP coannihilation are given in Appendixes G and H, respectively.

II. FORMALISM

A. Generic model of Majorana fermionic dark matter

Starting with the SM, we add two Z_2-odd, two-component Weyl spinor multiplets $\eta_{1,2} \sim (2I+1, \mp Y)$ under $SU_L(2) \times U(1)_Y$, and all SM particles are assigned to be Z_2 even. The introduction of the Z_2 symmetry assures the stability of DM. Without loss of generality, we take $Y \geq 0$. A mass term can be constructed as

$$-\mathcal{L}_m = \mu\lambda_{ij}\eta_2^i\eta_1^j + \mu\lambda_{ij}^*\bar{\eta}_2^i\bar{\eta}_1^j, \tag{3}$$

with

$$\lambda_{ij} \equiv \sqrt{2I+1}\langle II;00|Ii,Ij\rangle \tag{4}$$

proportional to the Clebsch-Gordan coefficient and $i, j = -I, \ldots, I$. This is actually a Dirac particle multiplet. The reason is explained below. We define

$$\xi^i \equiv \eta_2^i, \qquad \bar{\eta}^i \equiv \lambda_{ij}\bar{\eta}_1^j, \tag{5}$$

and the Dirac field with the ith component of isospin

$$\psi^i \equiv \begin{pmatrix} \xi^i \\ \bar{\eta}^i \end{pmatrix}. \tag{6}$$

Note that the hypercharge of ψ is Y. Since under SU(2) transformation we have

$$\begin{aligned} \xi'^i &= U_{ij}\eta_2^j = U_{ij}\xi^j, \\ \bar{\eta}'^i &= \lambda_{ik}U_{kl}^*\lambda_{lj}^{-1}\lambda_{jr}\bar{\eta}_1^r = U_{ij}\bar{\eta}^j, \end{aligned} \tag{7}$$

where we have used the similarity transformation of the SU(2) transformation matrix,[2]

$$\lambda_{ik}U_{kl}^*\lambda_{lj}^{-1} = U_{ij}. \tag{8}$$

Hence, the transform of the $(2I+1)$-multiplet of Dirac fields in ψ under SU(2) is

$$\psi'^i = U_{ij}\psi^j, \tag{9}$$

and the above mass term is simply

$$-\mathcal{L}_m = \mu\bar{\psi}\psi. \tag{10}$$

[2]This can be seen from $-(\vec{I})_{ij}^* = (-)^{-i}(\vec{I})_{-i,-j}(-)^j = [(-)^{I-i}\delta_{-i,k}](\vec{I})_{kl}[(-)^{-I+j}\delta_{l,-j}]$ and $\lambda_{ij} = (-)^{-I+i}\delta_{i,-j}$, i.e., $-(\vec{I})_{ij}^* = \lambda_{ik}^{-1}(\vec{I})_{kl}\lambda_{lj}$.

The component ψ^{-Y} with neutral charge could be a dark matter candidate. But in the $I \neq 0$ and $Y \neq 0$ case, ψ^{-Y} will induce a sizable SI-scattering cross section via Z-boson exchange ($\sim 10^{-39}$ cm^2) [45], which is ruled out by the present direct search data [19]. To clarify the situation, we switch back to the $\eta_{1,2}$ basis. By diagonalizing the mass matrix, we find that there are two neutral Majorana degenerate states $\chi_{1,2} \propto (\eta_1 \pm \eta_2)/\sqrt{2}$ with mass $|\mu\lambda_{Y,-Y}| = \mu$. Both of them can be dark matter, since their masses are degenerate. The dangerous Z-boson exchange diagram is from the $\chi_1 \to \chi_2$ vector current (the $\chi_i \to \chi_i$ current can only be an axial one). The above situation can be avoided if one lifts the mass degeneracy of $\chi_{1,2}$. To do so, we enlarge the mass matrix. The Z_2-odd WIMPs, $\eta_{1,2}$, can mix with additional Z_2-odd WIMPs in the presence of the Higgs field ϕ [with quantum number $(2, 1/2)$] and obtain a new mass term after spontaneous symmetry breaking (SSB). We consider all possible combinations of renormalizable interactions with $\eta_{1,2}$ coupled to the Higgs field,

$$\begin{aligned} &\text{(i)}\ \phi \times \eta_1 \times [\text{new}],\\ &\text{(ii)}\ \phi \times \eta_2 \times [\text{new}],\\ &\text{(iii)}\ \tilde{\phi} \times \eta_1 \times [\text{new}],\\ &\text{(iv)}\ \tilde{\phi} \times \eta_2 \times [\text{new}], \end{aligned} \tag{11}$$

where $\tilde{\phi}^i \equiv \epsilon_{ij}\phi^{*j}$ with $\epsilon_{ij} = \lambda_{ij}$ for $I = 1/2$ (i.e., $\epsilon_{ij} = -\epsilon_{ji}$ and $\epsilon_{1/2,-1/2} = 1$). The allowed quantum numbers of these new particles are given in Table. I.

The generic Lagrangian is given by

$$\begin{aligned} -\mathcal{L}_m = &\sum_{p=1}^{5} \mu_p \lambda^p_{ij} \eta^i_{2p} \eta^j_{2p-1} + \sum_{p=2}^{3} (g_{2p-1}\lambda^p_{ijk}\tilde{\phi}^i \eta^j_2 \eta^k_{2p-1} + g_{2p}\lambda^p_{ijk}\phi^i \eta^j_1 \eta^k_{2p})\\ &+ \sum_{p=4}^{5} (g_{2p-1}\lambda^p_{ijk}\phi^i \eta^j_2 \eta^k_{2p-1} + g_{2p}\lambda^p_{ijk}\tilde{\phi}^i \eta^j_1 \eta^k_{2p}) + \text{H.c.}, \end{aligned} \tag{12}$$

with

$$\begin{aligned} &\lambda^1_{ij} = \sqrt{2I+1}\langle II; 00|Ii, Ij\rangle,\\ &\lambda^2_{ij} = \lambda^4_{ij} = \sqrt{2I}\left\langle \left(I-\frac{1}{2}\right)\left(I-\frac{1}{2}\right); 00\middle| \left(I-\frac{1}{2}\right)i, \left(I-\frac{1}{2}\right)j\right\rangle,\\ &\lambda^3_{ij} = \lambda^5_{ij} = \sqrt{2I+2}\left\langle \left(I+\frac{1}{2}\right)\left(I+\frac{1}{2}\right); 00\middle| \left(I+\frac{1}{2}\right)i, \left(I+\frac{1}{2}\right)j\right\rangle, \end{aligned} \tag{13}$$

$$\begin{aligned} &\lambda^2_{ijk} = \lambda^4_{ijk} = \epsilon_{ir}\sqrt{2I}\left\langle I\left(I-\frac{1}{2}\right); \frac{1}{2}r\middle| Ij, \left(I-\frac{1}{2}\right)k\right\rangle,\\ &\lambda^3_{ijk} = \lambda^5_{ijk} = \epsilon_{ir}\sqrt{2I+2}\left\langle I\left(I+\frac{1}{2}\right); \frac{1}{2}r\middle| Ij, \left(I+\frac{1}{2}\right)k\right\rangle. \end{aligned} \tag{14}$$

Note that the imposed Z_2 symmetry can protect the DM against decays. Otherwise, DM can decay through, for example, the lepton number violation term and become unstable. Equation (12) can be used as a building block to built other multiplets. In principle, one can replace $\eta_{1,2}$ by the induced fields in Eq. (11) and involve additional fields. For simplicity, we do not do it here. In fact, a more complicated case can be readily generated by using the present case as a module.

These fields can be combined into Dirac fields with definite isospin and hypercharge quantum numbers,

$$\psi^i_{(p)} \equiv \begin{pmatrix} \xi^i_{(p)} \\ \bar{\eta}^i_{(p)} \end{pmatrix} \tag{15}$$

TABLE I. Summary of the eight types of additional multiplets induced by the four general types of couplings involving the Higgs field and $\eta_{1,2}$.

[New]	$SU(2)(I_\eta)$	$U_Y(1)$	Type	Couples with
η_3	$I-1/2$	$-(Y-\frac{1}{2})$	(iv)	$\tilde{\phi} \times \eta_2$, η_4
η_4	$I-1/2$	$Y-\frac{1}{2}$	(i)	$\phi \times \eta_1$, η_3
η_5	$I+1/2$	$-(Y-\frac{1}{2})$	(iv)	$\tilde{\phi} \times \eta_2$, η_6
η_6	$I+1/2$	$Y-\frac{1}{2}$	(i)	$\phi \times \eta_1$, η_5
η_7	$I-1/2$	$-(Y+\frac{1}{2})$	(ii)	$\phi \times \eta_2$, η_8
η_8	$I-1/2$	$Y+\frac{1}{2}$	(iii)	$\tilde{\phi} \times \eta_1$, η_7
η_9	$I+1/2$	$-(Y+\frac{1}{2})$	(ii)	$\phi \times \eta_2$, η_{10}
η_{10}	$I+1/2$	$Y+\frac{1}{2}$	(iii)	$\tilde{\phi} \times \eta_1$, η_9

with

$$\xi^i_{(p)} \equiv \eta^i_{2p}, \qquad \bar{\eta}^i_{(p)} \equiv \lambda^p_{ij}\bar{\eta}^j_{2p-1}, \tag{16}$$

for $p = 1, \ldots, 5$. Consequently, we have

$$\mu_p \lambda^p_{ij}\eta^j_{2p-1}\eta^i_{2p} = \mu_p \eta^i_{(p)}\xi^i_{(p)} = \mu_p \bar{\psi}^i_{(p)R}\psi^i_{(p)L}, \tag{17}$$

for $p = 1, \ldots, 5$,

$$\begin{aligned} g_{2p-1}\lambda^p_{ijk}\tilde{\phi}^i\eta^j_2\eta^k_{2p-1} &= g_{2p-1}[\lambda^p_{ijk}(\lambda^p)^{-1}_{kl}]\tilde{\phi}^i\xi^j_{(1)}\eta^l_{(p)} \\ &= g_{2p-1}[\lambda^p_{ijk}(\lambda^p)^{-1}_{kl}]\tilde{\phi}^i\bar{\psi}^l_{(p)R}\psi^j_{(1)L} \end{aligned} \tag{18}$$

and

$$\begin{aligned} g_{2p}\lambda^p_{ijk}\phi^i\eta^j_1\eta^k_{2p} &= g_{2p}[\lambda^p_{ijk}(\lambda^1)^{-1}_{jl}]\phi^i\eta^l_{(1)}\xi^k_{(2p)} \\ &= g_{2p}[\lambda^p_{ijk}(\lambda^1)^{-1}_{jl}]\phi^i\bar{\psi}^l_{(1)R}\psi^k_{(p)L}, \end{aligned} \tag{19}$$

for $p = 2, \ldots, 5$, giving

$$\begin{aligned} -\mathcal{L}_m = &\sum_{p=1}^{5}\mu_p\bar{\psi}^i_{(p)R}\psi^i_{(p)L} + \sum_{p=2}^{3}\{g_{2p-1}[\lambda^p_{ijk}(\lambda^p)^{-1}_{kl}]\tilde{\phi}^i\bar{\psi}^l_{(p)R}\psi^j_{(1)L} + g_{2p}[\lambda^p_{ijk}(\lambda^1)^{-1}_{jl}]\phi^i\bar{\psi}^l_{(1)R}\psi^k_{(p)L}\} \\ &+ \sum_{p=4}^{5}\{g_{2p-1}[\lambda^p_{ijk}(\lambda^p)^{-1}_{kl}]\phi^i\bar{\psi}^l_{(p)R}\psi^j_{(1)L} + g_{2p}[\lambda^p_{ijk}(\lambda^1)^{-1}_{jl}]\tilde{\phi}^i\bar{\psi}^l_{(1)R}\psi^k_{(p)L}\} + \text{H.c.} \end{aligned} \tag{20}$$

After SSB, the above Lagrangian will generate the mixing in these Dirac fields. We still do not have any Majorana particle.

The MSSM case can shed some light on this issue. In fact, the relevant MSSM multiplet corresponds to

$$I = Y = \frac{1}{2}, \qquad \eta_{1,2} = \tilde{H}_{1,2}, \qquad \eta_3, \qquad \eta_4 \propto \tilde{B}, \qquad \eta_5, \qquad \eta_6 \propto \tilde{W}, \qquad \text{without} \quad \eta_{7,8,9,10}. \tag{21}$$

The Majorana particles can only enter when $Y = 1/2$, where the quantum numbers of $\eta_{3(5)}$ and $\eta_{4(6)}$ are identical, and to have neutral particles, I can only be half-integers. Consequently, we have

$$Y = \frac{1}{2}, \qquad I = \frac{2n+1}{2}, \qquad \eta_3 = \text{sign}(\mu_2)(-1)^n\eta_4, \qquad \eta_5 = \text{sign}(\mu_3)(-1)^{n+1}\eta_6, \tag{22}$$

and $\mu_{2,3}$ change to $\mu_{2,3}/2$, to which we will stick throughout this work. Note that the additional signs in the relations of $\eta_{3,4}$ and $\eta_{5,6}$ are designed to absorb the signs of the corresponding Majorana mass terms [$\mu_{2,3}$; see Eq. (24) below].

The Lagrangian for the neutral WIMP mass term is

$$\begin{aligned} -\mathcal{L}^0_m = &\mu_1\lambda^1_{-\frac{1}{2},\frac{1}{2}}\eta_2^{-\frac{1}{2}}\eta_1^{\frac{1}{2}} + \frac{1}{2}\mu_2\lambda^2_{0,0}\eta^0_4\eta^0_3 + \frac{1}{2}\mu_3\lambda^3_{0,0}\eta^0_6\eta^0_5 + \mu_4\lambda^4_{-1,1}\eta_8^{-1}\eta_7^1 + \mu_5\lambda^5_{-1,1}\eta_{10}^{-1}\eta_9^1 \\ &+ g_3\lambda^2_{\frac{1}{2},-\frac{1}{2},0}\langle\tilde{\phi}^{\frac{1}{2}}\rangle\eta_2^{-\frac{1}{2}}\eta^0_3 + g_4\lambda^2_{-\frac{1}{2},\frac{1}{2},0}\langle\phi^{-\frac{1}{2}}\rangle\eta_1^{\frac{1}{2}}\eta^0_4 + g_5\lambda^3_{\frac{1}{2},-\frac{1}{2},0}\langle\tilde{\phi}^{\frac{1}{2}}\rangle\eta_2^{-\frac{1}{2}}\eta^0_5 + g_6\lambda^3_{-\frac{1}{2},\frac{1}{2},0}\langle\phi^{-\frac{1}{2}}\rangle\eta_1^{\frac{1}{2}}\eta^0_6 \\ &+ g_7\lambda^4_{-\frac{1}{2},-\frac{1}{2},1}\langle\phi^{-\frac{1}{2}}\rangle\eta_2^{-\frac{1}{2}}\eta^1_7 + g_8\lambda^4_{\frac{1}{2},\frac{1}{2},-1}\langle\tilde{\phi}^{\frac{1}{2}}\rangle\eta_1^{\frac{1}{2}}\eta_8^{-1} + g_9\lambda^5_{-\frac{1}{2},-\frac{1}{2},1}\langle\phi^{-\frac{1}{2}}\rangle\eta_2^{-\frac{1}{2}}\eta^1_9 + g_{10}\lambda^5_{\frac{1}{2},\frac{1}{2},-1}\langle\tilde{\phi}^{\frac{1}{2}}\rangle\eta_1^{\frac{1}{2}}\eta_{10}^{-1} + \text{H.c.} \end{aligned} \tag{23}$$

It can be simplified as

$$\begin{aligned} -\mathcal{L}^0_m = &\mu_1(-1)^{n+1}\eta_2^{-\frac{1}{2}}\eta_1^{\frac{1}{2}} + \frac{1}{2}\mu_2(-1)^n\eta^0_4\eta^0_3 + \frac{1}{2}\mu_3(-1)^{n+1}\eta^0_6\eta^0_5 + \mu_4(-1)^{n+1}\eta_8^{-1}\eta_7^1 + \mu_5(-1)^n\eta_{10}^{-1}\eta_9^1 \\ &+ g_3(-1)^n\langle\tilde{\phi}^{\frac{1}{2}}\rangle\eta_2^{-\frac{1}{2}}\eta^0_3 + g_4(-1)^{n+1}\langle\phi^{-\frac{1}{2}}\rangle\eta_1^{\frac{1}{2}}\eta^0_4 + g_5(-1)^{1-n}\langle\tilde{\phi}^{\frac{1}{2}}\rangle\eta_2^{-\frac{1}{2}}\eta^0_5 + g_6(-1)^{1-n}\langle\phi^{-\frac{1}{2}}\rangle\eta_1^{\frac{1}{2}}\eta^0_6 \\ &+ g_7(-1)^n\sqrt{\frac{n}{n+1}}\langle\phi^{-\frac{1}{2}}\rangle\eta_2^{-\frac{1}{2}}\eta^1_7 + g_8(-1)^{n+1}\sqrt{\frac{n}{n+1}}\langle\tilde{\phi}^{\frac{1}{2}}\rangle\eta_1^{\frac{1}{2}}\eta_8^{-1} \\ &+ g_9(-1)^{-n}\sqrt{\frac{n+2}{n+1}}\langle\phi^{-\frac{1}{2}}\rangle\eta_2^{-\frac{1}{2}}\eta^1_9 + g_{10}(-1)^{-n}\sqrt{\frac{n+2}{n+1}}\langle\tilde{\phi}^{\frac{1}{2}}\rangle\eta_1^{\frac{1}{2}}\eta_{10}^{-1} + \text{H.c.} \end{aligned} \tag{24}$$

With the basis $\Psi^{0T}_i = (\eta_1^{1/2}, \eta_2^{-1/2}, \eta^0_3, \eta^0_5, \eta^1_7, \eta_8^{-1}, \eta^1_9, \eta_{10}^{-1})$, the above Lagrangian after SSB can be written as

$$\mathcal{L}^0_m = -\frac{1}{2}\Psi^{0T}Y\Psi^0 + \text{H.c.}, \tag{25}$$

where the corresponding mass matrix Y takes the form

$$\begin{pmatrix}
0 & (-)^{n+1}\mu_1 & -\frac{g_4 v}{\sqrt{2}} & \frac{g_6 v}{\sqrt{2}} & 0 & \frac{(-1)^{n+1} g_8 v\sqrt{n}}{\sqrt{2(n+1)}} & 0 & \frac{(-1)^n g_{10} v\sqrt{n+2}}{\sqrt{2(n+1)}} \\
(-)^{n+1}\mu_1 & 0 & \frac{(-1)^n g_3 v}{\sqrt{2}} & \frac{(-1)^{n+1} g_5 v}{\sqrt{2}} & \frac{(-1)^n g_7 v\sqrt{n}}{\sqrt{2(n+1)}} & 0 & \frac{(-1)^n g_9 v\sqrt{n+2}}{\sqrt{2(n+1)}} & 0 \\
-\frac{g_4 v}{\sqrt{2}} & \frac{(-1)^n g_3 v}{\sqrt{2}} & \mu_2 & 0 & 0 & 0 & 0 & 0 \\
\frac{g_6 v}{\sqrt{2}} & \frac{(-)^{n+1} g_5 v}{\sqrt{2}} & 0 & \mu_3 & 0 & 0 & 0 & 0 \\
0 & \frac{(-1)^n g_7 v\sqrt{n}}{\sqrt{2(n+1)}} & 0 & 0 & 0 & (-1)^{n+1}\mu_4 & 0 & 0 \\
\frac{(-1)^{n+1} g_8 v\sqrt{n}}{\sqrt{2(n+1)}} & 0 & 0 & 0 & (-1)^{n+1}\mu_4 & 0 & 0 & 0 \\
0 & \frac{(-1)^n g_9 v\sqrt{n+2}}{\sqrt{2(n+1)}} & 0 & 0 & 0 & 0 & 0 & (-1)^n\mu_5 \\
\frac{(-1)^n g_{10} v\sqrt{n+2}}{\sqrt{2(n+1)}} & 0 & 0 & 0 & 0 & 0 & (-1)^n\mu_5 & 0
\end{pmatrix}. \tag{26}$$

In parallel with the neutralino sector in the MSSM, we work the model with $I = Y = 1/2$, and the Lagrangian for the neutral WIMP mass term must be modified as in Appendix A. Note that the sign convention of the Clebsch-Gordan coefficient is different from those usually used in quantum field theory. For example, we usually use $\pi^{\pm} = (\pi_1 \mp i\pi_2)/\sqrt{2}$, while the Clebsch-Gordan convention is $\pi^{\pm} = \mp(\pi_1 \mp i\pi_2)/\sqrt{2}$. Comparing to the MSSM, we then have the correspondences

$$\begin{aligned}
&\eta_1 = \tilde{H}_1, \qquad \eta_2 = \tilde{H}_2, \qquad \eta_3 = -i\lambda', \qquad \eta_5^{\pm,0} = -i(\mp\lambda_{\pm}, \lambda_3), \\
&g_3 v = \sqrt{2} m_Z \cos\beta \sin\theta_W, \qquad g_4 v = \sqrt{2} m_Z \sin\beta \sin\theta_W, \\
&g_5 v = \sqrt{2} m_Z \cos\beta \cos\theta_W, \qquad g_6 v = \sqrt{2} m_Z \sin\beta \cos\theta_W, \\
&\mu_4 = \mu_5 = 0, \qquad g_{7,8,9,10} = 0,
\end{aligned} \tag{27}$$

where the additional sign in front of λ_+ is to absorb the sign from the Clebsch-Gordan sign convention.

When diagonalizing the mass matrix in Eq. (26) and producing non-negative mass eigenvalues, one sometimes needs to absorb a negative sign resulting in purely imaginary matrix elements in the transition matrix. On the other hand, one should note that all parameters in the Lagrangian are assumed to be real before transforming the gauge eigenstates to mass eigenstates in this model. The whole Lagrangian in this model is then CP conserved. As noted after field redefinition, some couplings become purely imaginary. However, the whole Lagrangian should still be CP conserved (see Appendix E).

The Lagrangian for a single charged WIMP mass term is

$$\begin{aligned}
-\mathcal{L}_m^{\pm} = {} & \mu_1(-1)^n(\eta_2^{\frac{1}{2}}\eta_1^{-\frac{1}{2}} + \eta_2^{-\frac{3}{2}}\eta_1^{\frac{3}{2}}) + \frac{1}{2}\mu_2(-1)^{n+1}(\eta_4^1\eta_3^{-1} + \eta_4^{-1}\eta_3^1) + \frac{1}{2}\mu_3(-1)^n(\eta_6^1\eta_5^{-1} + \eta_6^{-1}\eta_5^1) \\
& + \mu_4(-1)^n(\eta_8^0\eta_7^0 + \eta_8^{-2}\eta_7^2) + \mu_5(-1)^{n+1}(\eta_{10}^0\eta_9^0 + \eta_{10}^{-2}\eta_9^2) + g_3(-1)^{n+1}\left(\sqrt{\frac{n}{n+1}}\langle\tilde{\phi}^{\frac{1}{2}}\rangle\eta_2^{\frac{1}{2}}\eta_3^{-1} + \sqrt{\frac{n+2}{n+1}}\langle\tilde{\phi}^{\frac{1}{2}}\rangle\eta_2^{-\frac{3}{2}}\eta_3^1\right) \\
& + g_4(-1)^n\left(\sqrt{\frac{n+2}{n+1}}\langle\phi^{-\frac{1}{2}}\rangle\eta_1^{\frac{3}{2}}\eta_4^{-1} + \sqrt{\frac{n}{n+1}}\langle\phi^{-\frac{1}{2}}\rangle\eta_1^{-\frac{1}{2}}\eta_4^1\right) + g_5(-1)^n\left(\sqrt{\frac{n+2}{n+1}}\langle\tilde{\phi}^{\frac{1}{2}}\rangle\eta_2^{\frac{1}{2}}\eta_5^{-1} + \sqrt{\frac{n}{n+1}}\langle\tilde{\phi}^{\frac{1}{2}}\rangle\eta_2^{-\frac{3}{2}}\eta_5^1\right) \\
& + g_6(-1)^n\left(\sqrt{\frac{n}{n+1}}\langle\phi^{-\frac{1}{2}}\rangle\eta_1^{-\frac{1}{2}}\eta_6^1 + \sqrt{\frac{n+2}{n+1}}\langle\phi^{-\frac{1}{2}}\rangle\eta_1^{\frac{3}{2}}\eta_6^{-1}\right) + g_7(-1)^{n+1}\left(\langle\phi^{-\frac{1}{2}}\rangle\eta_2^{\frac{1}{2}}\eta_7^0 + \sqrt{\frac{n-1}{n+1}}\langle\phi^{-\frac{1}{2}}\rangle\eta_2^{-\frac{3}{2}}\eta_7^2\right) \\
& + g_8(-1)^n\left(\sqrt{\frac{n-1}{n+1}}\langle\tilde{\phi}^{\frac{1}{2}}\rangle\eta_1^{\frac{3}{2}}\eta_8^{-2} + \langle\tilde{\phi}^{\frac{1}{2}}\rangle\eta_1^{-\frac{1}{2}}\eta_8^0\right) + g_9(-1)^{n-1}\left(\langle\phi^{-\frac{1}{2}}\rangle\eta_2^{\frac{1}{2}}\eta_9^0 + \sqrt{\frac{n+3}{n+1}}\langle\phi^{-\frac{1}{2}}\rangle\eta_2^{-\frac{3}{2}}\eta_9^2\right) \\
& + g_{10}(-1)^{n-1}\left(\sqrt{\frac{n+3}{n+1}}\langle\tilde{\phi}^{\frac{1}{2}}\rangle\eta_1^{\frac{3}{2}}\eta_{10}^{-2} + \langle\tilde{\phi}^{\frac{1}{2}}\rangle\eta_1^{-\frac{1}{2}}\eta_{10}^0\right) + \text{H.c.}
\end{aligned} \tag{28}$$

As mentioned previously, $\langle i|T^+|j\rangle$ used in quantum field theory is connected to Clebsch-Gordan coefficient $\langle m'|J^+|m\rangle$ used in quantum mechanics by a similarity transformation V,

$$\langle I_k,i|T^+|I_k,j\rangle = \sum_{m,m'}\langle I_k,i|V^\dagger|I_k,m'\rangle\langle I_k,m'|VJ^+V^\dagger|I_k,m\rangle\langle I_k,m|V|I_k,j\rangle. \tag{29}$$

When dealing with the single charged particles, the similarity transformation only changes the sign of positive charged particles with an integer isospin; namely, we only need to do the transform

$$\eta_k^{q_k+1} \to \eta'^{q_k+1}_k \equiv V\eta_k^{q_k+1} = (-1)^{\mathrm{mod}(2I_k,2)+1}\eta_k^{q_k+1}, \tag{30}$$

where q_k in $\eta_k^{q_k+1}$ is defined as the the third component of isospin corresponding to the neutral particle in the multiplet η_k with isospin I_k. With the basis $\Psi_i^{+T} = (\eta_1'^{3/2}, \eta_2'^{1/2}, \eta_3'^{1}, \eta_5'^{1}, \eta_7'^{2}, \eta_8'^{0}, \eta_9'^{2}, \eta_{10}'^{0})$ and $\Psi_i^{-T} = (\eta_1^{-1/2}, \eta_2^{-3/2}, \eta_3^{-1}, \eta_5^{-1}, \eta_7^{0}, \eta_8^{-2}, \eta_9^{0}, \eta_{10}^{-2})$, the Lagrangian in Eq. (28) becomes

$$\begin{aligned}
-\mathcal{L}_m^{\pm} &= \mu_1(-1)^n(\eta_2^+\eta_1^- + \eta_2^-\eta_1^+) + \frac{1}{2}\mu_2(\eta_3'^+\eta_3^- + \eta_3^-\eta_3'^+) + \frac{1}{2}\mu_3(\eta_5'^+\eta_5^- + \eta_5^-\eta_5'^+)\\
&\quad - \mu_4(-1)^n(\eta_8'^+\eta_7^- + \eta_8^-\eta_7'^+) - \mu_5(-1)^{n+1}(\eta_{10}'^+\eta_9^- + \eta_{10}^-\eta_9'^+)\\
&\quad + g_3(-1)^{n+1}\left(\sqrt{\frac{n}{n+1}}\langle\tilde{\phi}^0\rangle\eta_2^+\eta_3^- - \sqrt{\frac{n+2}{n+1}}\langle\tilde{\phi}^0\rangle\eta_2^-\eta_3'^+\right) + g_4\left(\sqrt{\frac{n+2}{n+1}}\langle\phi^0\rangle\eta_1^+\eta_3^- + \sqrt{\frac{n}{n+1}}\langle\phi^0\rangle\eta_1^-\eta_3'^+\right)\\
&\quad + g_5(-1)^n\left(\sqrt{\frac{n+2}{n+1}}\langle\tilde{\phi}^0\rangle\eta_2^+\eta_5^- - \sqrt{\frac{n}{n+1}}\langle\tilde{\phi}^0\rangle\eta_2^-\eta_5'^+\right) + g_6\left(-\sqrt{\frac{n}{n+1}}\langle\phi^0\rangle\eta_1^+\eta_5^- + \sqrt{\frac{n+2}{n+1}}\langle\phi^0\rangle\eta_1^-\eta_5'^+\right)\\
&\quad + g_7(-1)^{n+1}\left(\langle\phi^0\rangle\eta_2^+\eta_7^- - \sqrt{\frac{n-1}{n+1}}\langle\phi^0\rangle\eta_2^-\eta_7'^+\right) + g_8(-1)^n\left(\sqrt{\frac{n-1}{n+1}}\langle\tilde{\phi}^0\rangle\eta_1^+\eta_8^- - \langle\tilde{\phi}^0\rangle\eta_1^-\eta_8'^+\right)\\
&\quad + g_9(-1)^{n-1}\left(\langle\phi^0\rangle\eta_2^+\eta_9^- - \sqrt{\frac{n+3}{n+1}}\langle\phi^0\rangle\eta_2^-\eta_9'^+\right) + g_{10}(-1)^{n-1}\left(\sqrt{\frac{n+3}{n+1}}\langle\tilde{\phi}^0\rangle\eta_1^+\eta_{10}^- - \langle\tilde{\phi}^0\rangle\eta_1^-\eta_{10}'^+\right) + \mathrm{H.c.}
\end{aligned} \tag{31}$$

After SSB, it can be written as a compact form as

$$\mathcal{L}_m^{\pm} = -\frac{1}{2}(\Psi^+,\Psi^-)\begin{pmatrix}0 & X^T\\ X & 0\end{pmatrix}\begin{pmatrix}\Psi^+\\ \Psi^-\end{pmatrix} + \mathrm{H.c.}, \tag{32}$$

where X takes the form

$$\begin{pmatrix}
0 & (-)^n\mu_1 & \frac{-g_4v\sqrt{n}}{\sqrt{2(n+1)}} & \frac{g_6v\sqrt{n+2}}{\sqrt{2(n+1)}} & 0 & \frac{(-1)^{n+1}g_8v}{\sqrt{2}} & 0 & \frac{(-1)^ng_{10}v}{\sqrt{2}}\\
(-)^n\mu_1 & 0 & \frac{(-)^ng_3v\sqrt{n+2}}{\sqrt{2(n+1)}} & \frac{(-)^{n+1}g_5v\sqrt{n}}{\sqrt{2(n+1)}} & \frac{(-)^ng_7v\sqrt{n-1}}{\sqrt{2(n+1)}} & 0 & \frac{(-)^ng_9v\sqrt{n+3}}{\sqrt{2(n+1)}} & 0\\
\frac{g_4v\sqrt{n+2}}{\sqrt{2(n+1)}} & \frac{(-)^{n+1}g_3v\sqrt{n}}{\sqrt{2(n+1)}} & \mu_2 & 0 & 0 & 0 & 0 & 0\\
\frac{-g_6v\sqrt{n}}{\sqrt{2(n+1)}} & \frac{(-)^ng_5v\sqrt{n+2}}{\sqrt{2(n+1)}} & 0 & \mu_3 & 0 & 0 & 0 & 0\\
0 & \frac{(-1)^{n+1}g_7v}{\sqrt{2}} & 0 & 0 & 0 & (-)^{n+1}\mu_4 & 0 & 0\\
\frac{(-1)^ng_8v\sqrt{n-1}}{\sqrt{2(n+1)}} & 0 & 0 & 0 & (-)^{n+1}\mu_4 & 0 & 0 & 0\\
0 & \frac{(-)^{n-1}g_9v}{\sqrt{2}} & 0 & 0 & 0 & 0 & 0 & (-)^{n+1}\mu_5\\
\frac{(-)^{n-1}g_{10}v\sqrt{n+3}}{\sqrt{2(n+1)}} & 0 & 0 & 0 & 0 & 0 & (-)^{n+1}\mu_5 & 0
\end{pmatrix}. \tag{33}$$

Comparing to the chargino sector in the MSSM with $\psi_i^{+T} = (-i\lambda^+, \psi_{H_2}^1)$ and $\psi_j^{-T} = (-i\lambda^-, \psi_{H_1}^2)$, we have the following correspondences:

$$\eta_1^- = \psi_{H_1}^2, \quad \eta_2^+ = \psi_{H_2}^1, \quad \eta_5'^+ = -i\lambda^+, \quad \eta_5^- = -i\lambda^-,$$
$$g_5 v = \sqrt{2} m_Z \cos\beta \cos\theta_W, \quad g_6 v = \sqrt{2} m_Z \sin\beta \cos\theta_W,$$
$$\mu_4 = \mu_5 = 0, \quad g_{7,8,9,10} = 0. \tag{34}$$

Note that the Lagrangian for a single charged WIMP mass term with $I = Y = 1/2$ also needs to be modified as in Appendix A and the mass eigenstates of the neutral as well as single charged particles in the four-component notation are constructed in Appendix B.

B. Dark matter annihilation

The DM particles are thought to have been created thermally during the big bang and frozen out of thermal equilibrium in the early Universe with a relic density. The evolution of DM abundance is described by the Boltzmann equation,

$$\frac{dn_\chi}{dt} + 3Hn_\chi = -\langle \sigma_{\rm ann} v_{\rm M\phi l} \rangle [n_\chi n_{\bar\chi} - n_\chi^{\rm eq} n_{\bar\chi}^{\rm eq}], \tag{35}$$

where $H \equiv \dot{a}/a = \sqrt{4\pi^3 g_*(T) T^4/(45 M_{\rm PL}^2)}$ is the Hubble parameter, $M_{\rm PL}$ is the Plank mass, and g_* is the total effective number of the relativistic degrees of freedom [47,48]. $n_\chi(n_{\bar\chi})$ is the number density of DM particles, and $n_{\bar\chi} = n_\chi$ for Majorana fermions (that is, $\chi = \bar\chi$) as in this model. Equation (35) is measured in the cosmic comoving frame [49], and $\langle \sigma_{\rm ann} v_{\rm M\phi l} \rangle$ is the thermal averaged annihilation cross section times Mϕller velocity, which is defined by $v_{\rm M\phi l} \equiv \sqrt{(p_1 \cdot p_2)^2 - m_1^2 m_2^2}/(E_1 E_2) = \sqrt{|\mathbf{v}_1 - \mathbf{v}_2|^2 - |\mathbf{v}_1 \times \mathbf{v}_2|^2}$ with subscripts 1 and 2 labeling the two initial DM particles and velocities $\mathbf{v}_i \equiv \mathbf{p}_i/E_i (i = 1, 2)$.[3]

The DM particles became nonrelativistic when they froze out of thermal equilibrium in the early Universe. In this nonrelativistic limit, $\sigma_{\rm ann}(\chi\chi \to {\rm all}) v = a + b v^2 + O(v^4)$, where $v \equiv v_{\rm lab} = \sqrt{s(s - 4m_\chi^2)}/(s - 2m_\chi^2)$ and the Mandelstam variable $s = 2m_\chi^2(1 + 1/\sqrt{1 - v^2})$ in the lab frame. The velocity averaged DM annihilation cross section via Maxwell velocity distribution can be calculated [45] to be $\langle \sigma_{\rm ann} v \rangle = a + 6b/x + O(1/x^2)$ with the freeze-out temperature parameter $x \equiv m_\chi/T$. At the freeze-out temperature, the interaction rate of DM particles is equal to the expansion rate of Universe, namely, $\Gamma_f \equiv n_\chi^{eq} \langle \sigma_{\rm ann} v \rangle = H(T_f)$. From this freeze-out condition, x_f can be solved numerically by the equation [13,47]

$$x_f = \ln\left[c(c+2) \sqrt{\frac{45}{8}} \frac{g_\chi m_\chi M_{\rm PL} (a + 6b/x_f)}{2\pi^3 \sqrt{g_*(m_\chi/x_f)} x_f^{1/2}} \right], \tag{36}$$

where c is an order of unity parameter determined by matching the late time and early time in the freeze-out criterion. We take the usual value $c = 1/2$ since the exact value of c is not so significant to solve the numerical solution for x_f due to the logarithmic dependence in Eq. (36). Following the standard procedure [47] to solve Eq. (35), the relic CDM density $\Omega_{\rm DM} \equiv \rho_\chi/\rho_{\rm crit}$ can be approximately related to the velocity averaged annihilation cross section $\langle \sigma_{\rm ann} v \rangle$ as

$$\Omega_{\rm DM} h^2 \approx 1.04 \times 10^9 \frac{\rm GeV^{-1}}{M_{\rm PL} \sqrt{g_*(m_\chi)} J(x_f)}, \tag{37}$$

where

$$J(x_f) \equiv \int_{x_f}^\infty \frac{\langle \sigma_{\rm ann} v \rangle}{x^2} dx = a x_f^{-1} + 3b x_f^{-2} + O(x_f^{-3}). \tag{38}$$

When doing the calculation of DM relic density, we need to consider three exceptions [50]: coannihilation, forbidden channel annihilation, and annihilation near the pole. In this article, we focus on the model building and mainly consider the annihilation processes. The leading effect on coannihilation in this model will be discussed in Sec. IV. To solve the last two exceptions, we do not take the Taylor series expansion on v^2 in the s channel, and for each annihilation channel, we put a step function for the allowed threshold energy in the thermal average cross section as follows:

$$\langle \sigma_{\rm ann} v \rangle = \frac{x^{3/2}}{2\pi} \sum_{A,B} \int_0^\infty dv v^2 e^{-x v^2/4} [\sigma_{\rm ann}(\chi\chi \to A + B) v] \theta \times \left[2m_\chi^2 \left(1 + \frac{1}{\sqrt{1 - v^2}} \right) - (m_A + m_B)^2 \right]. \tag{39}$$

Instead of $a + 6b/x_f$, we replace it with the above thermal averaged cross section with $x = x_f$ in Eq. (36) and solve the value of x_f numerically. Then, we can get the DM relic density by modifying $J(x_f)$ in Eq. (38) as follows:

[3] In general, the collision is not collinear in the comoving frame. Hence, the Mϕller velocity is not equal to the relative velocity $v_{\rm rel} \equiv |\mathbf{v}_1 - \mathbf{v}_2|$. Nevertheless, it has been shown [49] that $\langle \sigma_{\rm ann} v_{\rm M\phi l} \rangle = \langle \sigma_{\rm ann} v_{\rm lab} \rangle^{\rm lab}$, where $v_{\rm lab} \equiv |\mathbf{v}_{1,\rm lab} - \mathbf{v}_{2,\rm lab}|$ is calculated in the lab frame with one of two initial particles being at rest.

$$J(x_f) \equiv \int_{x_f}^{\infty} \frac{\langle \sigma_{\rm ann} v \rangle}{x^2} dx$$
$$= \sum_{A,B} \int_0^{\infty} dv [\sigma_{\rm ann}(\chi\chi \to A + B) v][1 - {\rm erf}(v\sqrt{x_f}/2)]$$
$$\times \theta \left[2m_\chi^2 \left(1 + \frac{1}{\sqrt{1-v^2}} \right) - (m_A + m_B)^2 \right]. \quad (40)$$

We will calculate the relic density in the early Universe through the DM annihilation processes $(\chi\chi \to W^+W^-, ZZ, ZH, HH, f\bar{f})$. Figure 1 shows the corresponding Feynman diagrams. The corresponding Lagrangian and the matrix elements are shown in Appendixes C and D, respectively, and it is straightforward to obtain $\langle \sigma_{\rm ann} v \rangle$. Although the present DM relic density is determined by the velocity averaged cross section $\langle \sigma_{\rm ann} v \rangle$ of DM annihilation processes which ceased after the freeze-out stage in the cosmological scale, the DM annihilation to the SM particles would still occur today in regions of high DM density and result in the indirect search for end products as excesses relative to products from SM astrophysical processes. The results on $\langle \sigma_{\rm ann} v \rangle$ can be readily applied to the indirect search processes by using a typical velocity $v \simeq 300$ km/s (explained in Sec. III).

As we know that in the nonrelativistic limit, $\sigma_{\rm ann} v$ can be expressed as $a + bv^2 + O(v^4)$, where a is the s-wave contribution at zero relative velocity and bv^2 contains both the s- and p-waves contributions. $\sigma_{\rm ann} v$ is dominated by the s-wave term in indirect-detection calculations, while both s- and p-wave terms become important when dealing with the calculation of DM relic density.

It will be useful to recall some qualitative properties of the DM annihilation amplitudes in the channels of $\chi\chi \to W^+W^-, ZZ, ZH, HH, f\bar{f}$ [13,51]. Fermi statistics forces the two identical Majorana fermions with orbital angular momentum L and total spin S to satisfy $(-)^S = (-)^L$. The total angular momentum of the s-wave state is $J = 0$, and the CP is given by $CP = (-1)^{L+1} = -1$, while the p-wave state has $CP = +1$ [see Eqs. (E31) and (E33)].

The final-state W^+W^- can be produced via t-channel exchange of a single charged WIMP and s-channel exchange of a Higgs scalar or a Z boson (see Fig. 1). The final-state ZZ can be produced via t-channel exchange of a neutral WIMP and s-channel exchange of a Higgs scalar (see Fig. 1). Note that in the s-wave DM amplitude both gauge bosons in the final state are transversely polarized and governed via the t-channel exchange diagrams [13,51]. Also note that a binolike DM pair does not contribute to the s-wave amplitude [51].

The DM particles can annihilate into ZH via t-channel exchange of a neutral WIMP and s-channel exchange of a Z boson (see Fig. 1). The final-state ZH in a $L = 1$ configuration can match the angular momentum and the CP of the s-wave DM pair. Hence, the s-wave amplitude is allowed in this channel [13,51].

The DM particles can annihilate into two Higgs bosons via t-channel exchange of a neutral WIMP and s-channel exchange of a scalar Higgs (see Fig. 1). The s-wave scattering amplitude is vanishing since two scalars cannot be in a state with $J = 0$ and $CP = -1$ [13,51].

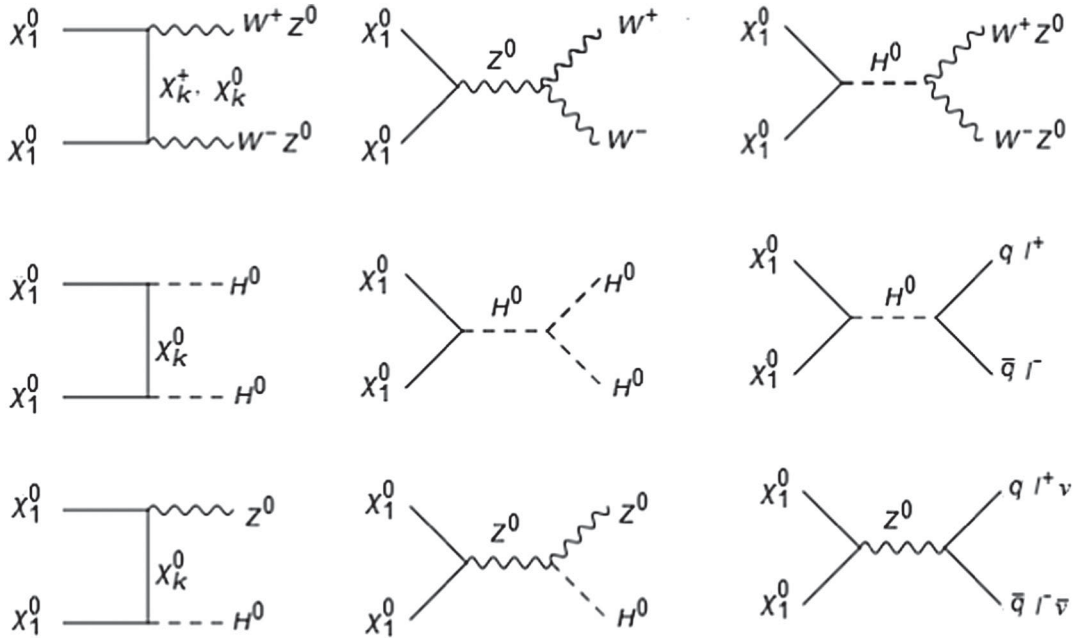

FIG. 1. The annihilation processes $(\chi\chi \to W^+W^-, ZZ, ZH, HH, f\bar{f})$.

The final-state fermion-antifermion pair $f\bar{f}$ can be produced via the s-channel exchange of a Higgs scalar or a Z boson (see Fig. 1). The Z exchange contributes to both the s- and p-wave matrix elements with chiral conserving interactions [51]. The final-state $f\bar{f}$ has $CP = (-)^{S+1}$. The s-wave DM pair requires the total spin $S = 0$ in the final state to conserve CP so that both the fermion and antifermion should have the same helicity. The Z-f-$\bar{f}$ couplings imply the fermion and the antifermion in opposite chirality and hence result in the helicity suppression of the s-wave amplitude. The Higgs scalar exchange only contributes to p-wave matrix elements (since the CP of Higgs boson is $+1$) with a fermion mass factor. Hence, the process $\chi\chi \to f\bar{f}$ favors a heavy fermion pair [13,51].

C. DM-nucleus elastic scattering cross section

To compare with the results of LUX, XENON100, and PICO-60 experiments, we calculate the SI and SD cross sections of DM scattering off ^{129,131}Xe nuclei and the SD cross section of DM scattering off CF_3I nuclei. We shall obtain $\bar{\sum}|M_{fi}|^2$ at $q^2 = 0$ first. In this model, the DM is composed of Majorana fermions so that the DM vector current matrix elements are vanishing. Hence, the Lagrangian in this model is given by

$$\mathcal{L} = \bar{\chi}\gamma_\mu\gamma_5\chi j^\mu_{Ah} + \bar{\chi}\gamma_\mu\gamma_5\chi j^\mu_{Vh} + \bar{\chi}\chi s_h + \bar{\chi}\gamma_5\chi s'_h. \tag{41}$$

where

$$s_h = a^q\bar{q}q, \qquad s'_h = a'^q\bar{q}q. \qquad j^\mu_{Vh} = b^q j^\mu_{Vq} = b^q\bar{q}\gamma_\mu q, \qquad j^\mu_{Ah} = d^q j^\mu_{Aq} = d^q\bar{q}\gamma\gamma_5 q, \tag{42}$$

and a^q, a'^q, b^q, and d^q are given in Appendix F. The corresponding scattering amplitude is

$$\begin{aligned} iM_{fi} &= \langle\chi(p'_\chi, s'_\chi), \mathcal{N}(p', s')|i\mathcal{L}(0)|\chi(p_\chi, s_\chi), \mathcal{N}(p, s)\rangle \\ &= i\kappa_\chi\bar{u}(p'_\chi, s'_\chi)\gamma_\mu\gamma_5 u(p_\chi, s_\chi)\langle\mathcal{N}(p', s')|j^\mu_{Ah} + j^\mu_{Vh}|\mathcal{N}(p, s)\rangle \\ &\quad + i\kappa_\chi\bar{u}(p'_\chi, s'_\chi)u(p_\chi, s_\chi)\langle\mathcal{N}(p', s')|s_h|\mathcal{N}(p, s)\rangle \\ &\quad + i\kappa_\chi\bar{u}(p'_\chi, s'_\chi)\gamma_5 u(p_\chi, s_\chi)\langle\mathcal{N}(p', s')|s'_h|\mathcal{N}(p, s)\rangle. \end{aligned} \tag{43}$$

In the above, $\kappa_\chi = 2$ for the Majorana fermions in this model, and $\kappa_\chi = 1$ for the Dirac fermions.

It is useful to define

$$\begin{aligned} \chi^{XY} &\equiv \frac{1}{2J_\chi + 1}\sum_{\text{spins}}\langle\chi(p_\chi, s_\chi)|(\bar{\chi}\chi)_X|\chi(p'_\chi, s'_\chi)\rangle\langle\chi(p'_\chi, s'_\chi)|(\bar{\chi}\chi)_Y|\chi(p_\chi, s_\chi)\rangle \\ W^{XY} &\equiv \frac{1}{2J_\mathcal{N} + 1}\sum_{\text{spins}}\langle\mathcal{N}(p', s')|O_{hX}|\mathcal{N}(p', s')\rangle\langle\mathcal{N}(p', s')|O_{hY}|\mathcal{N}(p, s)\rangle, \end{aligned} \tag{44}$$

where $X, Y = A$, V, S, P, and O_{hX} is the corresponding operator. For example, we have

$$\chi^{AA}_{\mu\nu} \equiv \frac{1}{2}\sum_{\text{spins}}\langle\chi(p'_\chi, s'_\chi)|\bar{\chi}\gamma_\mu\gamma_5\chi(0)|\chi(p_\chi, s_\chi)\rangle\langle\chi(p_\chi, s_\chi)|\bar{\chi}\gamma_\nu\gamma_5\chi(0)|\chi(p'_\chi, s'_\chi)\rangle, \tag{45}$$

or explicitly

$$\chi^{AA}_{\mu\nu} = ((p_\chi + p'_\chi)_\mu(p_\chi + p'_\chi)_\nu - g_{\mu\nu}4m^2_\chi + g_{\mu\nu}q^2 - q_\mu q_\nu)\kappa^2_\chi. \tag{46}$$

Similarly, for $X, Y = A$, V, we have

$$W^{XY}_{\mu\nu} \equiv \frac{1}{2J_\mathcal{N} + 1}\sum_{s,s'}\langle\mathcal{N}(p', s')|j_{Xh,\mu}(0)|\mathcal{N}(p, s)\rangle\langle\mathcal{N}(p, s)|j_{Yh,\nu}(0)|\mathcal{N}(p', s')\rangle, \tag{47}$$

$$W^{SS}_{\mu\nu} \equiv \frac{1}{2J_\mathcal{N} + 1}\sum_{s,s'}\langle\mathcal{N}(p', s')|s_h(0)|\mathcal{N}(p, s)\rangle\langle\mathcal{N}(p, s)|s_h(0)|\mathcal{N}(p', s')\rangle, \tag{48}$$

and so on.

Note that $q^2 = 0$ means $q = 0$ in all frames (see Appendix F). It is simpler to work in the lab frame (the rest frame of $\mathcal{N}$). The matrix elements of scalar, vector, and axial-vector current operators with initial- and final-state nucleus at rest are given by

$$\begin{aligned}
\langle \mathcal{N}(m_\mathcal{N}, s')|s_h(0)|\mathcal{N}(m_\mathcal{N}, s)\rangle &= 2m_\mathcal{N} f_{s\mathcal{N}}\delta_{ss'},\\
\langle \mathcal{N}(m_\mathcal{N}, s')|s'_h(0)|\mathcal{N}(m_\mathcal{N}, s)\rangle &= 2m_\mathcal{N} f'_{s\mathcal{N}}\delta_{ss'},\\
\langle \mathcal{N}(m_\mathcal{N}, s')|j_{Vh,\mu}(0)|\mathcal{N}(m_\mathcal{N}, s)\rangle &= 2g^0_\mu m_\mathcal{N}\delta_{ss'}Q_{V\mathcal{N}},\\
\langle \mathcal{N}(m_\mathcal{N}, s')|j^\mu_{Ah}(0)|\mathcal{N}(m_\mathcal{N}, s)\rangle &= 4g^\mu_i m_\mathcal{N} Q_{A\mathcal{N}}\langle J_\mathcal{N}, s'|(\vec{S}_\mathcal{N})_i|J_\mathcal{N}, s\rangle,
\end{aligned} \tag{49}$$

with

$$\begin{aligned}
Q_{V\mathcal{N}} &= Z(2b^u + b^d) + (A - Z)(2b^d + b^u),\\
Q_{A\mathcal{N}} &= d^q(\Delta^p_q\lambda_p + \Delta^n_q\lambda_n),\\
f^{(')}_{s\mathcal{N}} &= a^{('q)}(Zf_{sp} + (A - Z)f_{sn}),\\
f_{sp(n)} &= \sum_{q=u,d,s}\frac{m_{p(n)}}{m_q}f^{(p(n))}_{Tq} + \sum_{q=c,b,t}\frac{2}{27}\frac{m_{p(n)}}{m_q}\left(1 - \sum_{q'=u,d,s}f^{(p(n))}_{Tq'}\right),\\
\lambda_{p,n} &= \frac{\langle S_{p,n,z}\rangle_{\rm eff}}{J_\mathcal{N}}.
\end{aligned} \tag{50}$$

The derivation of the above formulas are given in Appendix F. Using

$$\begin{aligned}
\chi^{AA,\mu\nu}(q = 0) = \kappa^2_\chi 4(p^\mu_\chi p^\nu_\chi - g^{\mu\nu}m^2_\chi), \qquad \chi^{SS}(q = 0) = 4m^2_\chi,\\
\chi^{AS,\mu} = \chi^{AP,\mu} = \chi^{SP} = 0, \qquad \chi^{PP}(q = 0) = 0,
\end{aligned} \tag{51}$$

with $p_\chi = p'_\chi = (E_\chi, 0, 0, p^3_\chi)$,

$$(p^3_\chi)^2 = \frac{m^2_\chi v^2}{1 - v^2}, \tag{52}$$

in the nucleus rest frame and

$$\begin{aligned}
\sum_{s,s'}\langle J_\mathcal{N}, s'|(\vec{S}_\mathcal{N})_z|J_\mathcal{N}, s\rangle\delta_{ss'} &= 0,\\
\sum_{s,s'}\langle J_\mathcal{N}, s|(\vec{S}_\mathcal{N})_z|J_\mathcal{N}, s'\rangle\langle J_\mathcal{N}, s'|(\vec{S}_\mathcal{N})_z|J_\mathcal{N}, s\rangle &= \frac{1}{3}J_\mathcal{N}(J_\mathcal{N} + 1)(2J_\mathcal{N} + 1),\\
\sum_{s,s'}\langle J_\mathcal{N}, s|(\vec{S}_\mathcal{N})_i|J_\mathcal{N}, s'\rangle\langle J_\mathcal{N}, s'|(\vec{S}_\mathcal{N})_i|J_\mathcal{N}, s\rangle &= J_\mathcal{N}(J_\mathcal{N} + 1)(2J_\mathcal{N} + 1),
\end{aligned} \tag{53}$$

we obtain

$$\bar{\sum}|M_{fi}|^2 = \chi^{AA,\mu\nu}W^{AA}_{\mu\nu} + \chi^{AA,\mu\nu}W^{VV}_{\mu\nu} + \chi^{SS}W^{SS}, \tag{54}$$

where

$$\chi^{AA,\mu\nu}W^{AA}_{\mu\nu} = 64\kappa^2_\chi m^2_\mathcal{N} m^2_\chi\left(1 + \frac{v^2}{3(1 - v^2)}\right)Q^2_{A\mathcal{N}}J_\mathcal{N}(J_\mathcal{N} + 1), \tag{55}$$

$$\chi^{AA,\mu\nu}W^{VV}_{\mu\nu} = 16\kappa^2_\chi m^2_\mathcal{N} m^2_\chi\frac{v^2}{1 - v^2}Q^2_{V\mathcal{N}}, \tag{56}$$

$$\chi^{SS}W^{SS} = 16\kappa^2_\chi m^2_\chi m^2_\mathcal{N} f^2_\mathcal{N}. \tag{57}$$

Consequently, we have

$$\sum\!\!\!\!\!\!- |M_{fi}|^2(q^2=0) = 16 m_{\mathcal{N}}^2 m_\chi^2 \kappa_\chi^2 \left[\left(4+\frac{4v^2}{3(1-v^2)}\right) Q_{A\mathcal{N}}^2 J_{\mathcal{N}}(J_{\mathcal{N}}+1) + \frac{v^2}{1-v^2} Q_{V\mathcal{N}}^2 + f_{s\mathcal{N}}^2\right]. \tag{58}$$

Several comments are in order:

(i) Note that there is no interference between various interaction terms in iM_{fi}.

(ii) In the nucleus rest frame and at $q=0$, the matrix element of the space component of the vector current is vanishing, while the one of the time component of the axial-vector current is also vanishing; see Eq. (F14).

(iii) It seems that the matrix elements of $j_{A\chi\mu}$ and $j_{Vh,\mu}$ are orthogonal and hence the decay amplitude from the $j_{A\chi\mu} j^\mu_{Vh}$ contribution, i.e., $\chi^{AA,\mu\nu} W^{AA}_{\mu\nu}$, is vanishing. This is, however, untrue, since the rest frame of χ is not the rest frame of $\mathcal{N}$. Although the decay amplitude, see Eq. (56), is indeed suppressed by v [$v=\mathcal{O}(10^{-3})$], it is enhanced by $Q_{V\mathcal{N}}$, which contains large factors such as Z and A. The contribution from this term needs to be kept.

Usually, the direct search experiments report the cross section normalized to the interaction with a single nucleon (neutron/proton) since the target materials used in different direct search experiments are not the same. The normalization procedure is shown in Appendix F; we summarize the formulas below. The differential cross section is given by [see Eq. (F67)]

$$\frac{d\sigma_{A_i}}{d|\mathbf{q}|^2} = \frac{1}{4\mu_{A_i}^2 v^2}\left(\sigma_0^{\rm SI} F_{\rm SI}^2(|\mathbf{q}|^2) + \sigma_{0,pp}^{\rm SD} F_{pp}^2(|\mathbf{q}|^2) + \sigma_{0,nn}^{\rm SD} F_{nn}^2(|\mathbf{q}|^2) + \sigma_{0,pn}^{\rm SD} F_{pn}^2(|\mathbf{q}|^2)\right), \tag{59}$$

where

$$\begin{aligned}
\sigma_0^{\rm SI} &= \frac{\mu_{A_i}^2}{\pi}\kappa_\chi^2\left[\frac{v^2}{1-v^2} Q_{VA_i}^2 + f_{sA_i}^2\right],\\
\sigma_{0,pp(nn)}^{\rm SD} &= \frac{\mu_{A_i}^2}{\pi}\kappa_\chi^2\left[\left(4+\frac{4v^2}{3(1-v^2)}\right)\left(\sum d^q \Delta_q^{p(n)}\right)^2 \lambda_{p(n)}^2 J_{A_i}(J_{A_i}+1)\right],\\
\sigma_{0,pn}^{\rm SD} &= \frac{\mu_{A_i}^2}{\pi}\kappa_\chi^2\left[\left(4+\frac{4v^2}{3(1-v^2)}\right) 2\left(\sum d^q d^{q'} \Delta_q^p \Delta_{q'}^n\right)\lambda_p \lambda_n J_{A_i}(J_{A_i}+1)\right].
\end{aligned} \tag{60}$$

Note that in the above formulas the form factors do not depend on a^q, a'^q, b^q, and d^q in Eq. (41). It is better than those usually used in the literature, where d^qs are involved in the form factors. The DM-nucleus scattering cross section is

$$\begin{aligned}
\sigma_{A_i} &= \int d|\mathbf{q}|^2 \frac{d\sigma}{d|\mathbf{q}|^2}\\
&= (\sigma_0^{\rm SI} r_{\rm SI} + \sigma_{0,pp}^{\rm SD} r_{pp} + \sigma_{0,nn}^{\rm SD} r_{nn} + \sigma_{0,pn}^{\rm SD} r_{pn}),
\end{aligned} \tag{61}$$

where

$$r_j \equiv \int_0^{4\mu_{A_i}^2 v^2} \frac{d|\mathbf{q}|^2}{4\mu_{A_i}^2 v^2} F_j^2(|\mathbf{q}|), \tag{62}$$

with $j = {\rm SI}, pp, nn, pn$, and

$$\begin{aligned}
F_{pp(nn)}^2(|\mathbf{q}|) &\equiv \frac{S_{00}(|\mathbf{q}|) + S_{11}(|\mathbf{q}|) \pm S_{01}(|\mathbf{q}|)}{S_{00}(0) + S_{11}(0) \pm S_{01}(0)},\\
F_{pn}^2(|\mathbf{q}|) &\equiv \frac{S_{00}(|\mathbf{q}|) - S_{11}(|\mathbf{q}|)}{S_{00}(0) - S_{11}(0)}.
\end{aligned} \tag{63}$$

Finally, the spin-independent and spin-dependent scaled cross sections are defined as

$$\sigma_N^Z \equiv \frac{\sum_i \eta_i \sigma_{A_i}}{\sum_j \eta_j A_j^2 \frac{\mu_{A_j}^2}{\mu_p^2}} \tag{64}$$

and

$$\sigma_{p,n}^{\rm SD} \equiv \left(\sum_i \eta_i \sigma_{A_i}\right)\left(\sum_j \eta_j \frac{4\mu_{A_j}^2 \langle S_{p,n}\rangle_{\rm eff}^2 (J_{A_j}+1)}{3\mu_{p,n}^2 J_{A_j}}\right)^{-1}, \tag{65}$$

respectively. In this way, the data obtained from different experiments can be compared using σ_N^Z and $\sigma_{p,n}^{\rm SD}$.[4]

III. RESULTS

In parallel with the DM sector of the MSSM [13,28], we analyze the model with $I=1/2$ and $Y=1/2$. In this model, there are 13 parameters in total, five mass

[4]The terminology of spin-(in)dependent cross section is somewhat misleading. There are, in fact, two different normalizations, where both spin-dependent and spin-independent interactions are involved in $\sigma_{p,n}^{\rm SD}$ and σ_N^Z.

parameters $\mu_i (i = 1\text{–}5)$ and eight Yukawa couplings $g_i (i = 3\text{–}10)$, as shown in the mass matrices of neutral as well as single charged WIMPs in Eqs. (A4) and (A8), respectively. In principle, the 13 parameters can be reduced to fewer parameters under different considerations. First of all, let us see what is the minimal particle content which can make up the DM. In this model, the Majorana fermion can be generated purely by the singlet η_3, namely, only the mass parameter μ_2 being nonzero. Because of its quantum number $(2I, -(Y-1/2)) = (1, 0)$, it does not couple to the SM gauge bosons. It also does not couple to the SM Higgs boson since all Yakawa couplings are set to be zeros. Hence, it is inert and impossible to be a WIMP, unless some exotic Higgs boson is introduced [52]. Next, we consider the Majorana fermion generated by the two doublets η_1 and η_2, namely, only the parameter μ_1 being nonzero. Because of their quantum numbers $(2I+1, \mp Y) = (2, \mp 1/2)$, they couple to the SM gauge bosons but still do not couple to the SM Higgs boson. As mentioned previously, they are two degenerate Majorana states $\chi_{1,2} \propto (\eta_1 \pm \eta_2)/\sqrt{2}$ with the same mass μ_1. It results in an oversized DM-nucleus scattering cross section via Z-boson exchange from the $\chi_{1(2)} \to \chi_{2(1)}$ vector current. Nevertheless, the problem can be solved if one can lift the mass degeneracy of $\chi_{1,2}$. Hence, the minimal particle content to make up the DM is to combine these fermion doublets η_1, η_2 and the singlet η_3.

To have an overall understanding of the model, we will consider the following three typical cases: the neutralinolike, the reduced, and the extended cases (see Table II). For the neutralinolike case, only the parameters $\mu_{1\text{–}3}$ and $g_{3\text{–}6}$ are nonzero, and the Majorana DM is generated by $\eta_{1,2,3}$ and the triplet η_5. It contains four neutral Majorana fermions and two single charged fermions. Furthermore, depending on whether the grand unified theory (GUT) relation ($\mu_2 = \frac{5}{3}\mu_3 \tan^2\theta_W$) [53] or the $\tan\beta$ relation (note that $g_3 v = \sqrt{2} m_Z \cos\beta \sin\theta_W$, $g_4 v = \sqrt{2} m_Z \sin\beta \sin\theta_W$, $g_5 v = \sqrt{2} m_Z \cos\beta \cos\theta_W$, and $g_6 v = \sqrt{2} m_Z \sin\beta \cos\theta_W$) is imposed or not, we classify the neutralinolike case into four subcases: the neutralinolike I case with the GUT relation and $\tan\beta = 2$, the neutralinolike II case with the GUT relation and $\tan\beta = 20$, the neutralinolike III without the GUT relation but with $\tan\beta = 2$, and the neutralinolike IV case without the GUT and the $\tan\beta$ relations.

For the reduced case, only the parameters μ_1, μ_2, g_3, and g_4 are free with the minimal particle content (i.e., $\eta_{1,2,3}$). It contains three neutral Majorana fermions and one single charged fermion. For the extended case, all of the 13 model parameters are free with the maximal particle content (i.e., all η fields), and it contains six neutral Majorana fermions and four single charged fermions. In each case, we generate 10,000 random samples and survey the DM mass m_χ in the range of 1–2500 GeV by random sampling the mass couplings $\mu_i (i = 1\text{–}5)$ linearly in the range of 0–8000 GeV and the Yukawa coupling $g_i (i = 3\text{–}10)$ linearly in the range of 0–1 if these parameters are active.

For each sample, we numerically solve the mass eigenstates and eigenvalues, find the freeze-out temperature parameter x_f [see Eq. (36)], and obtain the DM thermal relic density $\Omega_\chi h^2$ via the calculations of DM annihilation processes $\chi\chi \to W^+W^-, ZZ, ZH, HH, f\bar{f}$ to compare with the observed relic density. We calculate the normalized SI and SD elastic cross sections ($\sigma_N^{\rm SI}$, $\sigma_n^{\rm SD}$, and $\sigma_p^{\rm SD}$) of DM scattering off ^{129,131}Xe nuclei to compare with the results of direct search experiments of LUX SI and XENON100 SD elastic cross sections of DM scattering off ^{129,131}Xe nuclei, respectively. We also calculate $\sigma_p^{\rm SD}$ for DM scattering off CF_{3I} nuclei to compare with the result of the PICO-60 experiment using CF_{3I} as a material target.

In the calculation of $\sigma_N^{\rm SI}$, we adopt the exponential form factor [13,24,25] for $F_{\rm SI}(|\mathbf{q}|)$, and we use the data in Ref. [54] for the nucleon parameters $f_{Tq}^{(p,n)}$ in Eq. (50). In calculation of $\sigma_{n,p}^{\rm SD}$, we adopt the structure factors $S_{00,01,11}(|\mathbf{q}|)$ for the ^{129,131}Xe nucleus in Ref. [55] and ^{19}F and ^{127}I (by Bonn A calculation) nuclei in Ref. [56] and use the experimental data in Refs. [54,57] for the quark spin component in a nucleon $\Delta_q^{p,n}$. For ^{129,131}Xe nuclei, we use the nuclear total angular momentum J and the predicted spin expectation values $\langle S_{p,n}\rangle$ in the calculation by Menendes *et al.* in Refs. [20,55] for $\langle S_{p,n,z}\rangle_{\rm eff}$ and the isotope abundance of ^{129,131}Xe in Refs. [20] for η_i. For ^{19}F and ^{127}I nuclei, we use the nuclear total angular momentum and the predicted spin expectation values in Refs. [58]. For simplicity, we only consider the case in which the second-lightest neutral particle χ_2 is dynamically forbidden to be produced from the $\chi_1 + {}^{129}\text{Xe} \to \chi_2 + {}^{129}\text{Xe}$ inelastic scattering process.

For the indirect search, we calculate the present velocity averaged cross section $\langle\sigma(\chi\chi \to W^+W^-, ZZ, ZH, HH, f\bar{f})v\rangle$ to compare with the Fermi-LAT results which provide six

TABLE II. Summary of three typical cases.

		Case A		Case B	Case C
Neutralinolike I	Neutralinolike II	Neutralinolike III	Neutralinolike IV	Reduced	Extended
GUT $\tan\beta = 2$	GUT $\tan\beta = 20$	No GUT $\tan\beta = 2$	No GUT		
$\eta_{1\text{–}3,5}$	$\eta_{1\text{–}3,5}$	$\eta_{1\text{–}3,5}$	$\eta_{1\text{–}3,5}$	$\eta_{1\text{–}3}$	$\eta_{1\text{–}3,5,7\text{–}10}$

TABLE III. Particle attribute distribution of sample sets.

	Case A				Case B	Case C
Percentage (%)	Neutralinolike I	Neutralinolike II	Neutralinolike III	Neutralinolike IV	Reduced	Extended
Higgsino-like ($\sim\eta_{1,2}$)	29	28	33	31	50	29
Binolike ($\sim\eta_3$)	71	72	33	34	49	34
Winolike ($\sim\eta_5$)	0	0	33	34	0	31
Non-neutralino-like ($\sim\eta_{9,10}$)	0	0	0	0	0	5
mixed	0.4	0.3	0.6	1.2	0.8	1.3

upper limits on $\langle\sigma(\chi\chi \to W^+W^-, b\bar{b}, u\bar{u}, \tau^+\tau^-, \mu^+\mu^-, e^+e^-)v\rangle$ from a combined analysis of 15 dSphs in an indirect search [23]. We know that the DM halo is immersed in the Galaxy. The speed of the Sun moving around the Galactic center is about 220 km/s at the local distance $r \approx 8.5$ kpc, and the Galactic circular rotation speed is about 230 km/s at radii $\approx$100 kpc [13,59]. On the other hand, the shortest and longest distances of these 15 dSphs from the Sun are $\approx$23 and 233 kpc, respectively [23]. Hence, we will use a typical DM velocity $v \simeq$ 300 km/s in the indirect-detection calculation.

Finally, we collect all allowed samples which satisfy all these 11 constraints, namely, one from the observed value of DM relic density; four from the direct detection of LUX, XENON100, and PICO-60 experiments; and six from the indirect detection of Fermi-LAT observations such that we can find the lower bound of DM mass with different particle attributes, the allowed range of the model parameters, and the coupling strengths in this model.

Before showing our results, we first define the different particle attributes, namely, Higgsino-, bino-, wino-, and non-neutralino-like particles if the main ingredient (composition fraction) $\geq$60% of a sample is in the state of $\eta_{1,2}$, η_3, η_5, and $\eta_{9,10}$ and is denoted by $\tilde{H}$-, $\tilde{B}$-, $\tilde{W}$-, and non-neutralino-like $\tilde{X}$ particles, respectively; otherwise, we call it a mixed particle. Let us first show the sample structures from six sample sets in Table III. We see that less than 1.3% of the samples is the mixed particles which can be ignored in each case. For the cases of neutralinolike I and II, the population ratio of $\tilde{H}$-like to $\tilde{B}$-like particles is roughly about 3 to 7. Because of the GUT relation, the $\tilde{W}$-like particles do not appear in these two cases. For the cases of neutralinolike III and IV, now without the GUT relation, plenty of $\tilde{W}$-like particles come out. In these two cases, $\tilde{H}$-, $\tilde{B}$-, and $\tilde{W}$-like particles are roughly equally distributed. For the reduced case, it is about 50/50 equally distributed for $\tilde{H}$- and $\tilde{B}$-like particles. For the extended case, it contains about 5% non-neutralino-like $\tilde{X}$ particles and is roughly equally distributed for $\tilde{H}$-, $\tilde{B}$-, and $\tilde{W}$-like particles. In the subsequent descriptions, we will use open circle, times, triangle, filled square, and filled circle to denote the Higgsino-, bino-, wino-, and non-neutralino-like and the mixed particles, respectively. The contour plot of the DM mass and composition in the μ_1-μ_3 plane for the neutralinolike case I is shown in Fig. 2. Note that the contour plot of the neutralino mass and composition in the MSSM [13] is successfully reproduced in Fig 2. Hence, the fermion multiplets η_1, η_2, η_3, and η_5 correspond to two doublets of Higgsinos, a singlet of bino, and a triplet of winos in the MSSM, respectively [recall Eq. (21)]. Nevertheless, the model does not contain particles corresponding to the sfermions and the second Higgs doublet in MSSM so that there does not exist the annihilation channels into the extra scalar states and scattering diagrams mediated by the extra scalars. On the other hand, the model does contain more Z_2-odd fermion particles with multiplets η_7, η_8, η_9, and η_{10}. Hence, this generic Majorana DM model is still quite different from the MSSM.

A. Case A: Neutralinolike cases

Both the neutralinolike I and II cases contain seven parameters, μ_{1-3}, g_{3-6}, which are subjected to the GUT and

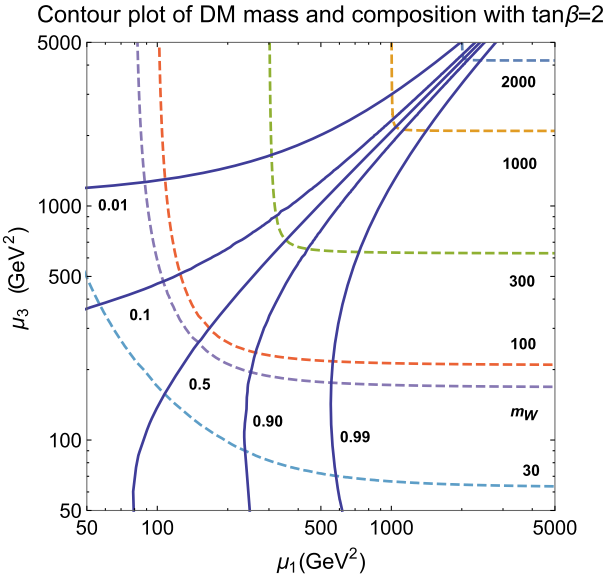

FIG. 2. Contour plot of the DM mass and composition in the μ_1-μ_3 plane for the neutralinolike I case. The broken curves are contours of DM mass m_χ, and the solid curves are contours of gauginolike (η_3^0 or η_5^0) fraction. Here, the GUT relation $\mu_2 = \frac{5}{3}\mu_3 \tan^2\theta_W$ has been used.

the $\tan\beta$ relations resulting in only two free parameters μ_1 and μ_2 (or μ_3). The neutralinolike III case is only subjected to the $\tan\beta$ relation resulting in three free parameters μ_{1-3}. Without the GUT and the $\tan\beta$ relations, all of these seven parameters in the neutralinolike IV case are free. We first emphasize on the description of the interplay among these constraints with the case of neutralinolike I using Figs. 3–5 and then tell the differences among these neutralinolike

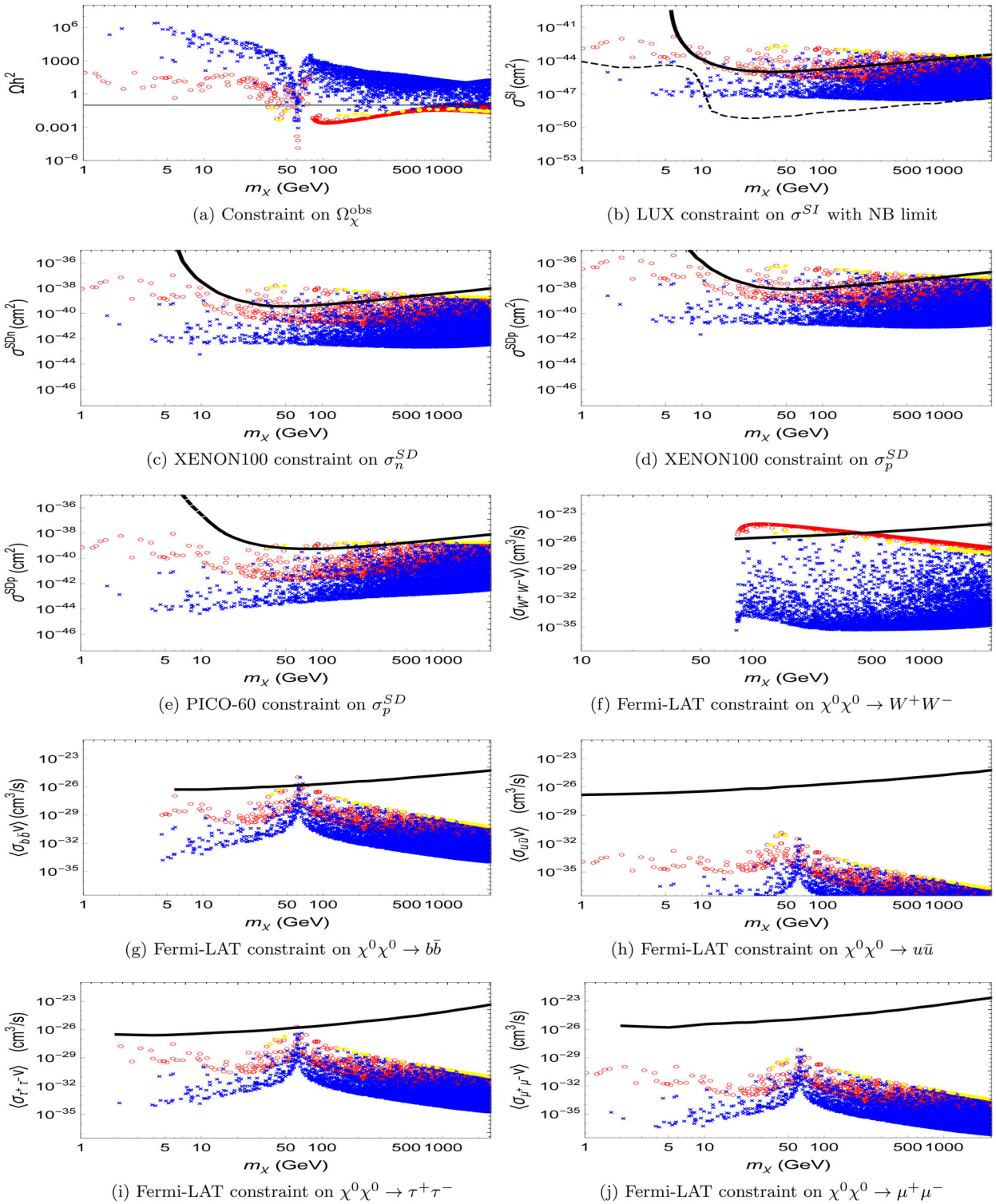

(a) Constraint on $\Omega_\chi^{\rm obs}$

(b) LUX constraint on σ^{SI} with NB limit

(c) XENON100 constraint on σ_n^{SD}

(d) XENON100 constraint on σ_p^{SD}

(e) PICO-60 constraint on σ_p^{SD}

(f) Fermi-LAT constraint on $\chi^0\chi^0 \to W^+W^-$

(g) Fermi-LAT constraint on $\chi^0\chi^0 \to b\bar{b}$

(h) Fermi-LAT constraint on $\chi^0\chi^0 \to u\bar{u}$

(i) Fermi-LAT constraint on $\chi^0\chi^0 \to \tau^+\tau^-$

(j) Fermi-LAT constraint on $\chi^0\chi^0 \to \mu^+\mu^-$

FIG. 3. Results for all samples with constraints in the case of neutralinolike I [open circle: Higgsino-like, times: binolike, filled circle: mixed].

cases in this subsection. The reduced case and the extended case are discussed in the next two subsections. For neutralinolike I case, we show the scatter plot of $\Omega_\chi h^2$ vs m_χ in Fig. 3(a). The horizontal line denotes the upper limit using the upper 3σ value of the observed relic density $\Omega_\chi h^2 = 0.1198 \pm 0.0026$. The samples sitting above the horizontal line are ruled out. We see that most of the $\tilde{B}$-like particles are ruled out, while the $\tilde{H}$-like particles tending to have smaller values in relic density with $m_\chi > M_W$ are safe. The $\Omega_\chi^{\rm obs} h^2$ constraint is the most stringent constraint since about 74% of samples is ruled out by this constraint. The results of DM-nucleon elastic scattering cross sections compared to the LUX $\sigma_N^{\rm SI}$, the XENON100 $\sigma_{n,p}^{\rm SD}$, and the PICO-60 $\sigma_p^{\rm SD}$ constraints are shown in Figs. 3(b)–3(e), respectively. Since the LUX constraint on $\sigma^{\rm SI}$ is the most stringent one among these four constraints, we should concentrate on Fig. 3(b). We find that the mixed and the $\tilde{H}$-like particles tend to have larger values in the DM-nucleon elastic scattering cross section, while the $\tilde{B}$-like particles tend to have smaller values. The samples sitting below the upper limit of the LUX SI-experiment [19] (solid curve) and above the line of the neutrino background (dashed curve) are allowed. We see that most of mixed particles, part of the $\tilde{H}$-like particles, and a few of $\tilde{B}$-like particles are ruled out by the LUX constraint so that about 96% of the samples is safe. However, most $\tilde{B}$-like particles sitting between these two lines [see Fig. 3(b)] have been ruled out by the $\Omega_\chi^{\rm obs} h^2$ constraint [see Fig. 3(a)], and hence only 23% of the samples survives. Furthermore, nearly 99% of the survived samples is $\tilde{H}$-like. It shows that the DM relic density and the direct search constraints are complementary to each other.

To compare with the Fermi-LAT constraints, we show the scatter plots of $\langle\sigma(\chi\chi \to W^+W^-, b\bar{b}, u\bar{u}, \tau^+\tau^-, \mu^+\mu^-)v\rangle$ vs m_χ in Figs. 3(f)–3(j), respectively. We do not show the plot of $\langle\sigma(\chi\chi \to e^+e^-)v\rangle$ since it is highly helicity suppressed as mentioned in Sec. II. B. The samples sitting above the Fermi-LAT constraints are ruled out. For the W^+W^- channel [see Fig. 3(f)], a $\tilde{B}$-like DM pair does not contribute to the s-wave amplitude (also mentioned in Sec. II. B) so that all values of $\langle\sigma_{\rm ann} v\rangle$ for the $\tilde{B}$-like particles are less than those values for the $\tilde{H}$-like and the mixed particles. We also see that part of the $\tilde{H}$-like and the mixed particles are ruled out by this constraint so that about 94% of samples is safe under this constraint. However, most $\tilde{B}$-like particles sitting below the limit are ruled out by the $\Omega_\chi^{\rm obs} h^2$ constraint, and hence only about 20% of the samples survives. In Figs. 3(f)–3(j), we see that, in general, the $\tilde{B}$-like particles tend to have smaller $\langle\sigma_{\rm ann} v\rangle$, while the $\tilde{H}$-like and the mixed particles tend to have larger $\langle\sigma_{\rm ann} v\rangle$. Note that all the DM particles annihilating into $f\bar{f}$ with the final fermion mass less than M_W have the similar resonance shapes with peaks at $m_\chi = m_Z/2$ and $m_H/2$. For $b\bar{b}$ and $\tau^+\tau^-$ channels, only a few DM candidates are ruled out by these two constraints, and for other channels, the constraints become less important when the final fermion mass is less than m_τ. Besides, we also give the scatter plots of velocity averaged cross sections $\langle\sigma(\chi\chi \to ZZ, HZ, t\bar{t}, HH)v\rangle$ vs m_χ in Fig. 4. Similar to the case of the W^+W^- channel, the $\tilde{B}$-like particles do not contribute

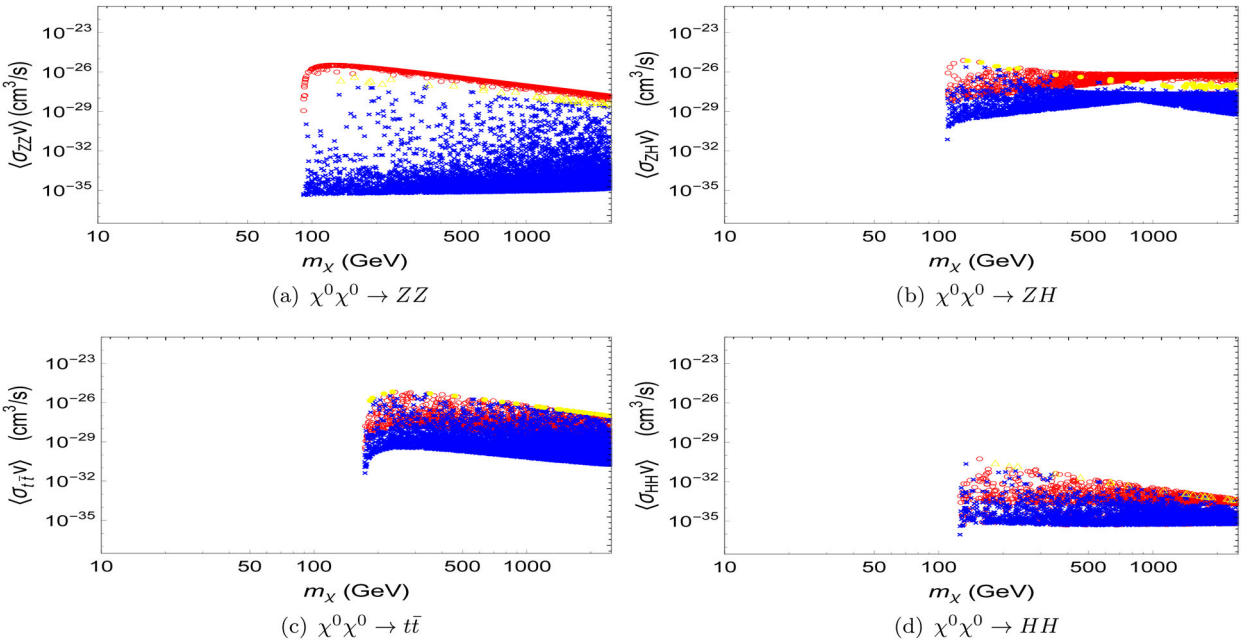

(a) $\chi^0\chi^0 \to ZZ$ (b) $\chi^0\chi^0 \to ZH$

(c) $\chi^0\chi^0 \to t\bar{t}$ (d) $\chi^0\chi^0 \to HH$

FIG. 4. Scatter plots of $\langle\sigma_{ZZ,ZH,t\bar{t},HH}v\rangle$ vs m_χ in the case of neutralinolike I [open circle: Higgsino-like, times: binolike, filled circle: mixed].

to the s-wave amplitude in the ZZ channel (mentioned in Sec. II. B) so that all the values of $\langle\sigma_{\rm ann}v\rangle$ for the $\tilde{B}$-like particles are less than those values for the $\tilde{H}$-like particles in the ZZ channel [see Fig. 4(a)]. In addition, the process $\chi\chi \to HH$ can only proceed from the p wave. It results in the fact that almost all values of $\langle\sigma_{\rm ann}v\rangle$ in the HH channel are less than those values in the ZZ, ZH, and $t\bar{t}$ channels [see Figs. 4(a)–(4d)]. Recall that the relic density is

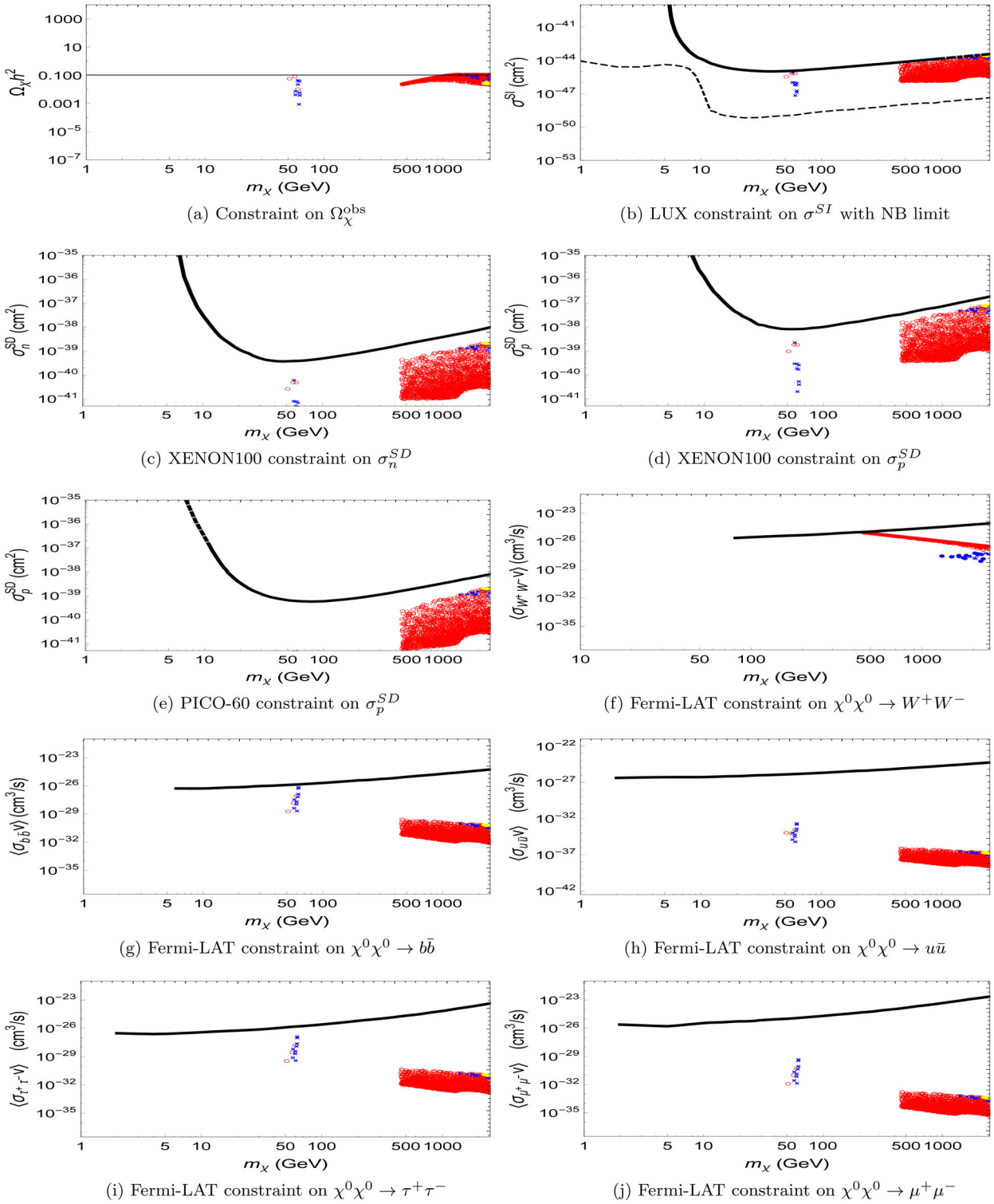

(a) Constraint on $\Omega_\chi^{\rm obs}$

(b) LUX constraint on σ^{SI} with NB limit

(c) XENON100 constraint on σ_n^{SD}

(d) XENON100 constraint on σ_p^{SD}

(e) PICO-60 constraint on σ_p^{SD}

(f) Fermi-LAT constraint on $\chi^0\chi^0 \to W^+W^-$

(g) Fermi-LAT constraint on $\chi^0\chi^0 \to b\bar{b}$

(h) Fermi-LAT constraint on $\chi^0\chi^0 \to u\bar{u}$

(i) Fermi-LAT constraint on $\chi^0\chi^0 \to \tau^+\tau^-$

(j) Fermi-LAT constraint on $\chi^0\chi^0 \to \mu^+\mu^-$

FIG. 5. Results for allowed samples satisfying all constraints in the neutralinolike I case [open circle: Higgsino-like, times: binolike, filled circle: mixed].

proportional to the inverse of $\langle\sigma_{\rm ann}v\rangle$, while $\langle\sigma_{\rm ann}v\rangle$ is dominated by the W^+W^- channel for $m_\chi > M_W$ and the $b\bar{b}$ channel for $m_\chi < M_W$. Therefore, the shape of the relic density in Fig. 3(a) can be easily understood from Figs. 3(f) and 3(g). The interplay of different observables are useful and instructive.

In Fig. 5, we redraw Fig. 3 only with the allowed samples which satisfy all the constraints. These plots are the predictions of the neutralinolike I case. We will also redraw the plots of Fig. 4 only with allowed samples later. We find that the direct detection of the SI cross section from DM scattering off nuclei and the indirect detection of the velocity averaged cross section from DM annihilating to W^+W^- are two more sensitive constraints as the allowed regions touch the corresponding upper limits. It means that they are more accessible for DM searches in the near future. Now, it is interesting to see how these constraints shape the allowed range of DM mass for a given particle attribute. In the following discussion, we will ignore the outlier samples with DM mass near the peaks, namely, $m_\chi \simeq M_Z/2$ and $M_H/2$ in Fig. 5. For the $\tilde{B}$-like particles, about 99% of them is ruled out by the DM relic density constraint. The LUX $\sigma_N^{\rm SI}$ constraint is complementary to the relic density constraint such that only the $\tilde{B}$-like particles with $m_\chi \gtrsim 1411$ GeV could be DM candidates [see Fig. 3(b)]. All of the $\tilde{H}$-like particles with mass $m_\chi \lesssim M_W$ GeV are ruled out by the DM relic density constraint, followed by the

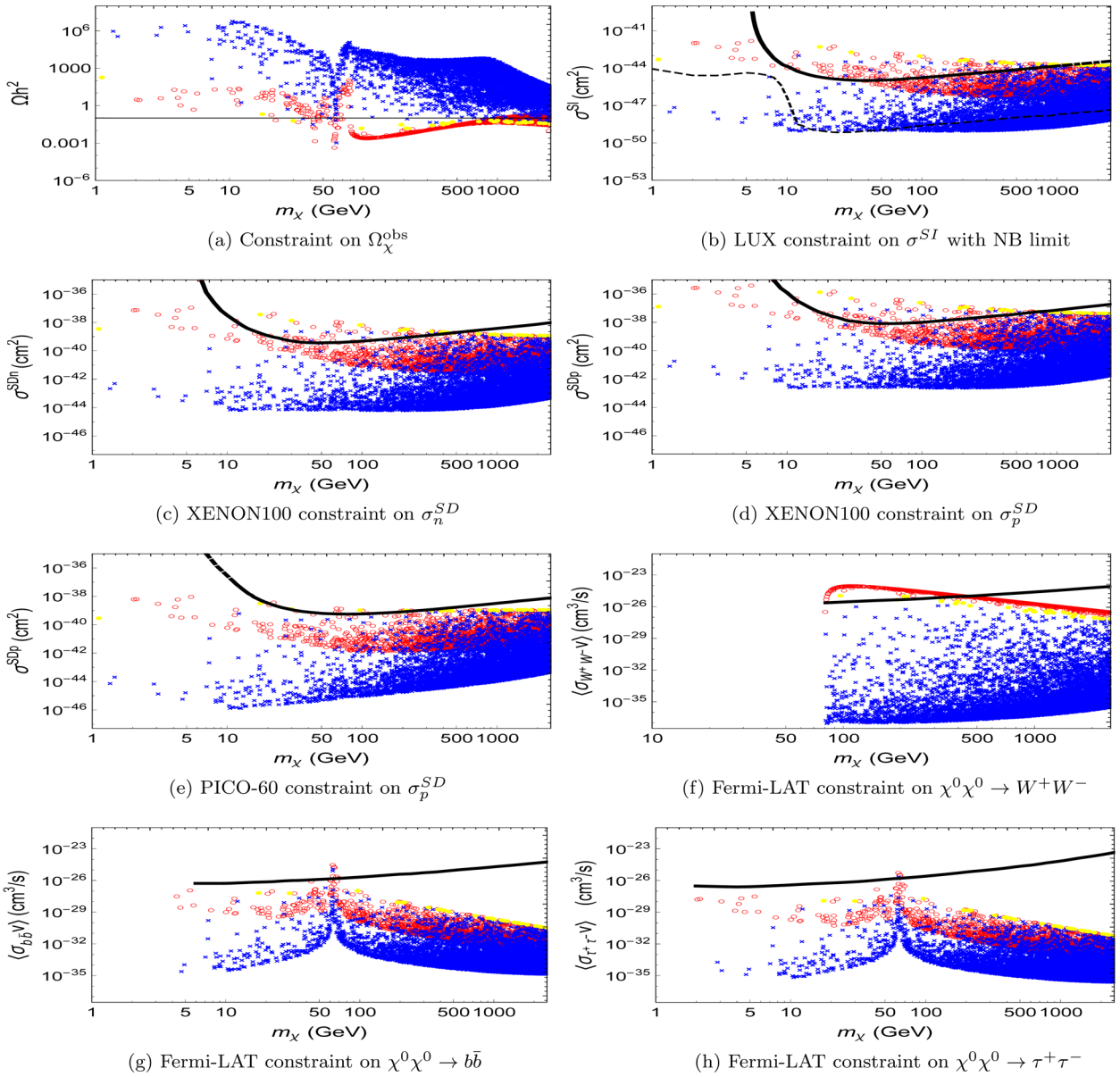

(a) Constraint on $\Omega_\chi^{\rm obs}$

(b) LUX constraint on σ^{SI} with NB limit

(c) XENON100 constraint on σ_n^{SD}

(d) XENON100 constraint on σ_p^{SD}

(e) PICO-60 constraint on σ_p^{SD}

(f) Fermi-LAT constraint on $\chi^0\chi^0 \to W^+W^-$

(g) Fermi-LAT constraint on $\chi^0\chi^0 \to b\bar{b}$

(h) Fermi-LAT constraint on $\chi^0\chi^0 \to \tau^+\tau^-$

FIG. 6. Results for all samples with constraints in the neutralinolike II case [open circle: Higgsino-like, times: binolike, filled circle: mixed].

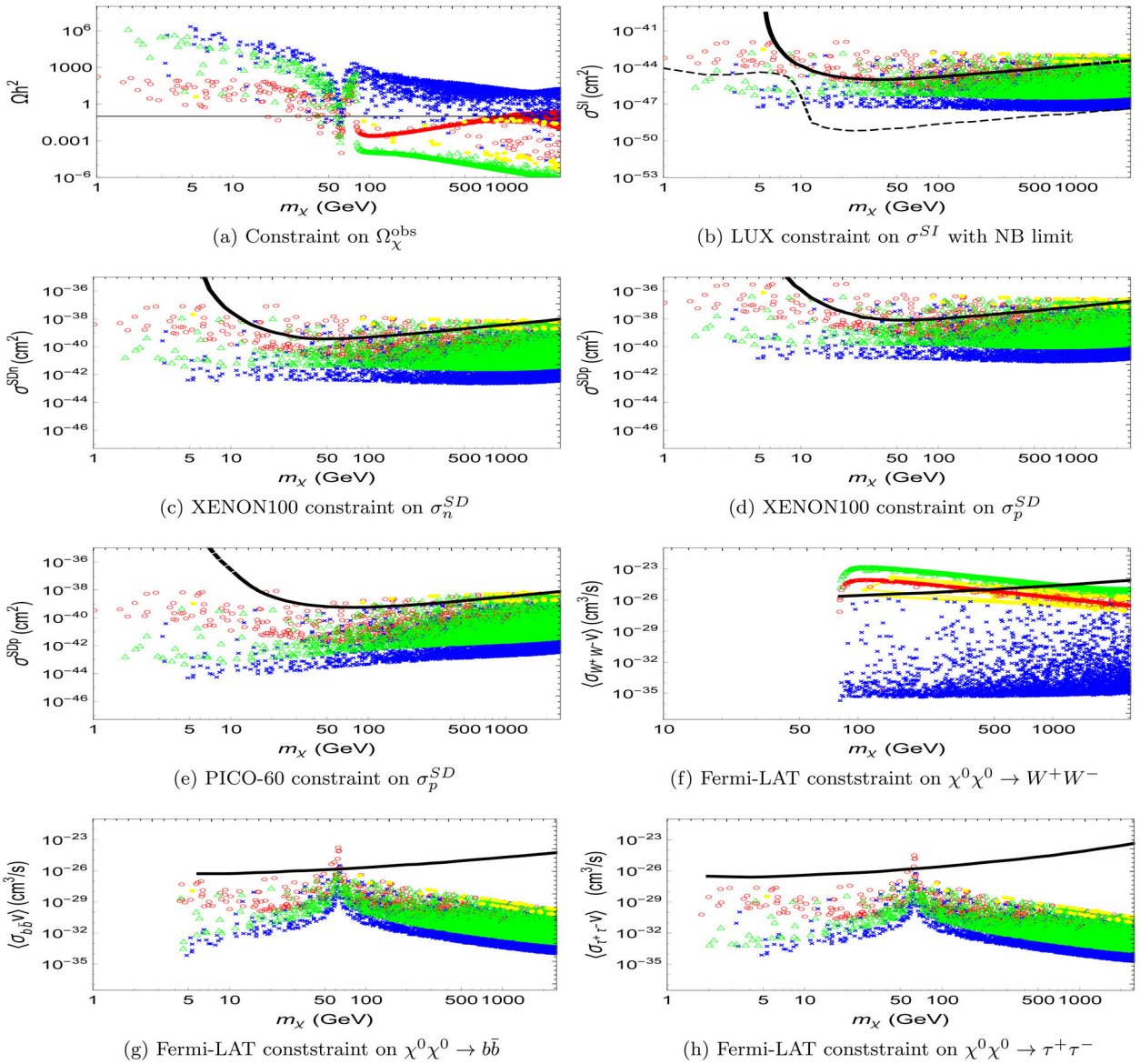

(a) Constraint on $\Omega_\chi^{\rm obs}$

(b) LUX constraint on σ^{SI} with NB limit

(c) XENON100 constraint on σ_n^{SD}

(d) XENON100 constraint on σ_p^{SD}

(e) PICO-60 constraint on σ_p^{SD}

(f) Fermi-LAT conststraint on $\chi^0\chi^0 \to W^+W^-$

(g) Fermi-LAT conststraint on $\chi^0\chi^0 \to b\bar{b}$

(h) Fermi-LAT conststraint on $\chi^0\chi^0 \to \tau^+\tau^-$

FIG. 7. Results for all samples with constraints in the case of neutralinolike III [open circle: Higgsino-like, times: binolike, triangle: winolike, filled circle: mixed].

Fermi-LAT $\langle(\sigma(\chi\chi \to b\bar{b})v\rangle$ constraint around $m_\chi \sim M_W$. All the $\tilde{H}$-like particles with $m_\chi > M_W$ are not ruled out by the observed relic density [see Fig. 3(a)], and all the $\tilde{H}$-like particles with $M_W < m_\chi \lesssim 456$ GeV are ruled out by Fermi-LAT $\langle(\sigma(\chi\chi \to W^+W^-)v\rangle$ constraint [see Fig. 3(f)], while $\tilde{H}$-like particles with $m_\chi \gtrsim 456$ GeV are still subject to the LUX $\sigma_N^{\rm SI}$ constraint. Therefore, without considering the outliers, the allowed mass regions for the $\tilde{B}$-like and the $\tilde{H}$-like particles in Fig. 5 can be understood.

After explaining the interplay among these constraints in the case of neutralinolike I, now we turn to see the differences among these neutralinolike cases. The results of other three cases with all samples are shown in Figs. 6–8. In these figures, we do not show the highly helicity suppressed plots of $\langle\sigma_{u\bar{u}}v\rangle$, $\langle\sigma_{\mu^+\mu^-}v\rangle$, and $\langle\sigma_{e^+e^-}v\rangle$. First of all, the $\tilde{W}$-like particles do not appear in the cases of neutralinolike I and II with different $\tan\beta$ values (see Figs. 3 and 6). It is highly unlikely to generate the $\tilde{W}$-like particles with the GUT relation.[5] In contrast, without the GUT relation, plenty of $\tilde{W}$-like particles can be generated as in the cases of neutralinolike III and IV (see Figs. 7 and 8). For the neutralinolike III case with a fixed $\tan\beta$, the $\tilde{W}$-like particles tend to have smaller values in $\Omega_\chi h^2$ and larger values in the cross section of DM scattering off nuclei and in the velocity averaged cross

[5]It does not mean that the $\tilde{W}$ component is vanishing, but it is not the dominant composition of DM particles in these cases.

section of DM annihilation to the SM particles than the $\tilde{B}$-like particles (see Fig. 7). For the neutralinolike IV case without fixing $\tan\beta$, only the $\tilde{W}$-like particles with $m_\chi \gtrsim M_W$ have smaller values in $\Omega_\chi h^2$ and greater values in $\langle\sigma_{W^+W^-}v\rangle$ than the $\tilde{B}$-like particles (see Fig. 8). It originates from the fact that a $\tilde{B}$-like DM pair does not contribute to the s-wave amplitude.

Among the neutralinolike cases, we see that either "a higher $\tan\beta$ value" (neutralinolike II, Fig. 6) or "without the GUT relation" (neutralinolike-III, IV, Figs. 7 and 8) gives a wider spread in each scatter plot as comparing to Fig. 3. With the DM relic constraint, 99%, 99%, 98%, and 60% of $\tilde{B}$-like particles are ruled out in the neutralinolike I–IV cases, respectively. After considering all constraints, less than 1% of $\tilde{B}$-like particles could be DM candidates for the cases of neutralinolike I–III. However, for the neutralinolike IV case, without the GUT and the $\tan\beta$ relations, it has the widest spread in each scatter plot among the neutralinolike cases so that up to 23% of $\tilde{B}$-like particles could be DM candidates. A closer look reveals that in the latter case more $\tilde{B}$-like particles have lower values in DM relic density [see Fig. 8(a)]. Therefore, more $\tilde{B}$-like particles are allowed in the neutralinolike IV case. On the other hand, with the LUX $\sigma_N^{\rm SI}$ constraint, 79%, 67%, 61%, and 51% of $\tilde{H}$-like particles survive in the neutralinolike I–IV cases, respectively [see Figs. 3, 6, 7, and 8(a)]. It means that in the case of either a

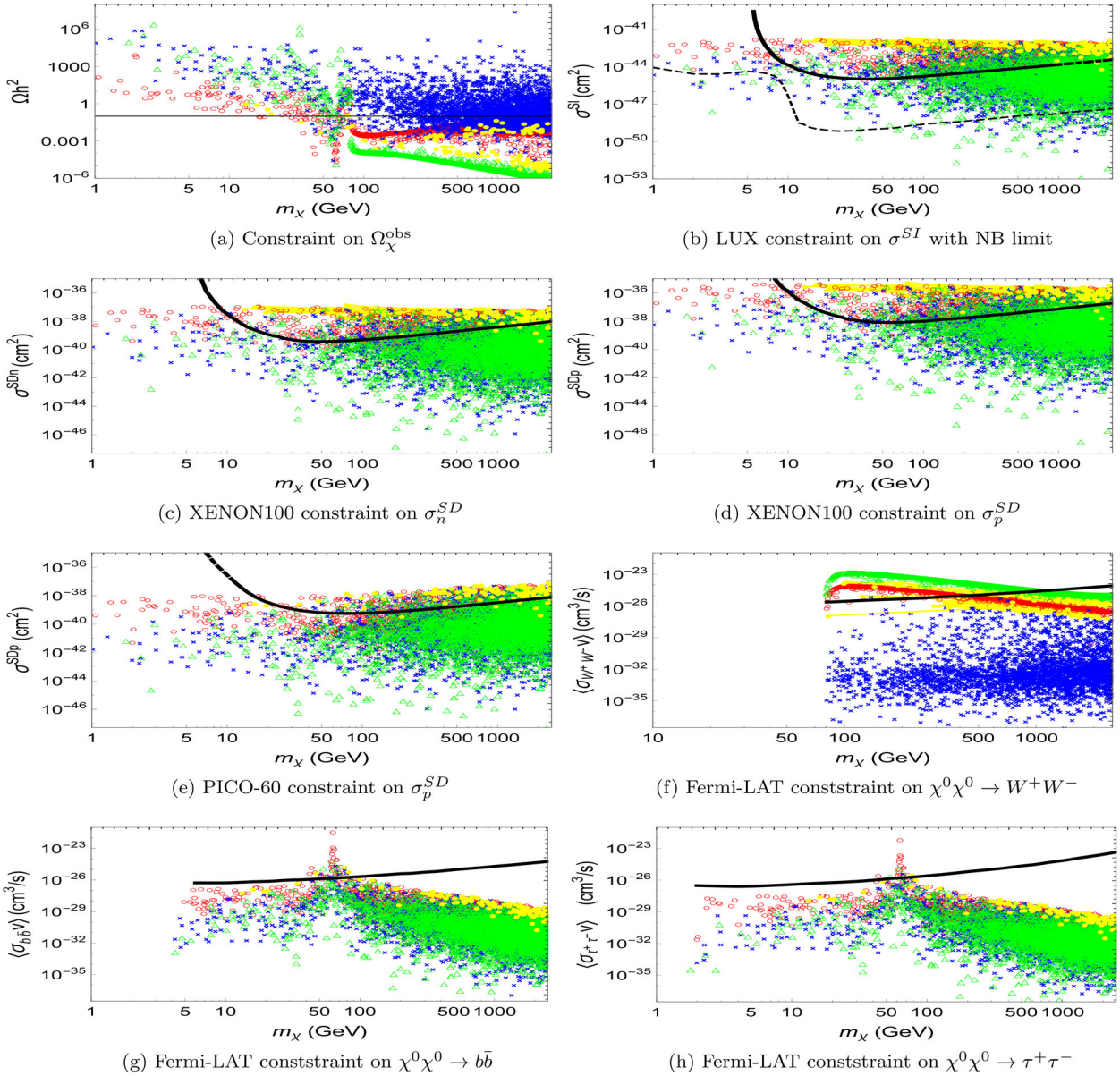

(a) Constraint on $\Omega_\chi^{\rm obs}$

(b) LUX constraint on σ^{SI} with NB limit

(c) XENON100 constraint on σ_n^{SD}

(d) XENON100 constraint on σ_p^{SD}

(e) PICO-60 constraint on σ_p^{SD}

(f) Fermi-LAT conststraint on $\chi^0\chi^0 \to W^+W^-$

(g) Fermi-LAT conststraint on $\chi^0\chi^0 \to b\bar{b}$

(h) Fermi-LAT conststraint on $\chi^0\chi^0 \to \tau^+\tau^-$

FIG. 8. Results for all samples with constraints in the case of neutralinolike IV [open circle: Higgsino-like, times: binolike, triangle: winolike, filled circle: mixed].

higher $\tan\beta$ or without the GUT relation more $\tilde{H}$-like particles spread toward larger values in $\sigma_N^{\rm SI}$; namely, fewer $\tilde{H}$-like particles (relative to neutralinolike I) can be allowed. After considering all constraints, 63%, 49%, 45%, and 46% of $\tilde{H}$-like particles are allowed in the neutralinolike I–IV cases, respectively. As for the mixed particles, it can be ignored since less than 0.1% of samples is allowed as the DM candidates in the neutralinolike cases.

The $\tilde{W}$-like particles can only appear in the cases without the GUT relation (neutralinolike III and IV; see Figs. 7 and 8). All the $\tilde{W}$-like particles with $m_\chi < M_W$ are ruled out mainly by the DM relic density constraint [see Figs. 7(a) and 8(a)], followed by the Fermi-LAT constraint via the DM annihilation to the $b\bar{b}$ channel around m_χ–M_W [see Figs. 7(g) and 8(g)]. All the $\tilde{W}$-like particles with $m_\chi > M_W$ are not ruled out by the observed relic density [see Figs. 7(a) and 8(a)], and all the $\tilde{W}$-like particles with $M_W < m_\chi \lesssim 1$ TeV are ruled out by the Fermi-LAT constraint via the DM annihilation to the W^+W^- channel [see Figs. 7(f) and 8(f)]. The remaining $\tilde{W}$-like particles with $m_\chi \gtrsim 1$ TeV are still subjected to the LUX, XENON100, and PICO-60 constraints [see Figs. 7(b)–7(e) and 8(b)–8(e)]. It results in about 45% and 39% of $\tilde{W}$-like particles being allowed to be DM candidates in the neutralinolike III and IV cases, respectively, and the allowed $\tilde{W}$-like particles are heavy ($m_\chi \gtrsim 1$ TeV).

In Figs. 9–11, we redraw Figs. 6–8 with the allowed samples, respectively. As in the case of neutralinolike I, we

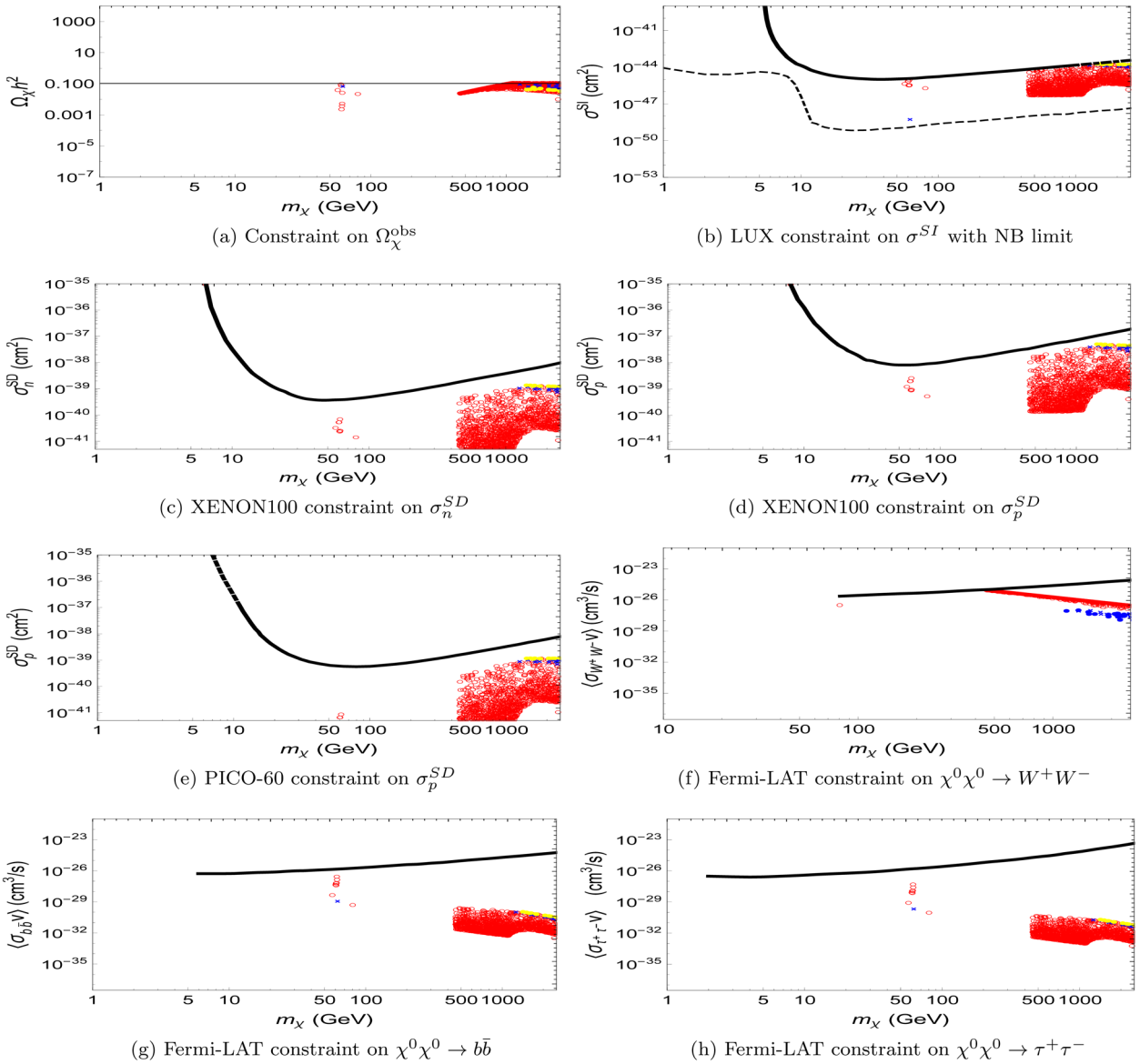

(a) Constraint on $\Omega_\chi^{\rm obs}$

(b) LUX constraint on σ^{SI} with NB limit

(c) XENON100 constraint on σ_n^{SD}

(d) XENON100 constraint on σ_p^{SD}

(e) PICO-60 constraint on σ_p^{SD}

(f) Fermi-LAT constraint on $\chi^0\chi^0 \to W^+W^-$

(g) Fermi-LAT constraint on $\chi^0\chi^0 \to b\bar{b}$

(h) Fermi-LAT constraint on $\chi^0\chi^0 \to \tau^+\tau^-$

FIG. 9. Results for allowed samples satisfying all constraints in the neutralinolike II case [open circle: Higgsino-like, times: binolike, filled circle: mixed].

still see that the direct detection of $\sigma_N^{\rm SI}$ and the indirect detection of $\langle\sigma(\chi\chi \to W^+W^-)v\rangle$ will be more accessible for DM searches in the near future. Hence, we focus on these two and the relic density plots in these figures. Note that in the following discussion we jump over the allowed outlier samples.

We see that most of $\tilde{B}$-like particles are ruled out by the $\Omega_\chi h^2$ constraint [see Figs. 6(a), 7(a), and 8(a)], followed by its complementary constraint of $\sigma_N^{\rm SI}$ [see Figs. 6(b), 7(b), and 8(b)]. With the GUT relation, the cases of neutralinolike I ($\tan\beta = 2$) and neutralinolike II ($\tan\beta = 20$) have similar results, where only the $\tilde{B}$-like particle with $m_\chi \gtrsim 1411$, 1258 GeV could be DM candidates, respectively (see Figs. 5 and 9). Without the GUT relation, the mass of the allowed $\tilde{B}$-like particle can lower down with $m_\chi \gtrsim 341$, 288 GeV in the cases of neutralinolike III and IV, respectively (see Figs. 10 and 11). Less than 0.3%, 0.3%, and 0.9% of the $\tilde{B}$-like samples are allowed in the cases of neutralinolike I, II, and III, respectively. Without the GUT relation, the allowed $\tilde{B}$-like samples become sparse in the neutralinolike III case. Note that the allowed $\tilde{B}$-like particles only attach to the LUX limit; in other words, the LUX limit is an active constraint, and consequently only the experiments of SI DM-nucleus scattering are accessible to the DM searches in the near future.

The $\tilde{H}$- and $\tilde{W}$-like particles with $m_\chi \lesssim M_W$ are ruled out by the $\Omega_\chi h^2$ constraint [see Figs. 6(a), 7(a), and 8(a)], followed by the $\langle\sigma(\chi\chi \to b\bar{b})v\rangle$ constraint

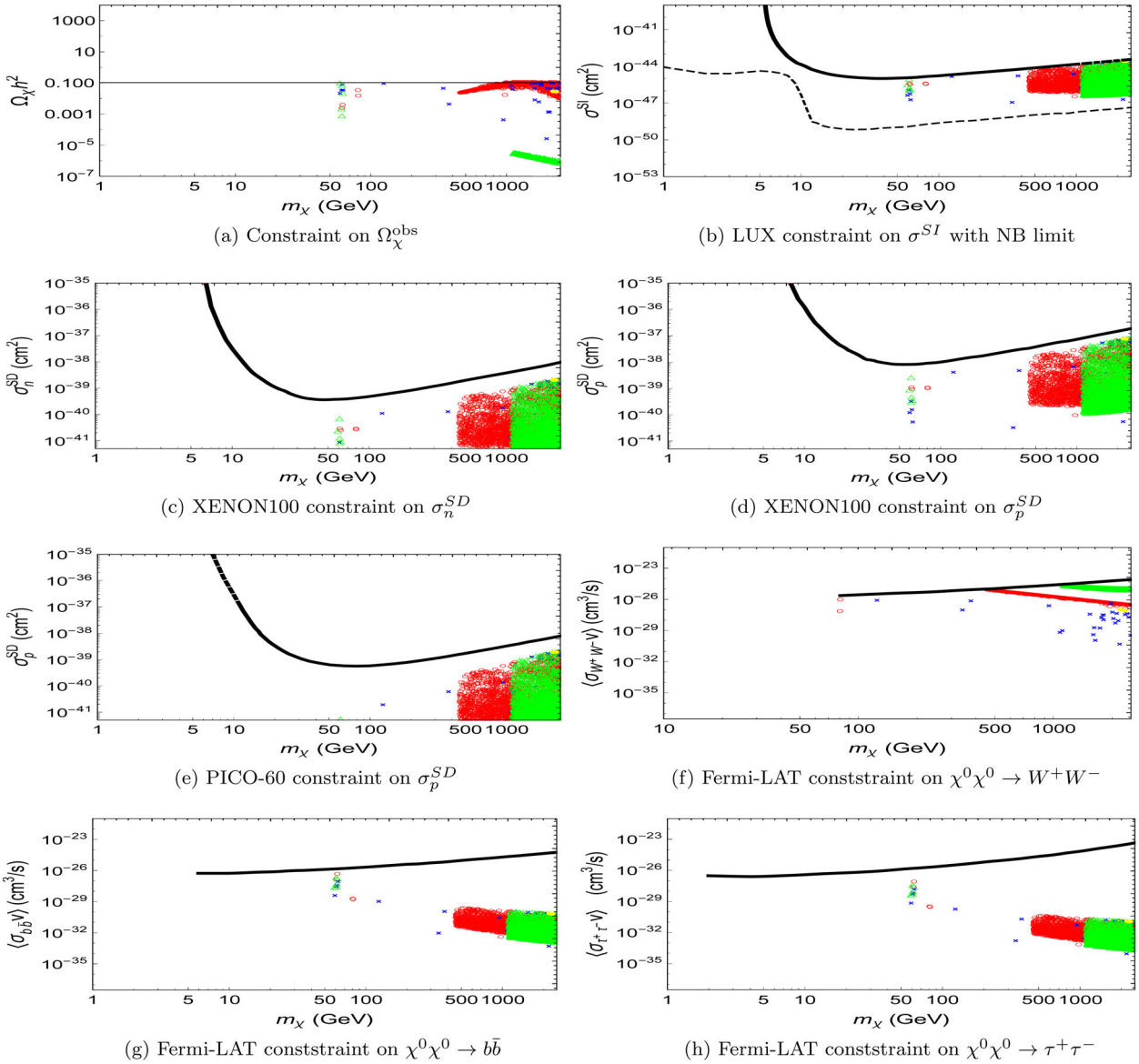

(a) Constraint on $\Omega_\chi^{\rm obs}$

(b) LUX constraint on σ^{SI} with NB limit

(c) XENON100 constraint on σ_n^{SD}

(d) XENON100 constraint on σ_p^{SD}

(e) PICO-60 constraint on σ_p^{SD}

(f) Fermi-LAT conststraint on $\chi^0\chi^0 \to W^+W^-$

(g) Fermi-LAT conststraint on $\chi^0\chi^0 \to b\bar{b}$

(h) Fermi-LAT conststraint on $\chi^0\chi^0 \to \tau^+\tau^-$

FIG. 10. Results allowed samples satisfying all constraints in the neutralinolike III case [open circle: Higgsino-like, times: binolike, triangle: winolike, filled circle: mixed].

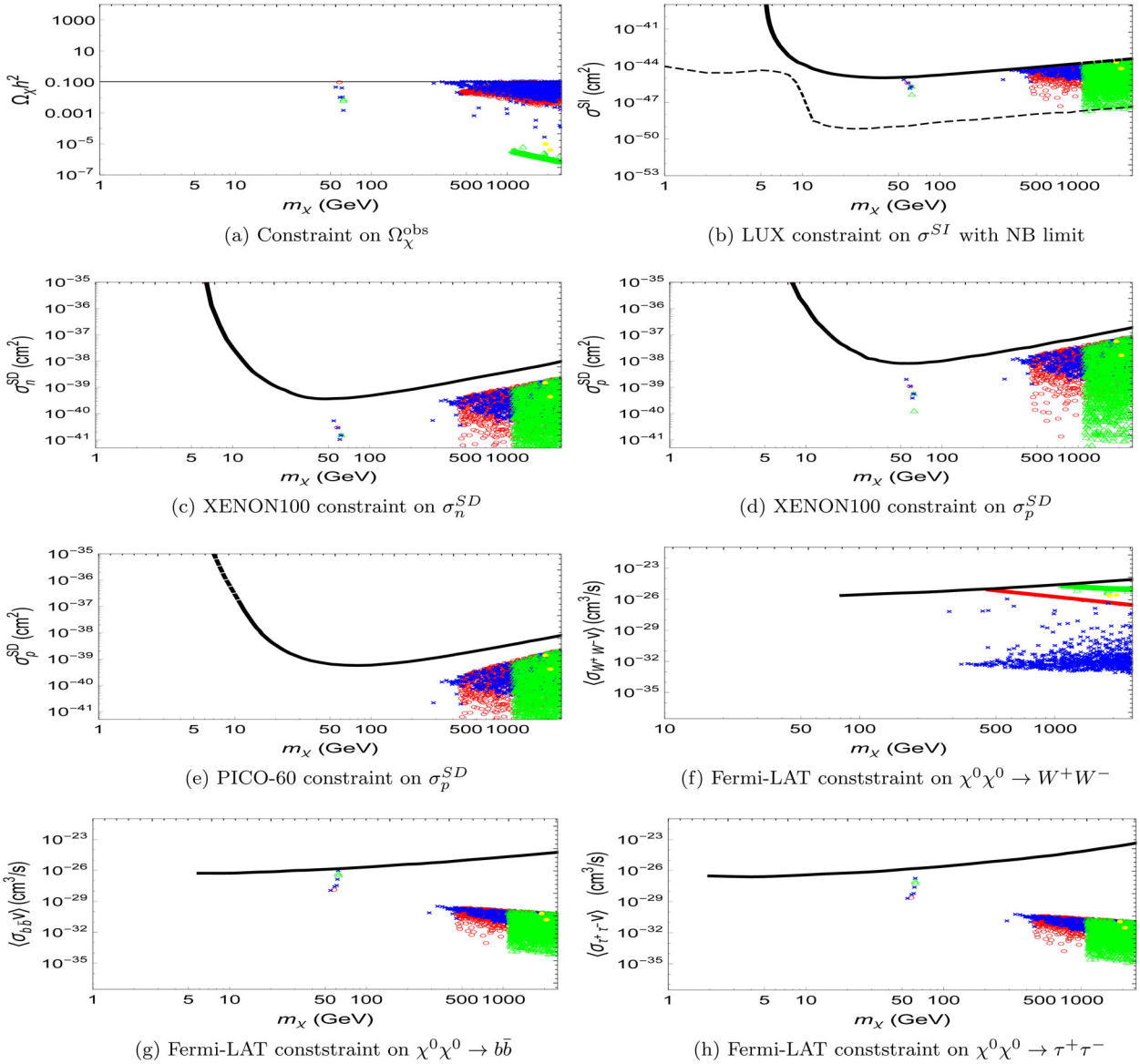

(a) Constraint on $\Omega_\chi^{\rm obs}$

(b) LUX constraint on σ^{SI} with NB limit

(c) XENON100 constraint on σ_n^{SD}

(d) XENON100 constraint on σ_p^{SD}

(e) PICO-60 constraint on σ_p^{SD}

(f) Fermi-LAT conststraint on $\chi^0\chi^0 \to W^+W^-$

(g) Fermi-LAT conststraint on $\chi^0\chi^0 \to b\bar{b}$

(h) Fermi-LAT conststraint on $\chi^0\chi^0 \to \tau^+\tau^-$

FIG. 11. Results for allowed samples satisfying all constraints in the neutralinolike IV case [open circle: Higgsino-like, times: binolike, triangle: winolike, filled circle: mixed].

[see Figs. 6(g), 7(g), and 8(g)], while the $\tilde{H}$- and $\tilde{W}$-like particles with $m_\chi \gtrsim M_W$ are mainly ruled out by the $\langle\sigma(\chi\chi \to W^+W^-)v\rangle$ [see Figs. 6–8(f)] and the $\sigma_N^{\rm SI}$ constraints [see Figs. 6–8(b)]. We see that the allowed lower mass bound of $\tilde{H}$-like DM candidates is about 455 GeV for all the neutralinolike cases (see Figs. 9–11), namely, independent of the GUT and the $\tan\beta$ relations for the $\tilde{H}$-like particles, while the allowed lower mass bound of $\tilde{W}$-like DM candidates is about 1100 GeV, which is independent of the $\tan\beta$ relation in the neutralinolike III and IV cases (see Figs. 10–11). On the contrary to the $\tilde{B}$-like DM candidates, $\tilde{H}$- and $\tilde{W}$-like DM candidates will be accessible in the direct search of $\sigma_N^{\rm SI}$ as well as the indirect search of $\langle\sigma(\chi\chi \to W^+W^-)v\rangle$ in the near future. Therefore, without considering the outlier samples, the allowed mass regions for $\tilde{H}$-like, $\tilde{B}$-like, and $\tilde{W}$-like in Figs. 9–11 can be understood. On the other hand, we find that the allowed $\tilde{H}$-like particles are highly pure, as 98%, 97%, 99%, and 99.9% of them are in the states of η_1 or η_2 with the composition fraction greater than 90% in the cases of neutralinolike I–IV respectively. However, only 39%, 5%, 55%, and 99% of the allowed $\tilde{B}$-like particles are in the state of η_3 with the composition fraction greater than 90% in the cases of neutralinolike I–IV respectively. That is because either the GUT relation or the $\tan\beta$ relation is imposed in the cases of neutralinolike I–III. As for the allowed $\tilde{W}$-like particles, 99.9% and 99.5% of them are in the state of η_5 with the composition fraction greater than 90% in neutralinolike III–IV, respectively.

B. Case B: Reduced case

For the reduced case, it contains a minimal particle content $\eta_{1,2,3}$ ($\tilde{H}$- and $\tilde{B}$-like) with four free parameters $\mu_{1,2}$ and $g_{3,4}$. Since η_5 ($\tilde{W}$-like) particles are absent, it is natural that the $\tilde{W}$-like particles do not appear in this case. We show the results in Fig. 12 with all samples. As in the neutralinolike cases, we show that all values of $\langle\sigma_{W^+W^-}v\rangle$ for the $\tilde{B}$-like particles should be less than those values for the $\tilde{H}$-like and the mixed particles in Fig. 12(f), which is consistent with the fact that a $\tilde{B}$-like DM pair does not contribute to the s-wave scattering amplitude.

As in the neutralinolike cases, we do not show the highly helicity suppressed plots of $\langle\sigma_{u\bar{u}}v\rangle$, $\langle\sigma_{\mu^+\mu^-}v\rangle$, and $\langle\sigma_{e^+e^-}v\rangle$. The reduced case contains more free parameters than the cases of neutralinolike I, II, and III, so it can have a wider spread in each scatter plot than the cases of neutralinolike I, II, and III as the $\tan\beta$ relations are not imposed. Therefore, although most $\tilde{B}$-like samples are ruled out by the $\Omega_\chi h^2$ constraint, we can still have plenty of $\tilde{B}$-like particles being allowed. As in the neutralinolike IV case, more $\tilde{B}$-like particles have lower values in $\Omega_\chi h^2$, and more $\tilde{H}$-like particles have larger values in $\sigma_N^{\rm SI}$ [see Figs. 12(a) and 12(b)]. Consequently, more $\tilde{B}$-like particles (relative to neutralinolike I, II, and III) and fewer $\tilde{H}$-like particles (relative to neutralinolike I) are allowed. We find that about 48% of the $\tilde{H}$-like particles and 23% of $\tilde{B}$-like particles could be DM candidates.

We redraw Fig. 12 in Fig. 13 but with the allowed samples only. As in the neutralinolike cases, the direct detection of $\sigma_N^{\rm SI}$ and the indirect detection of

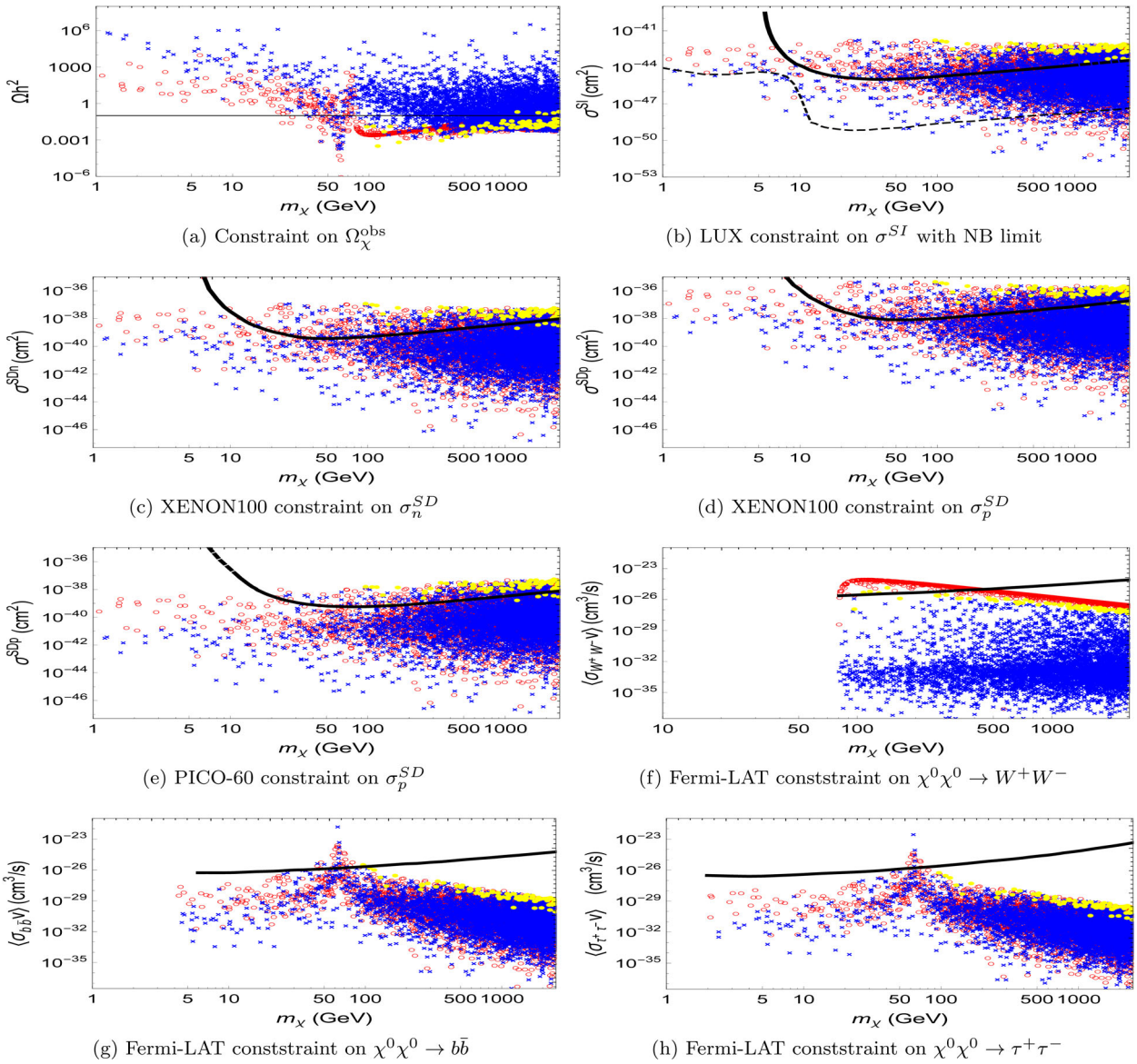

(a) Constraint on $\Omega_\chi^{\rm obs}$

(b) LUX constraint on σ^{SI} with NB limit

(c) XENON100 constraint on σ_n^{SD}

(d) XENON100 constraint on σ_p^{SD}

(e) PICO-60 constraint on σ_p^{SD}

(f) Fermi-LAT conststraint on $\chi^0\chi^0 \to W^+W^-$

(g) Fermi-LAT conststraint on $\chi^0\chi^0 \to b\bar{b}$

(h) Fermi-LAT conststraint on $\chi^0\chi^0 \to \tau^+\tau^-$

FIG. 12. Results for all samples with constraints in the reduced case [open circle: Higgsino-like, times: binolike, filled circle: mixed].

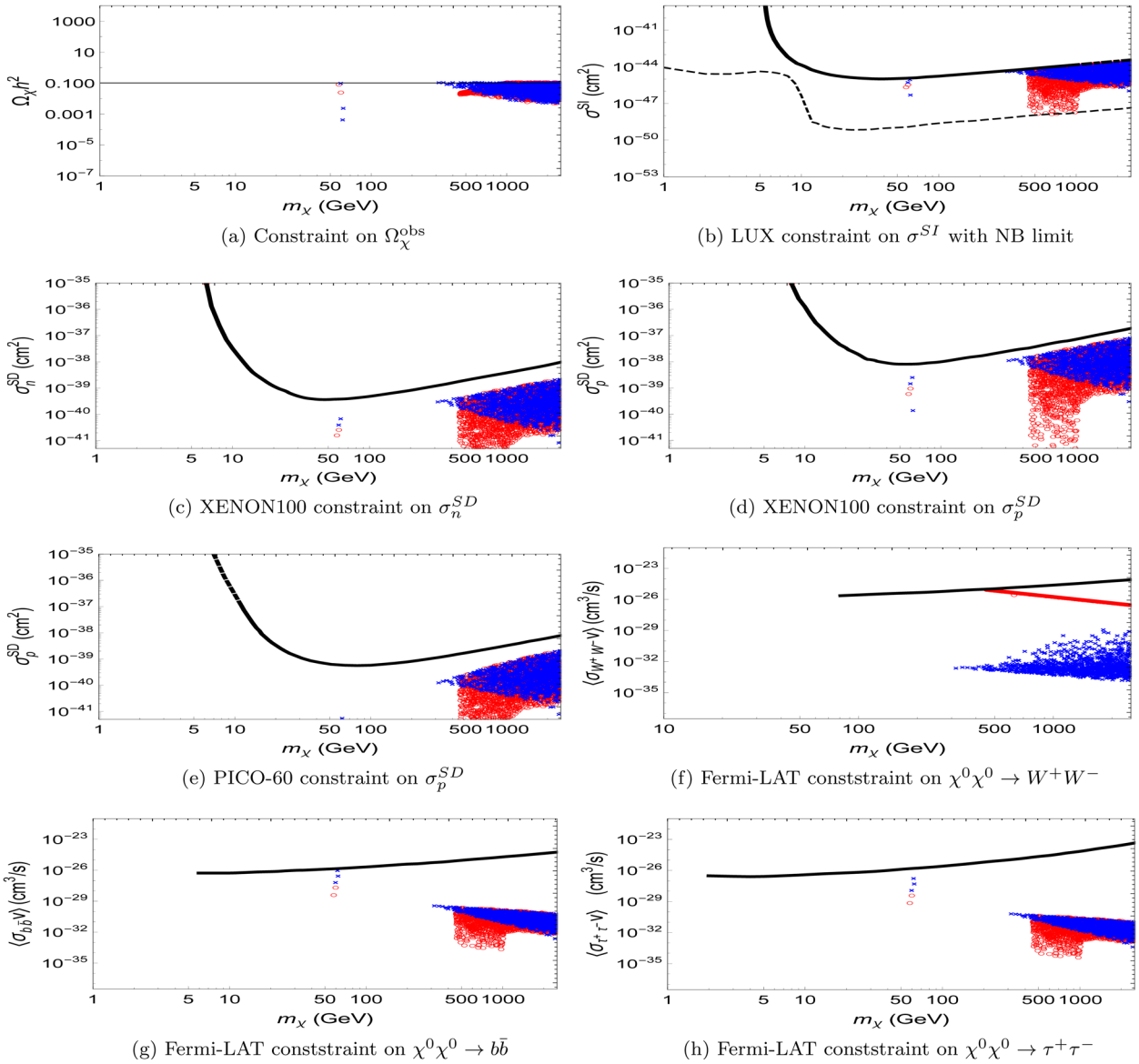

(a) Constraint on $\Omega_\chi^{\rm obs}$

(b) LUX constraint on σ^{SI} with NB limit

(c) XENON100 constraint on σ_n^{SD}

(d) XENON100 constraint on σ_p^{SD}

(e) PICO-60 constraint on σ_p^{SD}

(f) Fermi-LAT conststraint on $\chi^0\chi^0 \to W^+W^-$

(g) Fermi-LAT conststraint on $\chi^0\chi^0 \to b\bar{b}$

(h) Fermi-LAT conststraint on $\chi^0\chi^0 \to \tau^+\tau^-$

FIG. 13. Results for allowed samples satisfying all constraints in the reduced case [open circle: Higgsino-like, times: binolike, filled circle: mixed].

$\langle\sigma(\chi\chi \to W^+W^-)v\rangle$ will be more accessible for DM searches in the near future. Similarly, the $\tilde{B}$-like particles can be sensitively detected only through the experiments of SI DM-nucleus scattering, while the $\tilde{H}$-like particles can be sensitively detected through both the direct search in the SI experiments of DM-nucleus scattering and the indirect search in the observation of DM annihilation to the W^+W^- channel in the near future. Comparing Figs. 5, 9–11, and 13, we see that this case is closer to the neutralinolike IV case, but without $\tilde{W}$-like particles. Despite the fact that most of $\tilde{B}$-like particles are ruled out by the $\Omega_\chi h^2$ constraint, and further by LUX $\sigma^{\rm SI}$ constraint, more allowed $\tilde{B}$-like particles can lower the allowed mass range of $\tilde{B}$-like particles from $m_\chi \gtrsim 1$ TeV (as in the cases of neutralinolike I and II without the GUT relation) to $m_\chi \geq 317$ GeV. On the other hand, the $\tilde{H}$-like particles with $m_\chi \lesssim M_W$ are ruled out by the relic density and the Fermi-LAT $\langle\sigma(\chi\chi \to b\bar{b})v\rangle$ constraints, while the $\tilde{H}$-like particles with $m_\chi > M_W$ are subjected to the Fermi-LAT $\langle\sigma(\chi\chi \to W^+W^-)v\rangle$ and the LUX $\sigma_N^{\rm SI}$ constraints, so only the $\tilde{H}$-like particles with $m_\chi \gtrsim 454$ GeV could be the DM candidates. We also find that the allowed $\tilde{H}$- and $\tilde{B}$-like particles are highly pure, as 99.9% of both $\tilde{H}$- and $\tilde{B}$-like particles is in the states of $\eta_{1,2}$ and η_3, respectively, with their composition fractions greater than 90%.

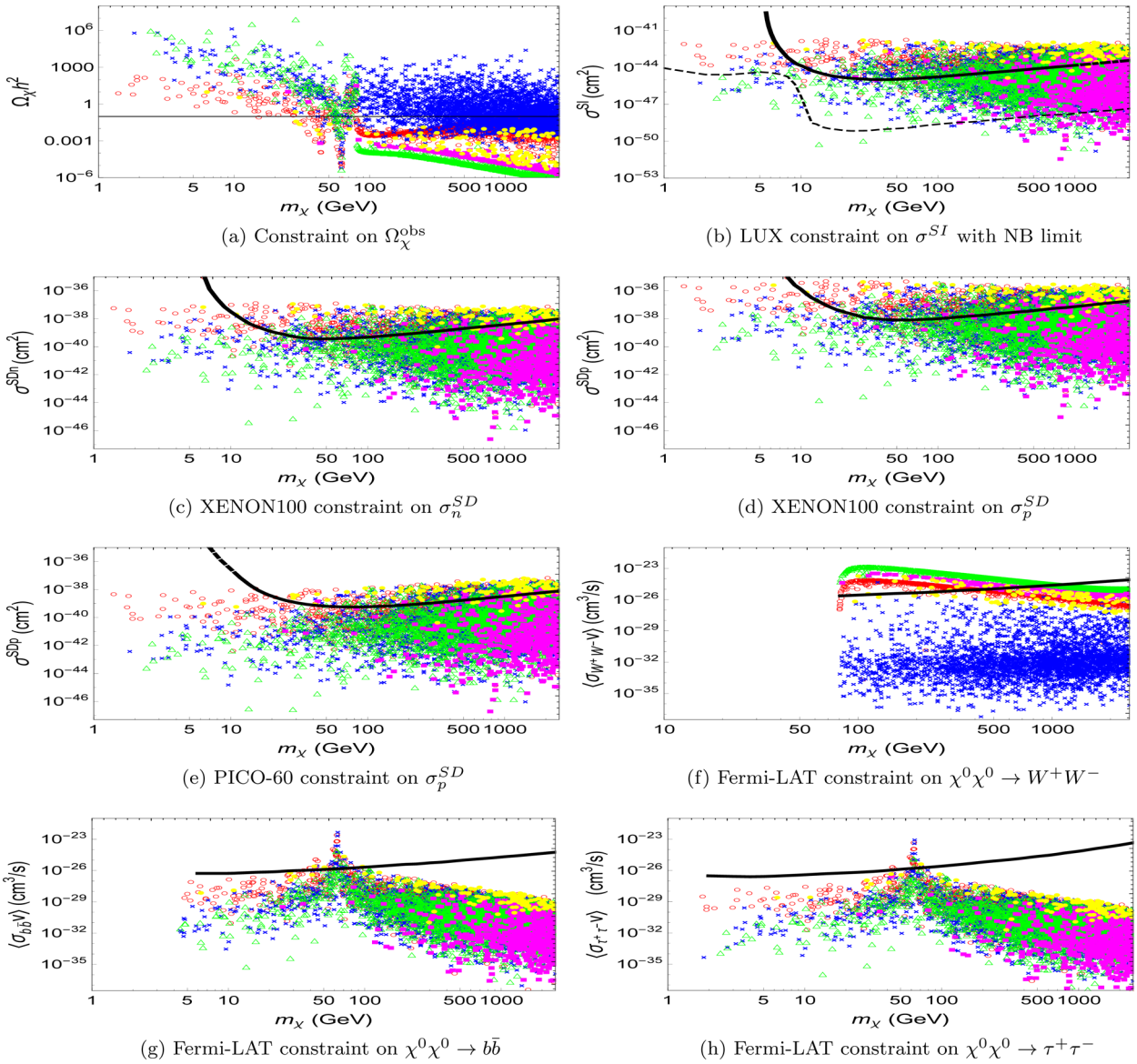

(a) Constraint on $\Omega_\chi^{\rm obs}$

(b) LUX constraint on σ^{SI} with NB limit

(c) XENON100 constraint on σ_n^{SD}

(d) XENON100 constraint on σ_p^{SD}

(e) PICO-60 constraint on σ_p^{SD}

(f) Fermi-LAT constraint on $\chi^0\chi^0 \to W^+W^-$

(g) Fermi-LAT constraint on $\chi^0\chi^0 \to b\bar{b}$

(h) Fermi-LAT constraint on $\chi^0\chi^0 \to \tau^+\tau^-$

FIG. 14. Results for all samples with constraints in the extended case [open circle: Higgsino-like, times: binolike, triangle: winolike, filled square: non-neutralino-like, filled circle: mixed].

C. Case C: Extended case

For the extended case, it has a maximal particle content with $\eta_{1\text{–}3,5,7\text{–}10}$. In addition to the $\tilde{W}$-like particles ($\sim\eta_5$), the non-neutralino-like $\tilde{X}$ particles ($\sim\eta_{9,10}$)[6] also appear in this case, and the latter contain about 5% of the samples. We show the results in Fig. 14 with all samples. As in other cases, we do not present the highly helicity suppressed plots of $\langle\sigma_{u\bar{u}}v\rangle$, $\langle\sigma_{\mu^+\mu^-}v\rangle$, and $\langle\sigma_{e^+e^-}v\rangle$, but we show that all values of $\langle\sigma_{W^+W^-}v\rangle$ for the $\tilde{B}$-like particles should be less than those values for the $\tilde{H}$-like and the mixed particles in Fig. 14(f), which is consistent with the fact that a $\tilde{B}$-like DM pair does not contribute to the s-wave scattering amplitude. In this case, all model parameters, $\mu_{1\text{–}5}$ and $g_{3\text{–}6}$, are free (without the GUT and the $\tan\beta$ relations), so it has the widest spread in each scatter plot among all cases. Without the GUT and the $\tan\beta$ relations, more $\tilde{B}$-like particles have lower values in $\Omega_\chi h^2$, and more $\tilde{H}$-like particles spread toward larger values in $\sigma_N^{\rm SI}$. Consequently, more $\tilde{B}$-like particles (relative to neutralinolike I, II, and III), and fewer $\tilde{H}$-like particles (relative to neutralinolike I) are allowed. [see Figs. 14(a) and 14(b)]. We find that 43% of $\tilde{H}$-like particles and up to 22% of $\tilde{B}$-like particles could be DM candidates.

We redraw Fig. 14 in Fig. 15, but with the allowed samples only. Similarly, we find that $\tilde{B}$-like DM candidates

[6]Note that $\eta_{7,8}$ do not have neutral particles, and hence they do not contribute to the dark matter compositions.

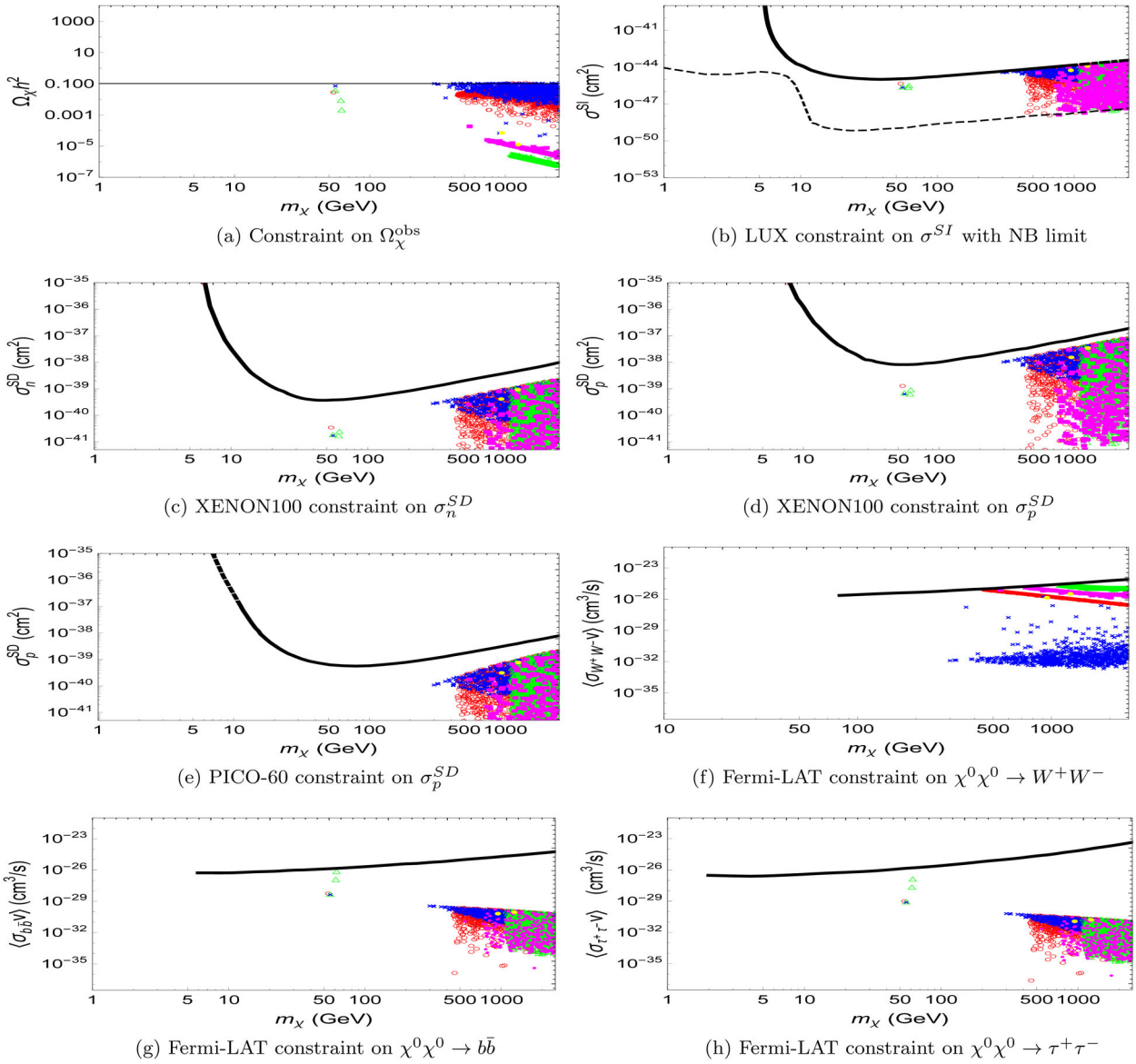

(a) Constraint on $\Omega_\chi^{\rm obs}$

(b) LUX constraint on σ^{SI} with NB limit

(c) XENON100 constraint on σ_n^{SD}

(d) XENON100 constraint on σ_p^{SD}

(e) PICO-60 constraint on σ_p^{SD}

(f) Fermi-LAT constraint on $\chi^0\chi^0 \to W^+W^-$

(g) Fermi-LAT constraint on $\chi^0\chi^0 \to b\bar{b}$

(h) Fermi-LAT constraint on $\chi^0\chi^0 \to \tau^+\tau^-$

FIG. 15. Results for allowed samples satisfying all constraints in the extended case [open circle: Higgsino-like, times: binolike, triangle: winolike, filled square: non-neutralino-like, filled circle: mixed].

are accessible only in the SI experiments of DM-nucleus scattering, while all other types of DM candidates can be sensitively detected from both the direct search in the SI experiments of DM-nucleus scattering and the indirect search in the observation of DM annihilation to the W^+W^- channel in the near future. Despite the fact that most of the $\tilde{B}$-like particles are ruled out by the $\Omega_\chi h^2$ constraint, and further by LUX $\sigma_N^{\rm SI}$ constraint, more allowed $\tilde{B}$-like DM candidates can lower the allowed mass range of $\tilde{B}$-like particles from $m_\chi \gtrsim 1$ TeV (as in the cases with the GUT relation) to $m_\chi \gtrsim 300$ GeV. The $\tilde{H}$-like particles with $m_\chi \lesssim M_W$ are ruled out by the relic density and the Fermi-LAT $\langle\sigma(\chi\chi \to b\bar{b})v\rangle$ constraints, while the $\tilde{H}$-like particles with $m_\chi > M_W$ are subjected to the Fermi-LAT $\langle\sigma(\chi\chi \to W^+W^-)v\rangle$ and the LUX $\sigma_N^{\rm SI}$ constraints, so only the $\tilde{H}$-like particles with $m_\chi \gtrsim 450$ GeV could be the DM candidates. Similarly, the $\tilde{W}$-like particles and the non-neutralino-like $\tilde{X}$ particles with $m_\chi \lesssim M_W$ are ruled out by the relic density and the Fermi-LAT $\langle\sigma(\chi\chi \to b\bar{b})v\rangle$ constraints, while the $\tilde{W}$-like particles and the non-neutralino-like $\tilde{X}$ particles with $m_\chi > M_W$ are subjected to the Fermi-LAT $\langle\sigma(\chi\chi \to W^+W^-)v\rangle$ and the LUX $\sigma_N^{\rm SI}$ constraints, so only the $\tilde{W}$-like particles and the non-neutralino-like $\tilde{X}$ particles with $m_\chi \gtrsim 1107$, 738 GeV, respectively, could be the DM candidates. We also find that about 31% of $\tilde{W}$-like particles and 62% of non-neutralino-like $\tilde{X}$ particles are allowed to be DM candidates. Furthermore, we find that the allowed $\tilde{H}$-, $\tilde{B}$-, and $\tilde{W}$-like particles and the

non-neutralino-like $\tilde{X}$ particles are highly pure, as 99.5%, 99.2%, 99.5%, and 95% of them are in the states of $\eta_{1,2}, \eta_3, \eta_5$, and $\eta_{9,10}$, respectively, with their composition fractions greater than 90%.

D. Summary and predictions

In this subsection, we will summarize the previous discussion and give some predictions. The allowed samples must satisfy all the constraints simultaneously, namely, the observed relic density $\Omega_\chi^{\rm obs}h^2$ constraint (below $+3\sigma$), the LUX constraint on $\sigma_N^{\rm SI}$, the XENON100 constraints on $\sigma_{n,p}^{\rm SD}$, the PICO-60 constraint on $\sigma_p^{\rm SD}$, and the Fermi-LAT constraints on $\langle\sigma(\chi\chi \to W^+W^-, b\bar{b}, u\bar{u}, \tau^+\tau^-, \mu^+\mu^-, e^+e^-)v\rangle$. For all cases, we find that most of the $\tilde{B}$-like particles are ruled out by the $\Omega_\chi h^2$ constraint, and further by the LUX $\sigma_N^{\rm SI}$ constraint; the $\tilde{H}$-like particles with $m_\chi \lesssim M_W$ are ruled out by the relic density and the Fermi-LAT $\langle\sigma(\chi\chi \to b\bar{b})v\rangle$ constraints, while the $\tilde{H}$-like particles with $m_\chi > M_W$ are subjected to the Fermi-LAT $\langle\sigma(\chi\chi \to W^+W^-)v\rangle$ and the LUX $\sigma_N^{\rm SI}$ constraints. For all cases, all values in $\langle\sigma_{W^+W^-}v\rangle$ for the $\tilde{B}$-like particles are smaller than those values for the $\tilde{H}$-like particles due to the fact that a $\tilde{B}$-like DM pair does not contribute to the s-wave scattering amplitude. Besides, the process of $\chi\chi \to f\bar{f}$ favors heavy fermions since the s-wave contribution is helicity suppressed. We see that the direct search of SI DM-nucleus elastic scattering and the indirect search of DM annihilation to the W^+W^- channel are more important. In other words, they will be sensitive to the DM searches in the near future.

Without considering the outlier samples, we show the allowed mass range of different particle attributes to detect DM in direct as well as indirect searches in Table IV. The upper values denote the lower mass bounds to detect DM in the direct search of SI DM-nucleus scattering experiments, and the lower intervals denote the mass interval suitable to detect DM in the indirect search of the DM annihilation process via the W^+W^- channel using the present limit and the projected limit, which is taken to be 1 order of magnitude lower than the present one. We see that the DM mass should be greater than 450, 288, 1090, and 738 GeV to detect the $\tilde{H}$-, $\tilde{B}$-, and $\tilde{W}$-like DM particles and the non-neutralino-like $\tilde{X}$ DM particles, respectively. Note that, unlike in the indirect case, we cannot infer the upper mass bound to detect DM in the direct search in this analysis. In other words, future direct searches can explore a larger DM mass range than the indirect one.

The Fermi-LAT constraint on $\langle\sigma(\chi\chi \to W^+W^-)v\rangle$ is more useful than other Fermi-LAT constraints with light $f\bar{f}$ in the final states. On the other hand, from the discussion of the properties of DM annihilation processes $\chi\chi \to W^+W^-, ZZ, ZH, HH, f\bar{f}$ in Sec. II. B, we know that only the process of $\chi\chi \to HH$ has no s-wave contribution and the process $\chi\chi \to f\bar{f}$ favors heavy fermion pairs. Hence, it is also important to study DM annihilation to gauge boson and heavy quark processes. In Fig. 16, we show our predictions on $\langle\sigma(\chi\chi \to ZZ, ZH, t\bar{t})v\rangle$ with the allowed samples. Their values of $\langle\sigma v\rangle$ can be as large as 10^{-26} cm^3/s. It will be useful to search DM with these processes.

In Table V, we summarize the distribution of the allowed samples satisfying all constraints. The two values in parentheses in the table show the percentages (with regard to the whole sample) of a specified particle attribute before and after being subjected to the constraints, respectively. For example, in the first row "$\tilde{H}$" and the first column "Neutralinolike I case" of the table, we see that there is 29% of the whole sample in the neutralinolike I case being $\tilde{H}$-like particles and only 18% of the whole sample being allowed $\tilde{H}$-like particles. Among the $\tilde{H}$-like particles, only 63% of them survives under the constraints, and this surviving rate is shown below the parentheses. From this table, we see that fewer $\tilde{H}$-like particles are allowed (relative to neutralinolike I) and fewer $\tilde{B}$-like particles

TABLE IV. Allowed mass ranges according to particle attributes to detect DM in the near future. The upper values denote the lower mass bounds (in units of GeV) to detect DM in the direct search of SI DM-nucleus scattering experiments, and the lower intervals denote the mass interval (in units of GeV) suitable for detecting DM in the indirect search of the DM annihilation process via the W^+W^- channel between the present limit and the projected limit, which is taken to be 1 order of magnitude lower than the present one.

	Case A				Case B	Case C
	Neutralinolike I	Neutralinolike II	Neutralinolike III	Neutralinolike IV	Reduced	Extended
$\tilde{H}$-like	456	457	457	454	454	450
	(456, 940)	(457, 937)	(457, 947)	(454, 947)	(454, 949)	(450, 927)
$\tilde{B}$-like	1411	1258	341	288	317	299
	X	X	X	X	X	X
$\tilde{W}$-like	X	X	1120	1090	X	1107
	X	X	(1120, 2500[a])	(1090, 2374)	X	(1107, 2080)
$\tilde{X}$-like	X	X	X	X	X	738
	X	X	X	X	X	(738, 1563)

[a]This value is originated from the limitation of our numerical analysis.

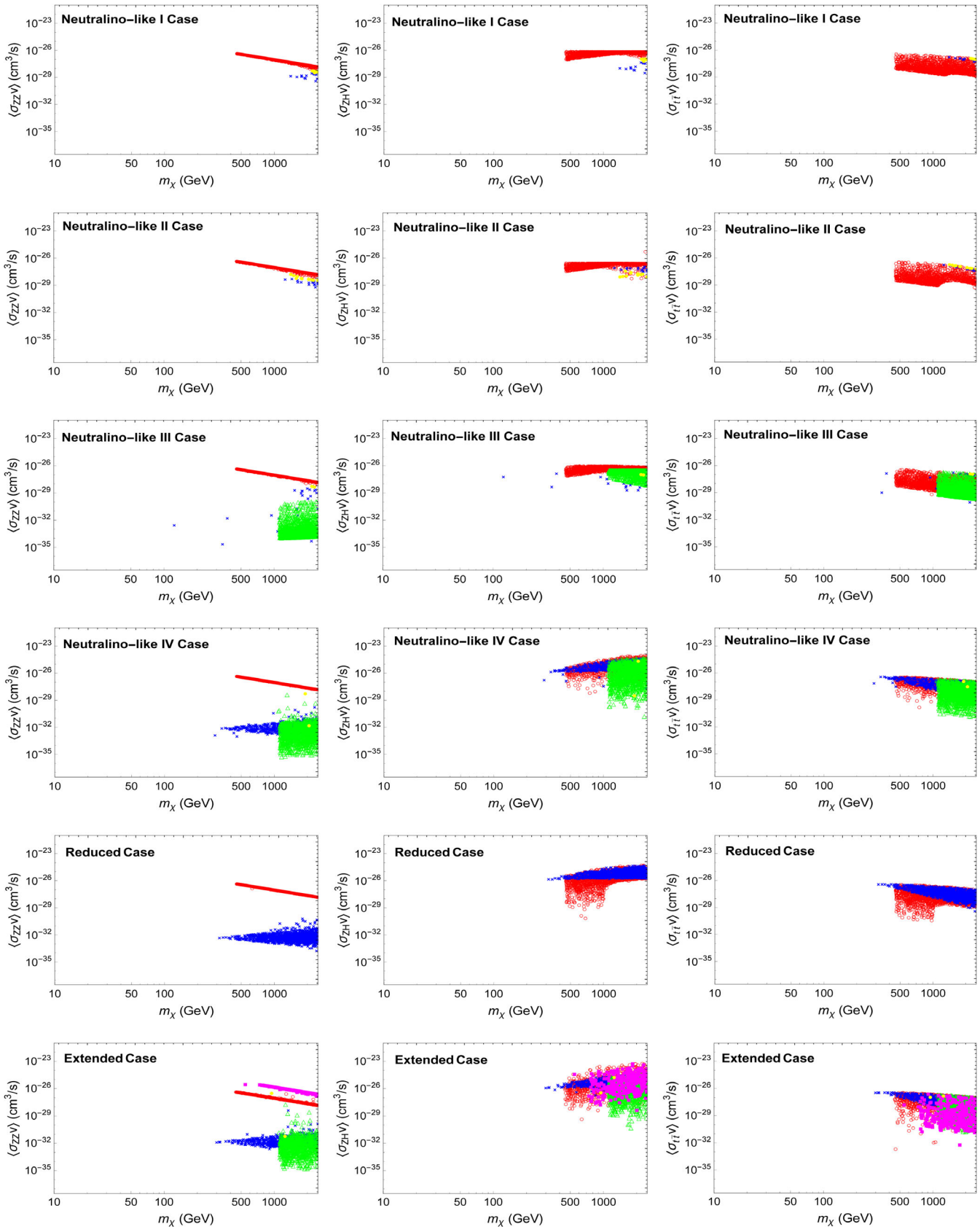

FIG. 16. Predictions of $\langle \sigma_{ZZ,ZH,t\bar{t}} v \rangle$ vs m_χ for allowed DM candidates [open circle: Higgsino-like, times: binolike, triangle: winolike, filled square: non-neutralino-like, filled circle: mixed].

TABLE V. Particle attribute distribution of the allowed DM candidates. The values in the first row $\tilde{H}$-like and the first column Neutralinolike I of the table mean that 29% of the whole sample in neutralinolike I case is $\tilde{H}$-like and only 18% of the whole sample is the allowed $\tilde{H}$-like particles, or equivalently, among the $\tilde{H}$-like particles, only 63% of them is allowed.

	Case A				Case B	Case C
%	Neutralinolike I	Neutralinolike II	Neutralinolike III	Neutralinolike IV	Reduced	Extended
$\tilde{H}$-like	(29, 18)	(28, 14)	(33, 15)	(31, 15)	(50, 24)	(29, 12)
	63	49	45	46	48	43
$\tilde{B}$-like	(71, 0.2)	(72, 0.2)	(33, 0.3)	(34, 8)	(49, 11)	(34, 7)
	0.3	0.3	0.9	23	23	22
$\tilde{W}$-like	X	X	(33, 15)	(34, 13)	X	(31, 10)
	X	X	45	39	X	31
$\tilde{X}$-like	X	X	X	X	X	(5, 3)
	X	X	X	X	X	62

can survive in the cases with the $\tan\beta$ relation (neutralinolike I–III). As mentioned before, it is due to the fact that a higher $\tan\beta$ value or without the GUT relation can give us wider spreads in the scatter plots. It results in the fact that more $\tilde{H}$-like particles spread into the prohibited region in the σ_N^{SI} scatter plot. On the other hand, with the $\tan\beta$ relation, fewer $\tilde{B}$-like particles can spread into the allowed region in the $\Omega_\chi h^2$ scatter plot.

TABLE VI. Allowed range for DM mass, model parameters, and effective couplings. The upper and lower intervals represent the allowed range for samples satisfying all the constraints with $\Omega_\chi h^2$ in the criteria C1 ($\leq +3\sigma$) and C2 (within $\pm 3\sigma$), respectively.

	Case A				Case B	Case C
	Neutralinolike I	Neutralinolike II	Neutralinolike III	Neutralinolike IV	Reduced	Extended
m_χ	(51.1, 2495.1)	(57.1, 2498.9)	(58.9, 2498.3)	(54.8, 2499.9)	(57.8, 2498.8)	(54.0, 2499.0)
	(1116.6, 2496.7)	(1018.2, 2471.4)	(947.7, 2454.6)	(332.6, 2464.6)	(316.6, 2481.7)	(299.0, 2383.5)
μ_1	(52.3, 6933.9)	(58.1, 3655.4)	(62.7, 7982.6)	(59.34, 7999.4)	(58.56, 7997.0)	(52.38, 7998.4)
	(1118.2, 2499.3)	(1019.1, 2473.8)	(980.4, 5452.8)	(901.6, 7896.2)	(953,9, 7953.3)	(1040.5, 7858.5)
μ_2	(58.4, 3814.3)	(0.214, 3823.5)	(59.80, 7999.9)	(56.99, 7999.4)	(61.67, 7998.2)	(56.7, 7996.9)
	(1430.8, 3811.4)	(2027.4, 3802.9)	(1781.6, 7979.6)	(339.5, 7970.8)	(323.4, 7977.4)	(305.4, 7134.6)
μ_3	(122.2, 7978.8)	(0.447, 7998.2)	(5.328, 7999.5)	(63.0, 7998.6)	X	(1.095, 7994.6)
	(2993.0, 7972.8)	(4240.9, 7955.1)	(1816.7, 7977.2)	(848.5, 7992.6)	X	(1305.3, 7951.2)
μ_4	X	X	X	X	X	(681.80, 7999.4)
	X	X	X	X	X	(681.80, 7633.5)
μ_5	X	X	X	X	X	(551.7, 7998.7)
	X	X	X	X	X	(551.7, 7771.8)
g_3	0.111	0.012	0.111	(1.40e-4, 0.999)	(2.86e-4, 0.999)	(2.57e-4, 0.999)
	0.111	0.012	0.111	(2.61e-2, 0.998)	(5.20e-4, 0.976)	(7.76e-3, 0.975)
g_4	0.221	0.247	0.221	(1.90e-4, 0.999)	(5.12e-4, 0.999)	(3.00e-4, 0.999)
	0.221	0.247	0.221	(5.20e-2, 0.994)	(8.50e-3, 0.996)	(8.38e-3, 0.988)
g_5	0.207	0.023	0.207	(1.26e-3, 0.999)	X	(6.00e-4, 0.999)
	0.207	0.023	0.207	(5.51e-3, 0.979)	X	(1.03e-2, 0.993)
g_6	0.413	0.462	0.413	(1.37e-5, 0.999)	X	(1.46e-4, 0.999)
	0.413	0.462	0.413	(1.31e-2, 0.994)	X	(1.91e-2, 0.995)
g_7	X	X	X	X	X	(6.47e-4, 0.999)
	X	X	X	X	X	(8.79e-3, 0.985)
g_8	X	X	X	X	X	(6.70e-4, 0.999)
	X	X	X	X	X	(6.70e-4, 0.998)
g_9	X	X	X	X	X	(1.02e-4, 0.999)
	X	X	X	X	X	(1.45e-2, 0.981)
g_{10}	X	X	X	X	X	(3.04e-5, 0.999)
	X	X	X	X	X	(1.98e-2, 0.994)
$\lvert a_q/m_q\rvert$	(9.3e-10, 9.02e-8)	(2.5e-10, 7.05e-8)	(1.52e-9, 9.08e-8)	(7.5e-10, 9.52e-8)	(5.6e-10, 9.03e-8)	(1.5e-11, 9.18e-8)
	(6.15e-9, 6.96e-8)	(3.69e-9, 1.28e-8)	(2.40e-9, 6.86e-8)	(4.87e-9, 6.95e-8)	(6.6e-10, 9.31e-8)	(1.5e-9, 7.28e-8)
$\lvert d_q\rvert$	(9.8e-11, 4.31e-8)	(5.7e-10, 8.62e-8)	(1.59e-10, 3.20e-8)	(9.1e-12, 5.70e-8)	(3.8e-13, 5.02e-8)	(1.7e-12, 3.62e-7)
	(1.38e-9, 1.57e-8)	(3.04e-9, 7.66e-9)	(2.17e-10, 1.26e-8)	(2.05e-11, 2.46e-8)	(3.4e-11, 3.19e-8)	(2.9e-12, 3.52e-8)

As shown in the table, in the neutralinolike III and IV and the extended cases, we have plenty of $\tilde{W}$-like particles. The $\tilde{W}$-particles with $m_\chi \lesssim M_W$ are ruled out by the relic density and the Fermi-LAT $\langle\sigma(\chi\chi \to b\bar{b})v\rangle$ constraints, while the $\tilde{W}$-particles with $m_\chi > M_W$ are subjected to the Fermi-LAT $\langle\sigma(\chi\chi \to W^+W^-)v\rangle$ constraint and the LUX $\sigma_N^{\rm SI}$ constraint. The fewer relations on model parameters give a wider spread in the scatter plots of $\Omega_\chi h^2$, $\sigma_N^{\rm SI}$, and $\langle\sigma(\chi\chi \to W^+W^-)$, resulting in lower surviving rates of $\tilde{W}$-like DM candidates, namely, 45%, 39%, and 31% in the neutralinolike III and IV and the extended cases, respectively. As for the non-neutralino-like $\tilde{X}$ particles, 62% of them could be DM candidates.

Including the allowed outlier samples, we show the allowed ranges of DM mass, mass parameters (μ_i), Yukawa couplings (g_i), and the effective couplings ($|a_q/m_q|$ and $|d_q|$) used in the calculation of DM scattering off ^{129,131}Xe nuclei and CF_3I nuclei in Table VI and the allowed ranges for the coupling strengths used in the calculation of DM annihilation processes in Table VII. In Table VII, we have used the following definitions:

TABLE VII. Allowed range for the coupling strengths. The upper and lower intervals represent the allowed range for samples satisfying all the constraints with $\Omega_\chi h^2$ in the criteria C1 ($\leq +3\sigma$) and C2 (within $\pm 3\sigma$), respectively.

	Case A				Case B	Case C
	Neutralinolike I	Neutralinolike II	Neutralinolike III	Neutralinolike IV	Reduced	Extended
$\lvert g_{11}^{L_H}\rvert$	(1.80e-3, 1.75e-1)	(4.84e-4, 2.49e-1)	(2.95e-3, 1.77e-1)	(1.45e-3, 1.85e-1)	(1.08e-3, 1.81e-1)	(2.85e-5, 1.78e-1)
	(1.20e-2, 1.35e-1)	(7.17e-3, 2.49e-1)	(4.66e-3, 1.33e-1)	(9.46e-3, 1.35e-1)	(1.33e-3, 1.81e-1)	(2.94e-3, 1.42e-1)
$\lvert g_{11}^{L_Z}\rvert$	(4.39e-6, 1.93e-3)	(2.57e-5, 3.87e-3)	(7.12e-6, 1.43e-3)	(4.07e-7, 2.56e-3)	(1.71e-8, 2.25e-3)	(7.81e-8, 1.62e-2)
	(6.20e-5, 7.03e-4)	(1.37e-4, 3.34e-4)	(9.73e-6, 5.62e-4)	(9.20e-7, 1.11e-3)	(1.51e-6, 1.43e-3)	(1.30e-7, 1.58e-3)
$\lvert g_{11}^{L_{W^-}}\rvert$	(3.95e-3, 3.28e-1)	(8.96e-4, 3.30e-1)	(1.22e-3, 6.53e-1)	(8.75e-6, 6.54e-1)	(1.35e-3, 3.28e-1)	(8.50e-7, 6.53e-1)
	(1.42e-1, 3.27e-1)	(3.26e-1, 3.27e-1)	(3.02e-2, 3.27e-1)	(5.06e-5, 3.27e-1)	(5.88e-3, 3.27e-1)	(4.03e-6, 3.26e-1)
$\lvert g_{11}^{R_{W^-}}\rvert$	(4.00e-3, 3.27e-1)	(1.07e-3, 3.27e-1)	(1.68e-3, 6.53e-1)	(2.04e-4, 6.54e-1)	(4.87e-3, 3.28e-1)	(1.72e-6, 6.54e-1)
	(1.40e-1, 3.27e-1)	(3.26e-1, 3, 27e-1)	(3.05e-2, 3.32e-1)	(2.45e-4, 3.38e-1)	(4.34e-3, 3.27e-1)	(1.72e-6, 3.29e-1)
$\lvert g_{12}^{L_H}\rvert$	(3.20e-3, 5.32e-2)	(1.28e-6, 1.08e-1)	(1.20e-3, 3.10e-1)	(2.17e-5, 9.35e-1)	(7.49e-7, 4.85e-1)	(6.46e-7, 8.89e-1)
	(3.32e-3, 5.32e-2)	(5.49e-3, 1.43e-2)	(2.65e-3, 5.43e-2)	(4.99e-4, 6.38e-1)	(6.10e-5, 4.08e-1)	(1.42e-5, 6.62e-1)
$\lvert g_{12}^{L_Z}\rvert$	(8.67e-6, 1.85e-1)	(4.79e-5, 1.85e-1)	(6.36e-6, 1.85e-1)	(5.36e-8, 1.85e-1)	(2.20e-3, 1.85e-1)	(4.66e-7, 3.71e-1)
	(7.99e-2, 1.85e-1)	(1.85e-1, 1.86e-1)	(1.63e-5, 1.85e-1)	(6.23e-6, 1.85e-1)	(3.68e-3, 1.85e-1)	(5.53e-7, 1.86e-1)
$\lvert g_{12}^{L_{W^-}}\rvert$	(2.67e-3, 5.49e-2)	(5.49e-3, 5.24e-2)	(1.72e-4, 2.84e-1)	(1.27e-4, 4.87e-1)	X	(5.47e-7, 3.80e-1)
	(1.00e-2, 2.00e-2)	(6.49e-3, 1.70e-2)	(5.88e-3, 1.27e-1)	(4.91e-4, 1.78e-1)	X	(1.07e-5, 7.41e-2)
$\lvert g_{12}^{R_{W^-}}\rvert$	(1.29e-3, 1.61e-2)	(3.20e-4, 1.54e-2)	(1.00e-6, 9.15e-2)	(1.27e-6, 1.63e-1)	X	(3.27e-7, 1.24e-1)
	(2.72e-3, 5.63e-3)	(8.50e-4, 3.78e-3)	(2.71e-3, 4.07e-2)	(2.87e-5, 5.58e-2)	X	(2.33e-5, 4.08e-2)
$\lvert g_{13}^{L_H}\rvert$	(1.65e-3, 1.66e-1)	(1.46e-3, 1.30e-1)	(3.65e-3, 3.10e-1)	(4.55e-4, 9.59e-1)	(2.26e-2, 9.81e-1)	(1.61e-5, 9.62e-1)
	(1.13e-1, 1.66e-1)	(1.28e-1, 1.30e-1)	(6.01e-2, 3.10e-1)	(3.00e-2, 6.94e-1)	(7.71e-2, 8.07e-1)	(6.51e-4, 6.24e-1)
$\lvert g_{13}^{L_Z}\rvert$	(1.12e-6, 1.06e-2)	(1.63e-5, 4.14e-3)	(8.73e-6, 7.07e-2)	(7.90e-7, 4.00e-2)	(9.52e-8, 6.86e-3)	(2.19e-7, 1.11e-1)
	(4.08e-4, 6.10e-4)	(9.45e-4, 1.60e-3)	(2.02e-4, 2.51e-3)	(5.62e-6, 1.64e-2)	(6.84e-6, 5.36e-3)	(1.18e-5, 2.85e-2)
$\lvert g_{13}^{L_{W^-}}\rvert$	X	X	X	X	X	(8.77e-8, 1.72e-1)
	X	X	X	X	X	(2.28e-5, 5.64e-2)
$\lvert g_{13}^{R_{W^-}}\rvert$	X	X	X	X	X	(5.66e-7, 6.79e-2)
	X	X	X	X	X	(2.46e-5, 2.32e-2)
$\lvert g_{14}^{L_H}\rvert$	(1.20e-1, 3.10e-1)	(1.03e-1, 2.42e-1)	(3.15e-5, 3.45e-1)	(1.88e-5, 9.84e-1)	X	(5.15e-5, 9.84e-1)
	(1.24e-1, 3.10e-1)	(2.41e-1, 2.42e-1)	(1.11e-1, 3.40e-1)	(3.49e-4, 7.46e-1)	X	(3.39e-4, 7.25e-1)
$\lvert g_{14}^{L_Z}\rvert$	(2.39e-4, 3.05e-3)	(5.74e-4, 5.01e-3)	(3.70e-8, 1.44e-2)	(2.05e-7, 5.46e-3)	X	(2.61e-10, 8.05e-2)
	(3.72e-4, 6.72e-4)	(1.10e-3, 1.78e-3)	(2.74e-4, 1.18e-3)	(5.59e-7, 4.34e-3)	X	(1.16e-6, 1.99e-2)
$\lvert g_{14}^{L_{W^-}}\rvert$	X	X	X	X	X	(2.79e-7, 1.66e-1)
	X	X	X	X	X	(8.19e-6, 2.31e-2)
$\lvert g_{14}^{R_{W^-}}\rvert$	X	X	X	X	X	(3.33e-7, 4.35e-2)
	X	X	X	X	X	(3.40e-6, 2.30e-2)
$\lvert g_{15}^{L_H}\rvert$	X	X	X	X	X	(5.86e-5, 9.49e-1)
	X	X	X	X	X	(5.62e-4, 6.25e-1)
$\lvert g_{15}^{L_Z}\rvert$	X	X	X	X	X	(3.24e-7, 2.63e-2)
	X	X	X	X	X	(1.20e-6, 1.46e-2)
$\lvert g_{16}^{L_H}\rvert$	X	X	X	X	X	(2.97e-5, 9.84e-1)
	X	X	X	X	X	(1.91e-4, 8.18e-1)
$\lvert g_{16}^{L_Z}\rvert$	X	X	X	X	X	(1.85e-8, 1.20e-2)
	X	X	X	X	X	(2.23e-6, 3.24e-3)

$g^{L_H}_{1j} = O^{L_H}_{1j}, g^{L_Z}_{1j} = \frac{g}{2\cos\theta_W} O^{L_Z}_{1j}$, and $g^{L,R_{W^-}}_{1j} = \frac{g}{\sqrt{2}} O^{L,R_{W^-}}_{1j}$. The allowed DM relic density should satisfy the condition $\Omega_\chi h^2 \leq 0.1198 + 3 \times 0.0026$. We consider two criterions: C1, having a less stringent constraint of the relic density with its value less than $+3\sigma$, and C2, having a more stringent constraint of the relic density with its value within $\pm 3\sigma$, from the observed mean value. In Tables VI and VII, the upper and lower intervals represent the allowed range for samples satisfying all the constraints with $\Omega_\chi h^2$ falling into the criteria C1 and C2, respectively.

IV. DISCUSSIONS AND CONCLUSIONS

A. Coannihilation

In addition to the annihilation, the coannihilation, namely, the annihilation from the other WIMPs, may affect the DM relic density in some parameter region. The coannihilation becomes significantly important when the WIMPs are nearly mass degenerate with DM [50]. In this subsection, we preliminarily explore the variation on the calculation of DM relic density when including the coannihilation. To see the leading effect of coannihilation, we consider two lightest neutral as well as two single charged WIMPs annihilating to the SM fermions through the s channel in the neutralinolike I case. The corresponding Feynman diagrams and Lagrangian are shown in Fig. 17 and Appendix C, respectively. The matrix elements for coannihilation are shown in Appendix H. The formulation for coannihilation is presented in Appendix G. To simplify the calculation of coannihilation, we have set the freeze-out temperature parameter $x_f = 25$.

Figures 18(a) and 18(b) show the scatter plots of relic density without and with coannihilation, respectively. We see that the Ωh^2 constraint affects the selection of the $\tilde{B}$-like particles a little but the selection of the $\tilde{H}$-like particles a lot. Most $\tilde{H}$-like particles with mass less than M_W ruled out originally become allowed now, while part of the $\tilde{H}$-like particles with mass greater than M_W allowed originally become ruled out now when including the leading effect of coannihilation.

To see the variation of DM relic density, we overlap Figs. 18(a) (in times) and 18(b) (in open circle) in Fig. 19(a). We also show the variation of DM relic density vs the mass fraction $\Delta m_2/m_\chi \equiv (\mathrm{Min}[m_{\chi^0_2}, m_{\chi^\pm_{1,2}}] - m_{\chi^0_1})/m_{\chi^0_1}$ in Fig. 19(b). Let $\Omega_{\rm new}$ and Ω denote the relic density with and without considering the coannihilation, respectively. Apart from a few samples around the poles, we find that $\Omega_{\rm new} \geq \Omega$ with $m_\chi \gtrsim m_W$, while $\Omega_{\rm new} \leq \Omega$ with $m_\chi \lesssim m_W$ in Fig. 19(c). We also find that the smaller mass fraction usually gives the greater value in $\Omega_{\rm new}/\Omega$ as shown in Fig. 19(d). We show the relic density vs DM mass m_χ and mass fraction $\Delta m_2/m_\chi$ with the allowed samples which satisfy all constraints in Figs. 19(e) and 19(f), respectively, and Figs. 19(g) and 19(h) for $\Omega_{\rm new}/\Omega$. In Figs. 19(e) and 19(f), the samples marked with open circle are allowed

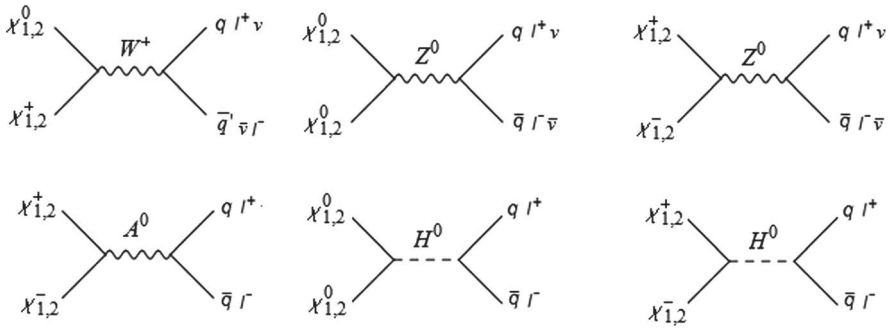

FIG. 17. The coannihilation processes ($\chi\chi \to$ SM fermions) through the s channel.

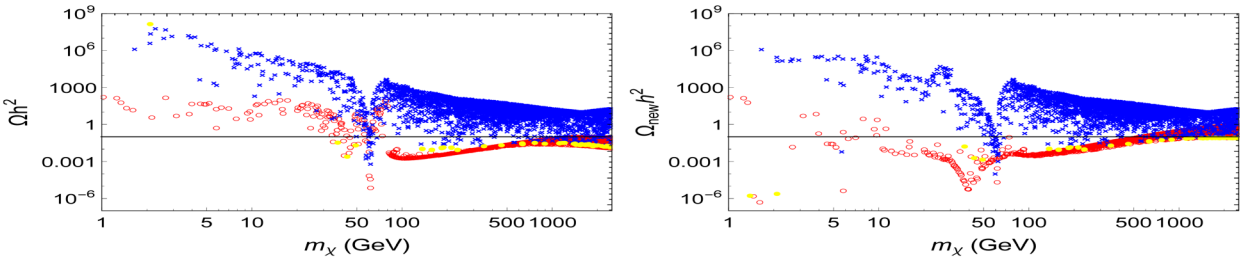

(a) Without coannihilation (b) With coannihilation

FIG. 18. Scatter plots of DM relic abundance before and after considering coannihilation in the neutralinolike I case [open circle: Higgsino-like, times: binolike, filled circle: mixed].

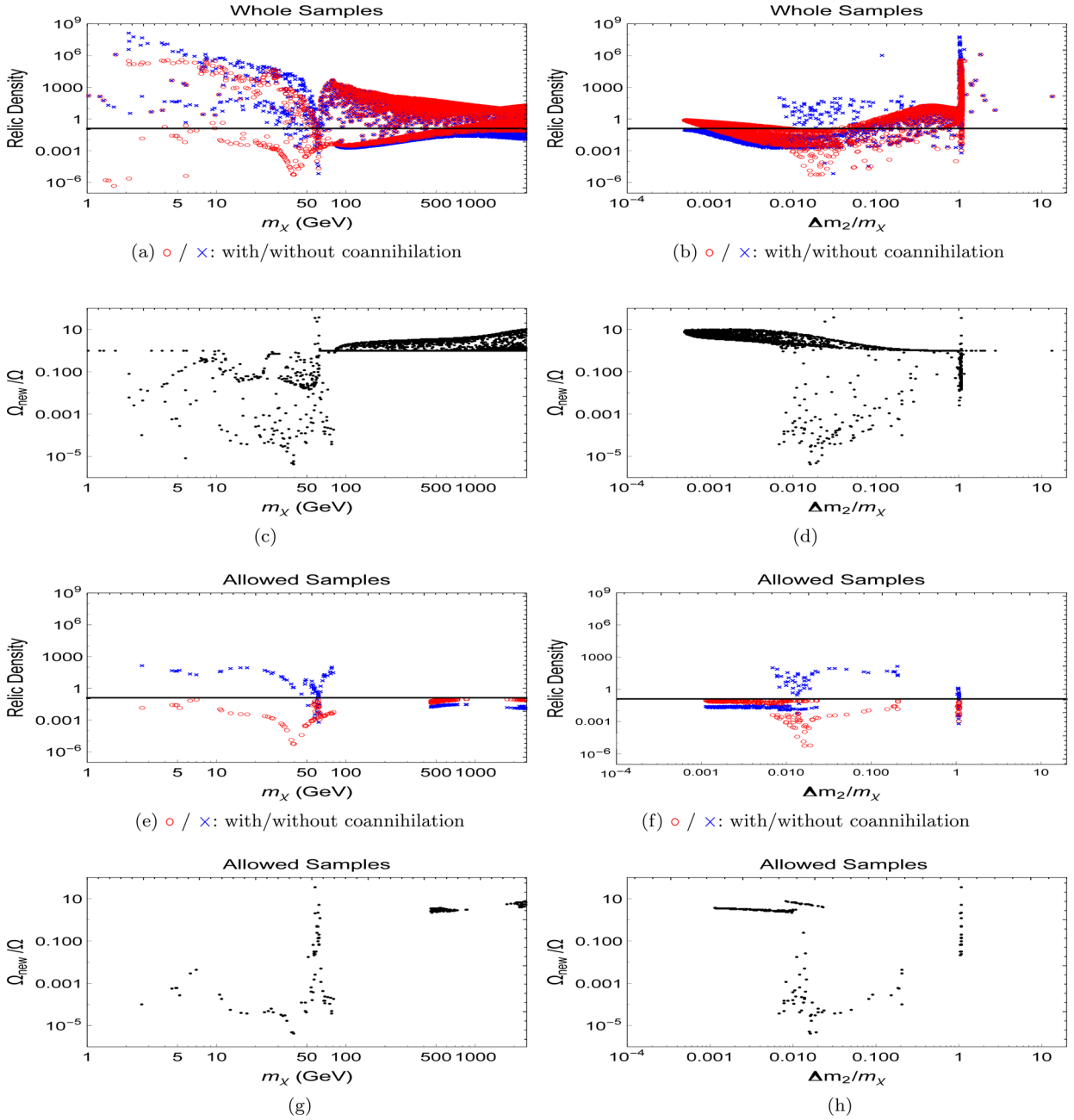

FIG. 19. Leading effect of coannihilation on DM relic abundance at $x_f = 25$ in the neutralinolike I case.

when including the coannihilation, and the samples marked with times correspond to the samples marked with open circle but only considering the annihilation.

In Figs. 20(a)–20(d), we only show the allowed samples in which the allowed regions touch the experimental upper limits, namely, in the plots of $\Omega_\chi h^2$, $\sigma^{\rm SI}$, $\langle\sigma_{W^+W^-}v\rangle$ and $\langle\sigma_{b\bar{b}}v\rangle$ vs DM mass m_χ, respectively. By comparing with the plots in Fig. 5, we see that the $\tilde{H}$-like particles with 10 GeV $\lesssim m_\chi \lesssim m_W$ will now be detectable in the near future through the direct search experiment of SI DM-nucleus elastic scattering, while originally detectable $\tilde{H}$-like particles with mass $950 \lesssim m_\chi \lesssim 1680$ GeV in the SI DM-nucleon scattering experiment will now not detectable when considering the leading effect of coannihilation.

B. Conclusions

In this work, we construct a generic model of Majorana fermionic dark matter. Starting with two Weyl spinor multiplets $\eta_{1,2} \sim (I, \mp Y)$ coupled to the Standard Model Higgs, six additional Weyl spinor multiplets with $(I \pm 1/2, \pm(Y \pm 1/2))$ are needed in general. It has 13 parameters in total, five mass parameters and eight Yukawa couplings. The DM sector of the minimal supersymmetric Standard Model is a special case of the model with

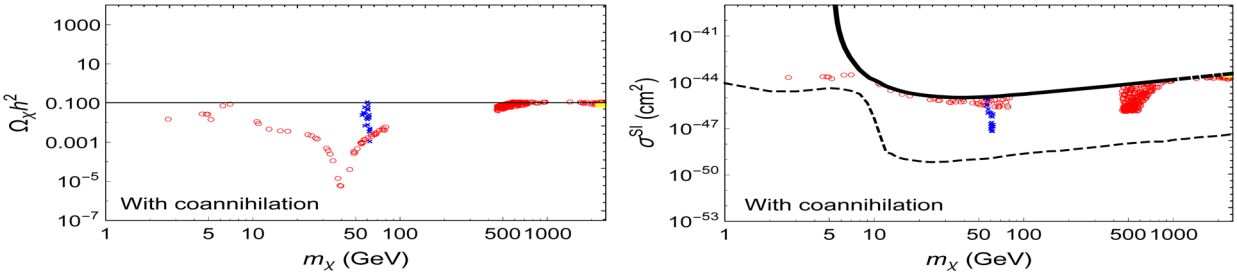

(a) Constraint on $\Omega_\chi^{\rm obs}$

(b) LUX constraint on σ^{SI} with NB limit

(c) Fermi-LAT constraint on $\chi^0\chi^0 \to W^+W^-$

(d) Fermi-LAT constraint on $\chi^0\chi^0 \to b\bar{b}$

FIG. 20. Results for allowed samples satisfying all constraints in the neutralinolike I case [open circle: Higgsino-like, times: binolike, filled circle: mixed].

$(I, Y) = (1/2, 1/2)$. Therefore, this model can be viewed as an extension of the neutralino DM sector. Nevertheless, this model does not have sfermions and the second Higgs as in the MSSM but have more Z_2-odd fermions. We consider three typical cases: the neutralinolike, the reduced, and the extended cases. For the neutralinolike case, we study four different scenarios (neutralinolike I–IV) according to whether the GUT relation on mass parameters or the $\tan\beta$ relation on the Yukawa couplings is imposed or not. For the reduced case, it has the minimal particle content, while the extended case has the maximal particle content. For each case, we generate 10,000 samples from the parameter space and survey the DM mass in the range of (1,2500) GeV. For each sample, we calculate the DM relic density $\Omega_\chi h^2$, the SI and SD DM-nucleon elastic scattering cross sections for direct searches, and the velocity averaged cross section of DM annihilation processes $\langle\sigma(\chi\chi \to W^+W^-, ZZ, ZH, HH, f\bar{f})v\rangle$ for an indirect search. We compare our results with 11 constraints from the observed DM relic density; the direct search of LUX, XENON100, and PICO-60 experiments; and the indirect search of Fermi-LAT data, respectively. We investigate the interplay of these three complementary searching strategies and tell the differences among the cases. For each case, we find the allowed DM candidates satisfying all the constraints and obtain the lower mass bounds of finding the $\tilde{H}$-, $\tilde{B}$-, $\tilde{W}$-, and non-neutralino-like DM particles. We discuss the properties of DM annihilation processes $\chi\chi \to W^+W^-, ZZ, ZH, HH, f\bar{f}$. We see that the processes of $\tilde{B}$-like particles annihilating to W^+W^- and ZZ do not have an s-wave contribution. The process $\chi\chi \to ZH$ is allowed to have an s-wave contribution, while the process $\chi\chi \to HH$ does not have an s-wave contribution. We also see that the process of $\chi\chi \to f\bar{f}$ has a helicity suppressed s-wave contribution. We find that the $\tilde{H}$- and $\tilde{B}$-like particles appear in all cases, and plenty of $\tilde{W}$-like particles can appear in the neutralinolike III and IV cases with the GUT relation relaxed and in the extended case. The non-MSSM-like $\tilde{X}$ particle can only appear in the extended case. We find that most of $\tilde{B}$-like particles are ruled out by the $\Omega_\chi h^2$ constraint and further by the LUX constraint; the $\tilde{H}$- and $\tilde{W}$-like particles and the non-neutralino-like $\tilde{X}$ particles with $m_\chi \lesssim M_W$ are ruled out by the $\Omega_\chi h^2$ and the Fermi-LAT $\langle\sigma(\chi\chi \to b\bar{b})v\rangle$ constraints, while the $\tilde{H}$- and $\tilde{W}$-like particles and the non-neutralino-like $\tilde{X}$ particles with $m_\chi > M_W$ are constrained by the Fermi-LAT $\langle\sigma(\chi\chi \to W^+W^-)v\rangle$ and the LUX $\sigma^{\rm SI}$ bounds. We note that in general the allowed $\tilde{H}$- and $\tilde{W}$-like particles and the non-neutralino-like $\tilde{X}$ particles are highly pure with composition fraction $\geq$90%. It is also true for $\tilde{B}$-like particles in the cases without GUT and $\tan\beta$ relations.

When we do not consider the coannihilation, we find the lower mass bounds to detect DM in the SI DM-nucleus scattering experiments and the suitable mass ranges to detect DM in the DM annihilation to the W^+W^- channel using the present limit and the projected limit (taken to be 1 order of magnitude lower than the present one). Apart from the outlier samples, the masses for finding the $\tilde{H}$-, $\tilde{B}$-, and $\tilde{W}$-like DM particles and the non-neutralino-like $\tilde{X}$ DM particles are given. The $\tilde{H}$-like particles can be detected

with DM mass $\gtrsim 450$ GeV in all cases. The $\tilde{B}$-like particles can be detected with mass $\gtrsim 1258$ GeV in the cases of neutralinolike I and II. On the other hand, the lower mass bound of $\tilde{B}$ can be as low as to 341 GeV to detect them for other cases. The $\tilde{W}$-like particles can be detected with DM mass $\gtrsim 1120$ GeV in the neutralinolike III and IV and the extended cases. Of course, the non-neutralino-like particles $\tilde{X}$ can only be detected with DM mass $\gtrsim 738$ GeV in the extended case. We also give the predictions on $\langle\sigma(\chi\chi \to ZZ, ZH, t\bar{t})v\rangle$ in the indirect search. The most rewarding way to find the DM particles in this model in the near future will be from the direct search of SI DM-nucleus scattering experiments and/or from the indirect search of DM annihilation processes via W^+W^-, ZZ, ZH, and $t\bar{t}$ channels. We also investigate the leading effect of coannihilation in the neutralinolike I case. The change is that the $\tilde{H}$-like particles with 10 GeV $\lesssim m_\chi \lesssim m_W$ will also be detectable through the direct search of the SI DM-nucleus scattering experiment in the near future, while $\tilde{H}$-like particles with mass $950 \lesssim m_\chi \lesssim 1680$ GeV will now become undetectable. The study of the generic Majorana fermion DM model can be further extended. The whole calculation of coannihilation is worthy of being probed further. The nonperturbative Sommerfeld effect also has not been implemented. These studies will be presented elsewhere. This work concentrates on $(I, Y) = (1/2, 1/2)$, but the formalism is generic and can be used to study with arbitrary (I, Y) quantum numbers.

ACKNOWLEDGMENTS

We thank Yi-Chin Yeh and Chung Kao for discussions. This research was supported by the Ministry of Science and Technology of Republic of China under Grant No. 104-2811-M-033-005 and in part by Grant No. 103-2112-M-033-002-MY3.

APPENDIX A: NEUTRAL AND CHARGED WIMP MASSES WITH $I = Y = 1/2$

For $I = Y = \frac{1}{2}$, η_7 and η_8 are singlets with charge ∓ 1; in other words, η_7^1 and η_8^{-1} are absent. The Lagrangian for the neutral WIMP mass term is modified as

$$\begin{aligned}-\mathcal{L}_m^0 =& \mu_1\lambda^1_{-\frac{1}{2},\frac{1}{2}}\eta_2^{-\frac{1}{2}}\eta_1^{\frac{1}{2}} + \frac{1}{2}\mu_2\lambda^2_{0,0}\eta_4^0\eta_3^0 + \frac{1}{2}\mu_3\lambda^3_{0,0}\eta_6^0\eta_5^0 \\ &+ \mu_5\lambda^5_{-1,1}\eta_{10}^{-1}\eta_9^1 + g_3\lambda^2_{\frac{1}{2},-\frac{1}{2},0}\langle\tilde{\phi}^{\frac{1}{2}}\rangle\eta_2^{-\frac{1}{2}}\eta_3^0 + g_4\lambda^2_{-\frac{1}{2},\frac{1}{2},0}\langle\phi^{-\frac{1}{2}}\rangle\eta_1^{\frac{1}{2}}\eta_4^0 \\ &+ g_5\lambda^3_{\frac{1}{2},-\frac{1}{2},0}\langle\tilde{\phi}^{\frac{1}{2}}\rangle\eta_2^{-\frac{1}{2}}\eta_5^0 + g_6\lambda^3_{-\frac{1}{2},\frac{1}{2},0}\langle\phi^{-\frac{1}{2}}\rangle\eta_1^{\frac{1}{2}}\eta_6^0 \\ &+ g_9\lambda^5_{-\frac{1}{2},-\frac{1}{2},1}\langle\phi^{-\frac{1}{2}}\rangle\eta_2^{-\frac{1}{2}}\eta_9^1 + g_{10}\lambda^5_{\frac{1}{2},\frac{1}{2},-1}\langle\tilde{\phi}^{\frac{1}{2}}\rangle\eta_1^{\frac{1}{2}}\eta_{10}^{-1} + \text{H.c.}\end{aligned} \tag{A1}$$

It can be simplified as

$$\begin{aligned}-\mathcal{L}_m^0 =& -\mu_1\eta_2^{-\frac{1}{2}}\eta_1^{\frac{1}{2}} + \frac{1}{2}\mu_2\eta_4^0\eta_3^0 - \frac{1}{2}\mu_3\eta_6^0\eta_5^0 + \mu_5\eta_{10}^{-1}\eta_9^1 \\ &+ g_3\langle\tilde{\phi}^{\frac{1}{2}}\rangle\eta_2^{-\frac{1}{2}}\eta_3^0 - g_4\langle\phi^{-\frac{1}{2}}\rangle\eta_1^{\frac{1}{2}}\eta_4^0 \\ &- g_5\langle\tilde{\phi}^{\frac{1}{2}}\rangle\eta_2^{-\frac{1}{2}}\eta_5^0 - g_6\langle\phi^{-\frac{1}{2}}\rangle\eta_1^{\frac{1}{2}}\eta_6^0 \\ &+ g_9\sqrt{2}\langle\phi^{-\frac{1}{2}}\rangle\eta_2^{-\frac{1}{2}}\eta_9^1 + g_{10}\sqrt{2}\langle\tilde{\phi}^{\frac{1}{2}}\rangle\eta_1^{\frac{1}{2}}\eta_{10}^{-1} + \text{H.c.}\end{aligned} \tag{A2}$$

With the basis $\Psi_i^{0T} = (\eta_1^{1/2}, \eta_2^{-1/2}, \eta_3^0, \eta_5^0, \eta_9^1, \eta_{10}^{-1})$, Eq. (A2) can be written as

$$\mathcal{L}_m^0 = -\frac{1}{2}\Psi^{0T}Y\Psi^0 + \text{H.c.}, \tag{A3}$$

where the corresponding mass matrix Y takes the form

$$\begin{pmatrix} 0 & -\mu_1 & -\frac{g_4 v}{\sqrt{2}} & \frac{g_6 v}{\sqrt{2}} & 0 & g_{10} v \\ -\mu_1 & 0 & \frac{g_3 v}{\sqrt{2}} & \frac{-g_5 v}{\sqrt{2}} & g_9 v & 0 \\ -\frac{g_4 v}{\sqrt{2}} & \frac{g_3 v}{\sqrt{2}} & \mu_2 & 0 & 0 & 0 \\ \frac{g_6 v}{\sqrt{2}} & \frac{-g_5 v}{\sqrt{2}} & 0 & \mu_3 & 0 & 0 \\ 0 & g_9 v & 0 & 0 & 0 & \mu_5 \\ g_{10} v & 0 & 0 & 0 & \mu_5 & 0 \end{pmatrix}. \tag{A4}$$

For $I = Y = \frac{1}{2}$, the Lagrangian for the single charged WIMP mass term is modified as

$$\begin{aligned}-\mathcal{L}_m^\pm =& \mu_1\eta_2^{\frac{1}{2}}\eta_1^{-\frac{1}{2}} + \frac{1}{2}\mu_3(\eta_6^1\eta_5^{-1} + \eta_6^{-1}\eta_5^1) + \mu_4\eta_8^0\eta_7^0 - \mu_5\eta_{10}^0\eta_9^0 \\ &+ g_5\sqrt{2}\langle\tilde{\phi}^{\frac{1}{2}}\rangle\eta_2^{\frac{1}{2}}\eta_5^{-1} + g_6\sqrt{2}\langle\phi^{-\frac{1}{2}}\rangle\eta_1^{-\frac{1}{2}}\eta_6^1 - g_7\langle\phi^{-\frac{1}{2}}\rangle\eta_2^{-\frac{1}{2}}\eta_7^0 \\ &+ g_8\langle\tilde{\phi}^{\frac{1}{2}}\rangle\eta_1^{\frac{-1}{2}}\eta_8^0 - g_9\langle\phi^{-\frac{1}{2}}\rangle\eta_2^{\frac{1}{2}}\eta_9^0 - g_{10}\langle\tilde{\phi}^{\frac{1}{2}}\rangle\eta_1^{-\frac{1}{2}}\eta_{10}^0 + \text{H.c.}\end{aligned} \tag{A5}$$

With the basis $\Psi_i^{+T} = (\eta_2'^{1/2}, \eta_5'^1, \eta_8'^0, \eta_{10}'^0)$ and $\Psi_i^{-T} = (\eta_1^{-1/2}, \eta_5^{-1}, \eta_7^0, \eta_9^0)$, the above Lagrangian becomes

$$\begin{aligned}-\mathcal{L}_m^\pm =& \mu_1\eta_2^+\eta_1^- + \frac{1}{2}\mu_3(\eta_5'^+\eta_5^- + \eta_5^-\eta_5'^+) - \mu_4\eta_8'^+\eta_7^- + \mu_5\eta_{10}'^+\eta_9^- \\ &+ g_5\sqrt{2}\langle\tilde{\phi}^0\rangle\eta_2^+\eta_5^- + g_6\sqrt{2}\langle\phi^0\rangle\eta_1^-\eta_5'^+ - g_7\langle\phi^0\rangle\eta_2^+\eta_7^- \\ &- g_8\langle\tilde{\phi}^0\rangle\eta_1^-\eta_8'^+ - g_9\langle\phi^0\rangle\eta_2^+\eta_9^- + g_{10}\langle\tilde{\phi}^0\rangle\eta_1^-\eta_{10}'^+ + \text{H.c.}\end{aligned} \tag{A6}$$

Hence, it can be written in the compact form as

$$\mathcal{L}_m^\pm = -\frac{1}{2}(\Psi^+, \Psi^-)\begin{pmatrix} 0 & X^T \\ X & 0 \end{pmatrix}\begin{pmatrix} \Psi^+ \\ \Psi^- \end{pmatrix} + \text{H.c.}, \tag{A7}$$

where X takes the form

$$\begin{pmatrix} \mu_1 & g_6 v & \frac{-g_8 v}{\sqrt{2}} & \frac{g_{10} v}{\sqrt{2}} \\ g_5 v & \mu_3 & 0 & 0 \\ \frac{-g_7 v}{\sqrt{2}} & 0 & -\mu_4 & 0 \\ \frac{-g_9 v}{\sqrt{2}} & 0 & 0 & \mu_5 \end{pmatrix}. \tag{A8}$$

APPENDIX B: MASS EIGENSTATES FOR THE NEUTRAL AND CHARGED WIMPs

For the neutral WIMPs, their four-component representations are of the form

$$\psi_k^0 = \begin{pmatrix} \eta_k^{q_k} \\ \bar{\eta}_k^{q_k} \end{pmatrix}. \tag{B1}$$

In the above, q_k is defined as the third component of the isospin of η_k as mentioned in the text. For $I = Y = 1/2$ with the basis $\Psi_i^{0T} = (\eta_1^{1/2}, \eta_2^{-1/2}, \eta_3^0, \eta_5^0, \eta_9^1, \eta_{10}^{-1})$, $q_i = (1/2, -1/2, 0, 0, 1, -1)$. The four-component mass eigenstates can be obtained by doing a transformation with a unitary matrix N as

$$\chi_i^0 \equiv \begin{pmatrix} \zeta_i^0 \\ \bar{\zeta}_j^0 \end{pmatrix} = (N_{ij} P_L + N_{ij}^* P_R)\psi_j^0 \tag{B2}$$

so that $M_D^0 \equiv N^* Y N^\dagger$ is a diagonal matrix with nonnegative entries $m_{\chi_k^0}$. Hence, the mass term in Eq. (25) becomes

$$\begin{aligned} \mathcal{L}_m^0 &= -\frac{1}{2}\Psi^{0T} Y \Psi^0 + \text{H.c.} \\ &= -\frac{1}{2}\sum_k m_{\chi_k^0} \bar{\chi}_k^0 \chi_k^0. \end{aligned} \tag{B3}$$

For the single charged WIMPs, their four-component representations are of the form

$$\psi_k^+ = \begin{pmatrix} \eta_k'^{q_k+1} \\ \bar{\eta}_k^{q_{k-1}} \end{pmatrix} \quad \text{and} \quad \psi_k^- = \begin{pmatrix} \eta_k^{q_k-1} \\ \bar{\eta}_k'^{q_{k+1}} \end{pmatrix}. \tag{B4}$$

For $I = Y = 1/2$, with the basis $\Psi_i^{+T} = (\eta_2'^{1/2}, \eta_5'^1, \eta_8'^0, \eta_{10}'^0)$, $q_i = (-1/2, 0, -1, -1)$ and $\Psi_i^{-T} = (\eta_1^{-1/2}, \eta_5^{-1}, \eta_7^0, \eta_9^0)$, $q_i = (1/2, 0, 1, 1)$, the four-component mass eigenstates can be obtained by doing the transformation with two unitary matrices U and V as

$$\begin{aligned} \chi_i &\equiv \begin{pmatrix} \zeta_i^+ \\ \bar{\zeta}_j^- \end{pmatrix} = (V_{ij} P_L + U_{ij}^* P_R)\psi_j^+ \quad \text{and} \\ \chi_i^c &= \begin{pmatrix} \zeta_j^- \\ \bar{\zeta}^+ \end{pmatrix} = (U_{ij} P_L + V_{ij}^* P_R)\psi_j^- \end{aligned} \tag{B5}$$

so that $M_D^\pm \equiv U^* X V^\dagger$ is a diagonal matrix with nonnegative entries $m_{\chi_k^+}$. Hence, the mass term in Eq. (A7) becomes

$$\begin{aligned} \mathcal{L}_m^\pm &= -\frac{1}{2}(\Psi^+, \Psi^-)\begin{pmatrix} 0 & X^T \\ X & 0 \end{pmatrix}\begin{pmatrix} \Psi^+ \\ \Psi^- \end{pmatrix} + \text{H.c.} \\ &= -\sum_k m_{\chi_k^+} \bar{\chi}_k \chi_k. \end{aligned} \tag{B6}$$

APPENDIX C: LAGRANGIAN FOR WIMPs INTERACTING WITH SM PARTICLES

The Lagrangian for WIMPs interacting with the SM gauge bosons in four-component notation can be derived from the following gauge invariance terms with two-component notation [28] using the generic Lagrangian in Eq. (12) and Appendixes A and B:

$$-(g T_{ij}^a V_\mu^a + g' y_i \delta_{ij} V_\mu')\bar{\psi}^i \bar{\sigma}^\mu \psi^j. \tag{C1}$$

In the following, we just write down the results.

For $I = Y = 1/2$, the Lagrangian of the W-boson interaction with the neutral and single charged WIMPs can be written as

$$\begin{aligned} \mathcal{L}_{\chi^0 \chi^\mp W^\pm} = -\frac{g}{\sqrt{2}}\{ & W_\mu^- [\bar{\chi}_i^0 \gamma^\mu (O_{ij}^{L_{W^-}} P_L + O_{ij}^{R_{W^-}} P_R)\chi_j^+] \\ & + W_\mu^+ [\bar{\chi}_i^+ \gamma^\mu (O_{ij}^{L_{W^+}} P_L + O_{ij}^{R_{W^+}} P_R)\chi_j^0]\}, \end{aligned} \tag{C2}$$

where

$$\begin{cases} O_{ij}^{L_{W^-}} = \sum_{k=1}^6 \sum_{l=1}^4 (-1)^{\text{mod}\,(2I_j,2)+1} N_{ik} T_{ki}^{+0T} V_{lj}^\dagger \quad \text{with} \quad O_{ij}^{L_{W^+}} = (O^{L_{W^-}})_{ij}^\dagger \\ O_{ij}^{R_{W^-}} = -\sum_{k=1}^6 \sum_{l=1}^4 N_{ik}^* T_{kj}^{0-} U_{lj}^T \quad \text{with} \quad O_{ij}^{R_{W^+}} = (O^{R_{W^-}})_{ij}^\dagger, \end{cases} \tag{C3}$$

and

$$T^{+0T}_{kl} = \begin{pmatrix} 0 & 0 & 0 & 0 \\ 1 & 0 & 0 & 0 \\ 0 & 0 & 0 & 0 \\ 0 & \sqrt{2} & 0 & 0 \\ 0 & 0 & 0 & 0 \\ 0 & 0 & 0 & \sqrt{2} \end{pmatrix}, \quad T^{0-}_{kl} = \begin{pmatrix} 1 & 0 & 0 & 0 \\ 0 & 0 & 0 & 0 \\ 0 & 0 & 0 & 0 \\ 0 & \sqrt{2} & 0 & 0 \\ 0 & 0 & 0 & 0 \\ 0 & 0 & 0 & \sqrt{2} \end{pmatrix}. \tag{C4}$$

The Lagrangian of the Z-boson interaction with the neutral WIMPs is

$$\mathcal{L}_{\chi^0_i\chi^0_j Z} = \frac{g}{2\cos\theta_W} Z_\mu \bar{\chi}^0_i \gamma^\mu (O^{L_Z}_{ij} P_L + O^{R_Z}_{ij} P_R)\chi^0_j, \tag{C5}$$

where

$$O^{L_Z}_{ij} = \sum_{k=1}^{6} q_k N_{ik} N^\dagger_{kj} \quad \text{with} \quad O^{R_Z}_{ij} = -O^{L_Z *}_{ij}. \tag{C6}$$

On the other hand, $O^{L_Z}_{11} = O^{L_Z *}_{11}$. Hence, the Lagrangian for the stable dark matter annihilation via the Z boson can be further simplified as

$$\mathcal{L}_{\chi^0_1\chi^0_1 Z} = -\frac{g}{2\cos\theta_W} O^{L_Z}_{11} Z_\mu \bar{\chi}^0_1 \gamma^\mu \gamma^5 \chi^0_1. \tag{C7}$$

The Lagrangian of the Higgs-boson interactions with the neutral WIMPs is

$$\mathcal{L}_{\chi^0_i\chi^0_j H^0} = -H^0 \bar{\chi}^0_i (O^{L_H}_{ij} P_L + O^{R_H}_{ij} P_R)\chi^0_j, \tag{C8}$$

where

$$O^{L_H}_{ij} = N^*_{ik} f_{kl} N^\dagger_{lj} \quad \text{with} \quad O^{R_H}_{ij} = (O^{L_H}_{ij})^*, \tag{C9}$$

and

$$f_{kl} = \begin{pmatrix} 0 & 0 & -\frac{g_4}{\sqrt{2}} & \frac{g_6}{\sqrt{2}} & 0 & g_{10} \\ 0 & 0 & \frac{g_3}{\sqrt{2}} & -\frac{g_5}{\sqrt{2}} & g_9 & 0 \\ -\frac{g_4}{\sqrt{2}} & \frac{g_3}{\sqrt{2}} & 0 & 0 & 0 & 0 \\ \frac{g_6}{\sqrt{2}} & \frac{g_5}{\sqrt{2}} & 0 & 0 & 0 & 0 \\ 0 & g_9 & 0 & 0 & 0 & 0 \\ g_{10} & 0 & 0 & 0 & 0 & 0 \end{pmatrix}. \tag{C10}$$

For coannihilation, we need the Lagrangian of the Z-boson interaction with the single charged WIMPs,

$$\mathcal{L}_{\chi^-_i\chi^+_j Z} = \frac{g}{\cos\theta_W} Z_\mu \bar{\chi}^+_i \gamma^\mu (O^{L^+_Z}_{ij} P_L + O^{R^+_Z}_{ij} P_R)\chi^+_j - eA_\mu \bar{\tilde{\chi}}^+_i \gamma^\mu \chi^+_i, \tag{C11}$$

where

$$O^{L^+_Z}_{ij} = -\frac{1}{2} V_{i1} V^*_{j1} - V_{i2} V^*_{j2} + \delta_{ij} \sin^2\theta_W,$$
$$O^{R^+_Z}_{ij} = -\frac{1}{2} U^*_{i1} U_{j1} - U^*_{i2} U_{j2} + \delta_{ij} \sin^2\theta_W. \tag{C12}$$

We also need the Lagrangian of the Higgs-boson interaction with the single charged WIMPs,

$$\mathcal{L}_{\chi^-_i\chi^+_j H^0} = H^0 \bar{\chi}^+_i (O^{L^+_H}_{ij} P_L + O^{R^+_H}_{ij} P_R)\chi^+_j, \tag{C13}$$

where

$$O^{L^+_H}_{ij} = U^*_{ik} h^L_{kl} V^\dagger_{lj} \quad \text{with} \quad O^{R^+_H}_{ij} = V_{ik} h^R_{kl} U^T_{lj} \tag{C14}$$

and

$$h^L_{lk} = \begin{pmatrix} 0 & -g_6 & \frac{g_8}{\sqrt{2}} & -\frac{g_1 0}{\sqrt{2}} \\ -g_5 & 0 & 0 & 0 \\ \frac{g_7}{\sqrt{2}} & 0 & 0 & 0 \\ \frac{g_9}{\sqrt{2}} & 0 & 0 & 0 \end{pmatrix} \quad \text{and}$$
$$h^R_{lk} = h^L_{kl}. \tag{C15}$$

APPENDIX D: MATRIX ELEMENTS FOR DARK MATTER ANNIHILATION

1. $\chi^0_1\chi^0_1 \to W^+W^-$

The dark matter can annihilate into W^+W^- via the t-channel exchange of a single charged WIMP and the s-channel exchange of a Z^0 boson or H^0 scalar corresponding to the matrix element

$$M(\chi^0_1\chi^0_1 \to W^+W^-) = M_{1a} + M_{1b} + 2M_{2a} + 2M_{3a}, \tag{D1}$$

where

$$
\begin{aligned}
M_{1a} &= -i\sum_k \frac{g^2}{2}\frac{1}{t-m^2_{\chi_k^+}}[\bar{v}(p_1)\gamma^\mu(O^{L_{W^-}}_{1k}P_L + O^{R_{W^-}}_{1k}P_R)(\not{p}_3 - \not{p}_1 + m_{\chi_k^+})\\
&\quad \times \gamma^\nu(O^{L_{W^+}}_{k1}P_L + O^{R_{W^+}}_{k1}P_R)u(p_2)\epsilon^*_\mu(p_3)\epsilon^*_\nu(p_4)],\\
M_{1b} &= -i\sum_k \frac{g^2}{2}\frac{1}{u-m^2_{\chi_k^+}}[\bar{v}(p_1)\gamma^\nu(O^{L_{W^+}}_{k1}P_L + O^{R_{W^+}}_{k1}P_R)(\not{p}_4 - \not{p}_1 + m_{\chi_k^+})\\
&\quad \times \gamma^\mu(O^{L_{W^-}}_{1k}P_L + O^{R_{W^-}}_{1k}P_R)u(p_2)\epsilon^*_\mu(p_3)\epsilon^*_\nu(p_4)],\\
M_{2a} &= -i\frac{g^2}{2}O^{L_Z}_{11}\frac{1}{s-M_Z^2+iM_Z\Gamma_Z}\bar{v}(p_1)\gamma^5[(\not{p}_3 - \not{p}_4)(\epsilon^*(p_3)\cdot\epsilon^*(p_4))\\
&\quad - \not{\epsilon}^*(p_4)(p_4\cdot\epsilon^*(p_3)) + \not{\epsilon}^*(p_3)(p_3\cdot\epsilon^*(p_4))],\\
M_{3a} &= -igM_W\frac{1}{s-M_H^2+iM_H\Gamma_H}\bar{v}(p_1)(O^{L_H}_{11}P_L + O^{R_H}_{11}P_R)u(p_2)\epsilon^*_\mu(p_3)\cdot\epsilon^*_\nu(p_4).
\end{aligned}
\tag{D2}
$$

2. $\chi_1^0\chi_1^0 \to H^0H^0$

The dark matter can annihilate into H^0H^0 via the s-channel exchange of a H^0 scalar and the t-channel exchange of a neutral WIMP corresponding to the matrix element

$$
M(\chi_1^0\chi_1^0 \to H^0H^0) = 2M_{1a} + M_{2a} + M_{2b} + M_{2c} + M_{2d},
\tag{D3}
$$

where

$$
\begin{aligned}
M_{1a} &= -ig\frac{3m_H^2}{2M_W}\frac{1}{s-m_H^2+im_H\Gamma_H}\bar{v}(p_1)(O^{L_H}_{11}P_L + O^{R_H}_{11}P_R)u(p_2),\\
M_{2a} &= -i\sum_k \frac{1}{t-m^2_{\chi_k^0}}\bar{v}(p_1)(O^{L_H}_{1k}P_L + O^{R_H}_{1k}P_R)(\not{p}_3 - \not{p}_1 + m_{\chi_0^+})(O^{L_H}_{k1}P_L + O^{R_H}_{k1}P_R)u(p_2),\\
M_{2b} &= -i\sum_k \frac{1}{u-m^2_{\chi_k^0}}\bar{v}(p_1)(O^{L_H}_{k1}P_L + O^{R_H}_{k1}P_R)(\not{p}_4 - \not{p}_1 + m_{\chi_0^+})(O^{L_H}_{1k}P_L + O^{R_H}_{1k}P_R)u(p_2),\\
M_{2c} &= -i\sum_k \frac{1}{u-m^2_{\chi_k^0}}\bar{v}(p_1)(O^{L_H}_{1k}P_L + O^{R_H}_{1k}P_R)(\not{p}_4 - \not{p}_1 + m_{\chi_0^+})(O^{L_H}_{k1}P_L + O^{R_H}_{k1}P_R)u(p_2),\\
M_{2d} &= -i\sum_k \frac{1}{t-m^2_{\chi_k^0}}\bar{v}(p_1)(O^{L_H}_{k1}P_L + O^{R_H}_{k1}P_R)(\not{p}_3 - \not{p}_1 + m_{\chi_0^+})(O^{L_H}_{1k}P_L + O^{R_H}_{1k}P_R)u(p_2).
\end{aligned}
\tag{D4}
$$

3. $\chi_1^0\chi_1^0 \to Z^0Z^0$

The dark matter can annihilate into Z^0Z^0 via the t-channel exchange of a neutral WIMP and the s-channel exchange of a H^0 scalar corresponding to the matrix element

$$
M(\chi_1^0\chi_1^0 \to Z^0Z^0) = M_{1a} + M_{1b} + M_{1c} + M_{1d} + 4M_{2a},
\tag{D5}
$$

where

$$M_{1a} = -i\left(\frac{g}{2\cos\theta_W}\right)^2 \frac{1}{t - m^2_{\chi^0_k}} [\bar{v}(p_1)\gamma^\mu (O^{L_Z}_{1k} P_L + O^{R_Z}_{1k} P_R)(\not{p}_3 - \not{p}_1 + m_{\chi^0_k})\gamma^\nu (O^{L_Z}_{k1} P_L + O^{R_Z}_{k1} P_R) u(p_2)]\epsilon^*_\mu(p_3)\epsilon^*_\nu(p_4),$$

$$M_{1b} = -i\left(\frac{g}{2\cos\theta_W}\right)^2 \frac{1}{u - m^2_{\chi^0_k}} [\bar{v}(p_1)\gamma^\nu (O^{L_Z}_{k1} P_L + O^{R_Z}_{k1} P_R)(\not{p}_4 - \not{p}_1 + m_{\chi^0_k})\gamma^\mu (O^{L_Z}_{1k} P_L + O^{R_Z}_{1k} P_R) u(p_2)]\epsilon^*_\mu(p_3)\epsilon^*_\nu(p_4),$$

$$M_{1c} = -i\left(\frac{g}{2\cos\theta_W}\right)^2 \frac{1}{u - m^2_{\chi^0_k}} [\bar{v}(p_1)\gamma^\nu (O^{L_Z}_{1k} P_L + O^{R_Z}_{1k} P_R)(\not{p}_4 - \not{p}_1 + m_{\chi^0_k})\gamma^\mu (O^{L_Z}_{k1} P_L + O^{R_Z}_{k1} P_R) u(p_2)]\epsilon^*_\mu(p_3)\epsilon^*_\nu(p_4),$$

$$M_{1d} = -i\left(\frac{g}{2\cos\theta_W}\right)^2 \frac{1}{t - m^2_{\chi^0_k}} [\bar{v}(p_1)\gamma^\mu (O^{L_Z}_{k1} P_L + O^{R_Z}_{k1} P_R)(\not{p}_3 - \not{p}_1 + m_{\chi^0_k})\gamma^\nu (O^{L_Z}_{1k} P_L + O^{R_Z}_{1k} P_R) u(p_2)]\epsilon^*_\mu(p_3)\epsilon^*_\nu(p_4),$$

$$M_{2a} = i\left(\frac{g}{2\cos\theta_W}\right) M_Z \frac{1}{s - M^2_H + iM_H\Gamma_H} [\bar{v}(p_1)(O^{L_H}_{11} P_L + O^{R_H}_{11} P_R) u(p_2)]. \tag{D6}$$

4. $\chi^0_1\chi^0_1 \to H^0Z^0$

The dark matter can annihilate into H^0Z^0 via the t-channel exchange of a neutral WIMP and s-channel exchange of a Z^0 boson corresponding to the matrix element

$$M(\chi^0_1\chi^0_1 \to HZ) = M_{1a} + M_{1b} + 4M_{2a}, \tag{D7}$$

where

$$M_{1a} = i\frac{g}{2\cos\theta_W}\frac{1}{t - m^2_{\chi^0_k}} [\bar{v}(p_1)\gamma^\mu (O^{L_Z}_{1k} P_L + O^{R_Z}_{1k} P_R)(\not{p}_3 - \not{p}_1 + m_{\chi^0_k})(O^{L_H}_{k1} P_L + O^{R_H}_{k1} P_R) u(p_2)]\epsilon^*_\mu(p_3),$$

$$M_{1b} = i\frac{g}{2\cos\theta_W}\frac{1}{u - m^2_{\chi^0_k}} [\bar{v}(p_1)(O^{L_H}_{k1} P_L + O^{R_H}_{k1} P_R)(\not{p}_3 - \not{p}_1 + m_{\chi^0_k})(O^{L_Z}_{1k} P_L + O^{R_Z}_{1k} P_R)\gamma^\mu u(p_2)]\epsilon^*_\mu(p_3),$$

$$M_{2a} = -i\left(\frac{g}{2\cos\theta_W}\right)^2 O^{L_Z}_{11} M_Z \frac{1}{s - M^2_Z + iM_Z\Gamma_Z} [\bar{v}(p_1)\gamma^\alpha\gamma^5 u(p_2)]\epsilon^*_\alpha(p_3). \tag{D8}$$

5. $\chi^0_1\chi^0_1 \to f\bar{f}$

The dark matter can annihilate into $f\bar{f}$ via the s-channel exchange of a Z^0 boson or a H^0 scalar corresponding to the matrix element

$$M(\chi^0_1\chi^0_1 \to f\bar{f}) = 2M_{1a} + 2M_{2a}, \tag{D9}$$

where

$$M_{1a} = i\left(\frac{g}{2\cos\theta_W}\right)^2 O^{L_Z}_{11} M_Z \frac{1}{s - M^2_Z + iM_Z\Gamma_Z} g_{\alpha\mu} [\bar{v}(p_1)\gamma^\alpha\gamma^5 u(p_2)][\bar{u}(p_3)\gamma^\mu](g^f_V + g^f_A\gamma^5) v(p_4)],$$

$$M_{2a} = -i\frac{gm_f}{2M_W}\frac{1}{s - M^2_H + iM_H\Gamma_H} [\bar{v}(p_1)(O^{L_H}_{11} P_L + O^{R_H}_{11} P_R) u(p_2)][\bar{u}(p_3) v(p_4)] \tag{D10}$$

with $g^f_V = \frac{1}{2}T^f_{3L} - Q^f \sin^2\theta_W$, and $g^f_A = -\frac{1}{2}T^f_{3L}$.

APPENDIX E: *CP* symmetry

Before transforming the gauge eigenstates to mass eigenstates, all parameters in the Lagrangian are assumed to be real in this model. The Lagrangian is CP conserved. After field redefinition, some parameters become purely imaginary. The Lagrangian should still be CP conserved. We explicitly show this and a useful application below.

The CP transformation of a four-component field is given by

$$\mathcal{C}P\chi_i(x)\mathcal{P}^\dagger\mathcal{C}^\dagger = \rho_{CP,\chi_i}\gamma_0\chi_i^c(\tilde{x}) = \rho_{CP,\chi_i}\gamma_0 C\bar{\chi}_i^T(\tilde{x}), \quad \text{(E1)}$$

with the phase ρ_{CP,χ_i} for χ_i, $\tilde{x}^\mu \equiv x_\mu$ and $C = i\gamma_2\gamma_0$. For a Majorana field, we have $\chi_i^c = \rho_{M,\chi_i}\chi_i$, where ρ_{M,χ_i} is a phase. Equation (E1) implies that $\rho_{CP,\chi_i}\rho_{M,\chi_i}$ is purely imaginary [60]. This can be seen by using $v(\vec{p},s) = C\bar{u}^T(\vec{p},s)$, $u(\vec{p},s) = C\bar{v}^T(\vec{p},s)$, $\gamma_0 u(\vec{p},s) = u(-\vec{p},-s)$, $\gamma_0 v(\vec{p},s) = -v(\vec{p},-s)$,

$$\mathcal{C}P\chi_i(x)\mathcal{P}^\dagger\mathcal{C}^\dagger = \rho_{CP,\chi_i}\gamma_0\chi_i^c(\tilde{x}) = \rho_{CP,\chi_i}\rho_{M,\chi_i}\gamma_0\chi_i(\tilde{x}), \quad \text{(E2)}$$

and

$$\chi_i(x) = \int \frac{d^3p}{(2\pi)^3 2E}(b_i(\vec{p},s)u(\vec{p},s)e^{-ip\cdot x} + b_i^\dagger(\vec{p},s)\rho_{M\chi_i}^* v(\vec{p},s)e^{ip\cdot x}), \quad \text{(E3)}$$

which imply

$$\mathcal{C}Pb_i^\dagger(\vec{p},s)(\mathcal{C}P)^\dagger = \rho_{CP,\chi_i}^*\rho_{M,\chi_i}^* b_i^\dagger(-\vec{p},-s) = -\rho_{CP,\chi_i}\rho_{M,\chi_i} b_i^\dagger(-\vec{p},-s). \quad \text{(E4)}$$

Hence, the phase $\rho_{CP,\chi_i}\rho_{M,\chi_i}$ is purely imaginary.

As shown in Appendix B, the neutral WIMP mass eigenstates are defined (in two-component notation) by

$$\zeta_i^0 = N_{ij}\eta_j^0. \quad \text{(E5)}$$

In the above, the superscript in η_j here denotes the charge instead of the third component of isospin, and N is a unitary matrix satisfying

$$N^* Y N^{*T} = M_D^0, \quad \text{(E6)}$$

where M_D^0 is a diagonal matrix with non-negative entries. Note, in the case one obtains a negative mass in the first place, the negative sign in front of the mass m_i can be absorbed in N_{ij} with N_{ij} being purely imaginary in the corresponding i row.

The four-component neutral Majorana states are defined as

$$\chi_i^0 = \begin{pmatrix} \zeta_i^0 \\ \bar{\zeta}_i^0 \end{pmatrix} = \begin{pmatrix} N_{ij}\eta_i^0 \\ N_{ij}^*\bar{\eta}_i^0 \end{pmatrix} = N_{ij}P_L\psi_i^0 + N_{ij}^* P_R\psi_i^0, \quad \text{(E7)}$$

where

$$\psi_i^0 \equiv \begin{pmatrix} \eta_i^0 \\ \bar{\eta}_i^0 \end{pmatrix}. \quad \text{(E8)}$$

From above definition, we have $\psi_i^{0c} = \psi_i^0$ and $\chi_i^{0c} = \chi_i^0$ so that $\rho_{M,\chi_i} = \rho_{M,\psi_i} = 1$.

For some given i, N_{ij} are real, which gives

$$\chi_i^0 = \begin{pmatrix} N_{ij}\eta_i^0 \\ N_{ij}\bar{\eta}_i^0 \end{pmatrix} = N_{ij}\psi_i^0 = N_{ij}(P_L\psi_i^0 + P_R\psi_i^0). \quad \text{(E9)}$$

We now assume that ψ_i^0 has common $\rho_{CP,\psi}$ for all i. Therefore, we have

$$\mathcal{C}P\psi_i^0(x)\mathcal{P}^\dagger\mathcal{C}^\dagger = \rho_{CP,\psi}\gamma_0\psi_i^0(\tilde{x}). \quad \text{(E10)}$$

For the case of real N_{ij} for some i, we now have

$$\mathcal{C}P\chi_i^0(x)\mathcal{P}^\dagger\mathcal{C}^\dagger = N_{ij}\mathcal{C}P\psi_i^0(x)\mathcal{P}^\dagger\mathcal{C}^\dagger = \rho_{CP,\psi}\gamma_0 N_{ij}\psi_i^0(\tilde{x}). \quad \text{(E11)}$$

We obtain for the real N_{ij} case

$$\rho_{CP,\chi_i} = \rho_{CP,\psi}. \quad \text{(E12)}$$

If for some i, N_{ij} are imaginary, i.e., $N_{ij}^* = -N_{ij}$, we now have

$$\chi_i^0 = \begin{pmatrix} N_{ij}\eta_i^0 \\ N_{ij}^*\bar{\eta}_i^0 \end{pmatrix} = \begin{pmatrix} N_{ij}\eta_i^0 \\ -N_{ij}\bar{\eta}_i^0 \end{pmatrix} = N_{ij}(-\gamma_5)\psi_i^0 = N_{ij}(P_L\psi_i^0 - P_R\psi_i^0). \quad \text{(E13)}$$

Note that the relative sign of $P_L\tilde{\psi}_i^0$ and $P_R\tilde{\psi}_i^0$ is the key to absorbing the minus of the mass term, which consists of left-handed and right-handed fields at the same time. The CP transformation of χ_i^0 is

$$\mathcal{C}P\chi_i^0(x)\mathcal{P}^\dagger\mathcal{C}^\dagger = N_{ij}(-\gamma_5)\mathcal{C}P\psi_i^0(x)\mathcal{P}^\dagger\mathcal{C}^\dagger = \rho_{CP,\psi}(-\gamma_5)\gamma_0 N_{ij}\psi_i^0(\tilde{x}) = -\rho_{CP,\psi}\gamma_0\chi_i^0(\tilde{x}). \quad \text{(E14)}$$

We obtain for the imaginary N_{ij} case

$$\rho_{CP,\chi_i} = -\rho_{CP,\psi}. \quad \text{(E15)}$$

Consider a Hermitian operator $\mathcal{O}(x)$:

$$\mathcal{O}_{ij}(x) = v_{ij}\bar{\chi}_i(x)\gamma_\mu T^a A^{a\mu}(x)\chi_j(x) + a_{ij}\bar{\chi}_i(x)\gamma_\mu\gamma_5 T^a A^{a\mu}(x)\chi_j(x) + [v_{ij}\bar{\chi}_i(x)\gamma_\mu T^a A^{a\mu}(x)\chi_j(x) + a_{ij}\bar{\chi}_i(x)\gamma_\mu\gamma_5 T^a A^{a\mu}(x)\chi_j(x)]^\dagger. \quad \text{(E16)}$$

For example, in Eq. (C5), we have

$$v_{ij} = \frac{g}{4\cos\theta_W}(O_{ij}^{L_Z} + O_{ij}^{R_Z}),$$
$$a_{ij} = \frac{g}{4\cos\theta_W}(-O_{ij}^{L_Z} + O_{ij}^{R_Z}) \tag{E17}$$

with $O_{ij}^{L_Z} = \sum_{k=1}^{6} q_k N_{ik} N_{kj}^{\dagger}$ and $O_{ij}^{R_Z} = -O_{ij}^{L_{Z^*}}$.

Under CP transformation, the operator transforms as

$$\begin{aligned}\mathcal{CP}\mathcal{O}_{ij}(x)\mathcal{P}^{\dagger}\mathcal{C}^{\dagger} = {} & v_{ij}\rho^{*}_{CP,\chi_i}\rho_{CP,\chi_j}[\bar{\chi}_i(\tilde{x})\gamma_\mu T^a A^{a\mu}(\tilde{x})\chi_j(\tilde{x})]^{\dagger} \\ & + a_{ij}\rho^{*}_{CP,\chi_i}\rho_{CP,\chi_j}[\bar{\chi}_i(\tilde{x})\gamma_\mu\gamma_5 T^a A^{a\mu}(\tilde{x})\chi_j(\tilde{x})]^{\dagger} \\ & + v^{*}_{ij}\rho_{CP,\chi_i}\rho^{*}_{CP,\chi_j}\bar{\chi}_i(\tilde{x})\gamma_\mu T^a A^{a\mu}(\tilde{x})\chi_j(\tilde{x}) \\ & + a^{*}_{ij}\rho_{CP,\chi_i}\rho^{*}_{CP,\chi_j}\bar{\chi}_i(\tilde{x})\gamma_\mu\gamma_5 T^a A^{a\mu}(\tilde{x})\chi_j(\tilde{x}).\end{aligned} \tag{E18}$$

To have CP symmetry, one requires

$$\mathcal{CP}\int d^4x\mathcal{O}_{ij}(x)\mathcal{P}^{\dagger}\mathcal{C}^{\dagger} = \int d^4x\mathcal{O}_{ij}(\tilde{x}) = \int d^4x\mathcal{O}_{ij}(x) \tag{E19}$$

so that

$$v_{ij}\rho^{*}_{CP,\chi_i}\rho_{CP,\chi_j} = v^{*}_{ij}, \qquad a_{ij}\rho^{*}_{CP,\chi_i}\rho_{CP,\chi_j} = a^{*}_{ij}. \tag{E20}$$

In the case both χ_i^0 and χ_j^0 contain only real (or imaginary) N_{ik}, N_{jr}, Eq. (E17) gives

$$v^{*}_{ij} = v_{ij}, \qquad a^{*}_{ij} = a_{ij}, \tag{E21}$$

and with Eq. (E12), we have

$$v_{ij}\rho^{*}_{CP,\chi_i}\rho_{CP,\chi_j} = v^{*}_{ij}, \qquad a_{ij}\rho^{*}_{CP,\chi_i}\rho_{CP,\chi_j} = a^{*}_{ij}. \tag{E22}$$

Hence, $\mathcal{O}$ is CP conserved.

In the case that χ_i^0 is with a real N_{ik}, but χ_j^0 is with a imaginary N_{jr}, Eq. (E17) gives

$$v^{*}_{ij} = -v_{ij}, \qquad a^{*}_{ij} = -a_{ij}, \tag{E23}$$

and Eqs. (E12) and (E15) give

$$\rho_{CP,\chi_i} = \rho_{CP,\tilde{\psi}} = -\rho_{CP,\chi_j}. \tag{E24}$$

It implies

$$v_{ij}\rho^{*}_{CP,\chi_i}\rho_{CP,\chi_j} = v^{*}_{ij}, \qquad a_{ij}\rho^{*}_{CP,\chi_i}\rho_{CP,\chi_j} = a^{*}_{ij}. \tag{E25}$$

The operator $\mathcal{O}$ is CP conserved as expected.

In the center-of-mass frame of two Majorana particles, which are in a definite angular momentum configuration, the state is given by

$$\begin{aligned}|^{2S+1}L_J, J_z\rangle = {} & \sum_{m,s_z,s_z'}\int\frac{d^3p}{2E}f_{J_z m}(\vec{p})\mathcal{S}_m(s_z,s_z')b^{\dagger} \\ & \times(\vec{p},s_z)b^{\dagger}(-\vec{p},s_z')|0\rangle,\end{aligned} \tag{E26}$$

where

$$f_{J_z m}(\vec{p}) \equiv \langle L,M,S,m|L,S;J,J_z\rangle Y_{LM}(\hat{p})R(|\vec{p}|), \tag{E27}$$

with $\langle L,M,S,m|L,S;J,J_z\rangle$ as the Clebsch-Gordan coefficient and $R(|\vec{p}|)$ as the radial wave function. Note that it is easier to use spin instead of helicity basis here. For the spin wave function, we have

$$\mathcal{S}_m(s_z,s_z') = (-1)^{S+1}\mathcal{S}_m(s_z',s_z). \tag{E28}$$

The spherical harmonic wave function has the following property:

$$Y_{LM}(-\hat{p}) = (-1)^L Y_{LM}(\hat{p}). \tag{E29}$$

Note that

$$b^{\dagger}(\vec{p},s_z)b^{\dagger}(-\vec{p},s_z')|0\rangle = -b^{\dagger}(-\vec{p},s_z')b^{\dagger}(\vec{p},s_z)|0\rangle; \tag{E30}$$

the above relations of χ_m and Y_{LM} lead to

$$(-)^{L+S} = 1. \tag{E31}$$

Since

$$\mathcal{CP}b^{\dagger}(\vec{p},s_z)b^{\dagger}(-\vec{p},s_z')|0\rangle = -b^{\dagger}(-\vec{p},s_z)b^{\dagger}(\vec{p},s_z')|0\rangle, \tag{E32}$$

where we use the fact that the phase $\rho_{CP}\rho_M$ is purely imaginary, we have

$$\begin{aligned}\mathcal{CP}|^{2S+1}L_J, J_z\rangle &= -\sum_{m,s_z,s_z'}\int\frac{d^3p}{2E}f_{J_z m}(\vec{p})\mathcal{S}_m(s_z,s_z')b^{\dagger} \\ &\quad\times(-\vec{p},s_z)b^{\dagger}(\vec{p},s_z')|0\rangle \\ &= (-)^{L+1}|^{2S+1}L_J, J_z\rangle,\end{aligned} \tag{E33}$$

where we have made use of $f_{J_z m}(-\vec{p}) = (-)^L f_{J_z m}(\vec{p})$. Note that for a $f\bar{f}$ pair a similar argument leads to $\mathcal{CP}|^{2S+1}L_J, J_z\rangle = (-)^{S+1}|^{2S+1}L_J, J_z\rangle$.

As CP is a good quantum number, it can be used as a selection rule in dark matter annihilation processes, when the initial state has a specific L (and S) configuration.

APPENDIX F: FORMULAS FOR DM-NUCLEUS ELASTIC SCATTERING CROSS SECTION

The derivations of the DM-nucleus elastic scattering cross section in the literature are scattered and usually with different approximations, normalizations, and notations. It will be useful to rederive the formulas here.

1. Kinematics

We consider the elastic scattering of

$$\chi(p_\chi) + \mathcal{N}(p) \to \chi(p'_\chi) + \mathcal{N}(p'). \tag{F1}$$

We define

$$q \equiv p' - p = p_\chi - p'_\chi, \quad P \equiv p + p', \quad P_\chi \equiv p_\chi + p'_\chi,$$
$$S \equiv (p^{(\prime)} + p_\chi^{(\prime)})^2 = m_{\mathcal{N}}^2 + m_\chi^2 + 2p^{(\prime)} \cdot p_\chi^{(\prime)}. \tag{F2}$$

In particular, we have

$$q^2 = 2m_{\mathcal{N}}^2 - 2p \cdot p' = 2m_\chi^2 - 2p_\chi \cdot p'_\chi, \tag{F3}$$

and, in the center-of-mass frame,

$$q^2 = (E' - E)^2 - (|\vec{p}'_{\rm cm}|^2 + |\vec{p}_{\rm cm}|^2 - 2\vec{p}'_{\rm cm} \cdot \vec{p}_{\rm cm})$$
$$= 2|\vec{p}_{\rm cm}|^2(\cos\theta - 1). \tag{F4}$$

When $q^2 = 0$, we must have $|\vec{p}_{\rm cm}| = 0$ or $\cos\theta = 1$. In either case, it gives $q = 0$. Therefore, in elastic scattering, $q^2 = 0$ implies $q = 0$ in the center-of-mass frame and in all other frames.

In the lab frame, $p = (m_{\mathcal{N}}, \vec{0})$ and $p_\chi = (m_\chi + m_\chi v^2/2, m_\chi \vec{v})$. We obtain

$$S = (m_{\mathcal{N}} + m_\chi)^2 \left(1 + \frac{\mu_{\mathcal{N}}}{m_{\mathcal{N}} + m_\chi} v^2\right), \tag{F5}$$

where $\mu_{\mathcal{N}} \equiv m_\chi m_{\mathcal{N}}/(m_{\mathcal{N}} + m_\chi)$ is the reduced mass. The center-of-mass energy of the whole system is

$$E_{\rm cm} = \sqrt{s} = m_{\mathcal{N}} + m_\chi + \frac{1}{2}\mu_{\mathcal{N}} v^2, \tag{F6}$$

as expected.

The center-of-mass velocity in the lab frame is $m_\chi \vec{v}/(m_{\mathcal{N}} + m_\chi)$. Boosting the frame by $-m_\chi \vec{v}/(m_{\mathcal{N}} + m_\chi)$, we obtain the velocity of p and p_χ at the center-of-mass frame as $-m_\chi \vec{v}/(m_{\mathcal{N}} + m_\chi)$ and $\vec{v} m_{\mathcal{N}}/(m_{\mathcal{N}} + m_\chi)$, respectively. Hence, we have

$$|\vec{p}_{\rm cm}| = \mu_{\mathcal{N}} v, \tag{F7}$$

and $q^2 = 2\mu_{\mathcal{N}}^2 v^2(\cos\theta - 1)$.

2. Effective Lagrangian for direct searches

In this model, we have scalar-scalar, psudo-scalar-scalar, axial-axial, and axial-vector interactions for direct searches. The process of DM-nucleus scattering is nonrelativistic, so we can use the effective Lagrangian which can be derived from the Lagrangian in Appendix C to calculate the related SI and SD cross sections. We just give the results as below. The effective Lagrangians for scalar-scalar and pseudo-scalar-scalar interactions are

$$\mathcal{L}^{SS} = \sum_q a^q \bar{\chi}_1^0 \chi_1^0 \bar{q} q, \qquad \mathcal{L}^{PS} = \sum_q a'^q \bar{\chi}_1^0 \gamma_5 \chi_1^0 \bar{q} q, \tag{F8}$$

where

$$a^q = i \frac{g m_q}{2 M_W m_H^2} \mathrm{Re}(O_{11}^{L_H}),$$
$$a'^q = \frac{g m_q}{2 M_W m_H^2} \mathrm{Im}(O_{11}^{L_H}), \tag{F9}$$

and the effective Lagrangians for axial-axial and axial-vector interactions are

$$\mathcal{L}^{AA} = \sum_q d^q \bar{\chi}_1^0 \gamma^\mu \gamma^5 \chi_1^0 \bar{q} \gamma_\mu \gamma^5 q,$$
$$\mathcal{L}^{AV} = \sum_q b^q \bar{\chi}_1^0 \gamma^\mu \gamma^5 \chi_1^0 \bar{q} \gamma_\mu q, \tag{F10}$$

where

$$d^q = -\frac{i}{2}\left(\frac{g}{M_W}\right)^2 O_{11}^{L_Z} g_A,$$
$$b^q = -2i\left(\frac{g}{M_W}\right)^2 O_{11}^{L_Z} g_V \tag{F11}$$

with $g_A = -\frac{1}{2} T_{3L}^q$ and $g_V = \frac{1}{2} T_{3L}^q - \sin^2\theta_W Q^q$.

3. Vector, axial-vector current, scalar, and pseudoscalar matrix elements in the $q = 0$ limit

Using parity transformation, one can see that the matrix elements of vector (j_{Vh}), axial-vector current (j_{Ah}), scalar (s_h), and pseudoscalar (p_h) matrix elements should satisfy the relations

$$\langle \mathcal{N}(p', s')|j_{V(A)h,\mu}(x)|\mathcal{N}(p, s)\rangle = \langle \mathcal{N}(p', s')|P^\dagger P j_{V(A)h,\mu}(x) P^\dagger P|\mathcal{N}(p, s)\rangle$$
$$= \pm \eta_P^* \eta_P \langle \mathcal{N}(\tilde{p}', s')|j^\mu_{V(A)h}(\tilde{x})|\mathcal{N}(\tilde{p}, s)\rangle$$
$$= \pm \langle \mathcal{N}(\tilde{p}', s')|j^\mu_{V(A)h}(\tilde{x})|\mathcal{N}(\tilde{p}, s)\rangle,$$
$$\langle \mathcal{N}(p', s')|s_h(p_h)(x)|\mathcal{N}(p, s)\rangle = \pm \langle \mathcal{N}(\tilde{p}', s')|s_h(p_h)(\tilde{x})|\mathcal{N}(\tilde{p}, s)\rangle, \tag{F12}$$

where $\tilde{p}^\mu$, $\tilde{x}^\mu \equiv p_\mu$, x_μ, ηs are phases and s, s' are spin (S_z) quantum numbers.

From Eq. (F12), it is clear that in the case of $p = p'$ and in the momentum rest frame, $p = (m_{\mathcal{N}}, \vec{0})$, we have

$$\langle \mathcal{N}(m_{\mathcal{N}}, s')|j_{V(A)h,\mu}(0)|\mathcal{N}(m_{\mathcal{N}}, s)\rangle = \pm\langle \mathcal{N}(m_{\mathcal{N}}, s')|j^{\mu}_{V(A)h}(0)|\mathcal{N}(m_{\mathcal{N}}, s)\rangle, \tag{F13}$$

which gives

$$\langle \mathcal{N}(m_{\mathcal{N}}, s')|j_{Vh,i}(0)|\mathcal{N}(m_{\mathcal{N}}, s)\rangle = 0, \qquad \langle \mathcal{N}(m_{\mathcal{N}}, s')|j_{Ah,0}(0)|\mathcal{N}(m_{\mathcal{N}}, s)\rangle = 0. \tag{F14}$$

These imply that $\langle \mathcal{N}(p', s')|j_{Vh,i}(x)|\mathcal{N}(p, s)\rangle$ and $\langle \mathcal{N}(p', s')|j_{Ah,0}(x)|\mathcal{N}(p, s)\rangle$ are suppressed in the nonrelativistic limit: $p \simeq p' \simeq (m_{\mathcal{N}}, \vec{0})$.

We consider the vector current case first. From the first equation of Eq. (F14), we obtain

$$\langle \mathcal{N}(m_{\mathcal{N}}, s')|j_{Vh,\mu}(0)|\mathcal{N}(m_{\mathcal{N}}, s)\rangle = (2m_{\mathcal{N}}\delta_{s's}F_{\mathcal{N}}(0), \vec{0}), \tag{F15}$$

where $F_{\mathcal{N}}$ is the form factor and the $\delta_{ss'}$ factor is obtained as $j_{Vh,0}$ is a singlet under rotation. We can write it in a covariant form:

$$\langle \mathcal{N}(p, s')|j_{Vh,\mu}(0)|\mathcal{N}(p, s)\rangle = 2p_\mu F_{\mathcal{N}}(0)\delta_{s's}. \tag{F16}$$

In the case of nonvanishing but small q, we have

$$\langle \mathcal{N}(p', s')|j_\mu(x)|\mathcal{N}(p, s)\rangle \simeq (p_\mu + p'_\mu)F_{\mathcal{N}}(q^2)\delta_{s,s'}\exp[i(p' - p)\cdot x]. \tag{F17}$$

Now, we want to find $F_{\mathcal{N}}(0)$. From $Q \equiv \int d^3x j_{Vh,0}(0, \vec{x})$, we have

$$\int d^3x\langle \mathcal{N}(p', s')|j_{Vh,0}(x)|\mathcal{N}(p, s)\rangle = (p_0 + p'_0)F_{Vh}(q^2)\delta_{s,s'}\int d^3x\exp[i(p' - p)\cdot x] + \ldots, \tag{F18}$$

giving

$$\langle \mathcal{N}(p', s')|Q|\mathcal{N}(p, s)\rangle = (E + E')\delta_{s,s'}F_{\mathcal{N}}(q^2)\exp[i(E' - E)t](2\pi)^3\delta^3(\vec{p} - \vec{p}'). \tag{F19}$$

Therefore, we have

$$Q_{\mathcal{N}}\langle \mathcal{N}(p', s')|\mathcal{N}(p, s)\rangle = F_{\mathcal{N}}(0)\delta_{s,s'}(2\pi)^3 2E\delta^3(\vec{p} - \vec{p}'), \tag{F20}$$

which implies

$$F_{\mathcal{N}}(0) = Q_{\mathcal{N}}, \tag{F21}$$

and, hence, the vector current matrix elements in $q = 0$ case and in the $p^{(\prime)}$ rest frame is

$$\begin{aligned}&\langle \mathcal{N}(m_{\mathcal{N}}, s')|j_{Vh,0}(0)|\mathcal{N}(m_{\mathcal{N}}, s)\rangle = 2m_{\mathcal{N}}\delta_{ss'}F(0) = 2m_{\mathcal{N}}\delta_{ss'}Q_{V\mathcal{N}},\\ &\langle \mathcal{N}(m_{\mathcal{N}}, s')|j_{Vh,i}(0)|\mathcal{N}(m_{\mathcal{N}}, s)\rangle = 0.\end{aligned} \tag{F22}$$

These results will be useful in later discussion. For

$$j_{hV,\mu} = b^q j_{qV,\mu} = b^u\bar{u}\gamma_\mu u + b^d\bar{d}\gamma_\mu d + \ldots, \tag{F23}$$

it can be proved, by using the isospin invariant, that

$$Q_{Vp} = 2b^u + b^d \equiv f_{Vp}, \qquad Q_{Vn} = b^u + 2b^d \equiv f_{Vn}. \tag{F24}$$

Hence, the corresponding charge is

$$Q_{V\mathcal{N}} = ZQ_{Vp} + (A-Z)Q_{Vn} = Z(2b^u + b^d) + (A-Z)(b^u + 2b^d). \tag{F25}$$

We now turn to the axial-vector case. We start from

$$\begin{aligned}\langle \mathcal{N}(p',s')|j^i_{Aq}(0)|\mathcal{N}(p,s)\rangle &= \langle \mathcal{N}(p',s')|\bar{q}\gamma^i\gamma_5 q(0)|\mathcal{N}(p,s)\rangle \\ &= 2\langle \mathcal{N}(p',s')|\bar{q}\gamma_0\frac{\vec{\Sigma}}{2}q(0)|\mathcal{N}(p,s)\rangle \\ &\simeq 2\langle \mathcal{N}(p',s')|\bar{q}\frac{\vec{\Sigma}}{2}q(0)|\mathcal{N}(p,s)\rangle,\end{aligned} \tag{F26}$$

where the nonrelativistic approximation is used in the last line and note that the operator is spin density in the quark degree of freedom. Changing the degree of freedom from a quark to a nucleon, as one usually does in effective theory, we have

$$\begin{aligned}\langle \mathcal{N}(p',s')|\bar{q}\frac{\vec{\Sigma}}{2}q(0)|\mathcal{N}(p,s)\rangle &= \langle \mathcal{N}(p',s')|\left(\Delta^p_q\bar{p}\frac{\vec{\Sigma}}{2}p(0) + \Delta^n_q\bar{n}\frac{\vec{\Sigma}}{2}n(0)\right)|\mathcal{N}(p,s)\rangle \\ &\equiv \langle \mathcal{N}(p',s')|(\Delta^p_q\vec{s}_p(0) + \Delta^n_q\vec{s}_n(0))|\mathcal{N}(p,s)\rangle,\end{aligned} \tag{F27}$$

where $\Delta^q_{p(n)}$ is the quark spin proportion in a proton (neutron).

Note that spin operators $S_{p,n,\mathcal{N}}$ are related to $\vec{s}_{p,n,\mathcal{N}}$ by

$$\vec{S}_{p,n,\mathcal{N}} = \int d^3x\vec{s}_{p,n,\mathcal{N}}(0,\vec{x}). \tag{F28}$$

We consider the nonrelativistic case, $p \simeq (m_{\mathcal{N}},\vec{0})$, $q \simeq 0$,

$$\langle \mathcal{N}(p,s')|\vec{s}_{p,n,\mathcal{N}}(x)|\mathcal{N}(p,s)\rangle \simeq 2m_{\mathcal{N}}\langle J_{\mathcal{N}},s'|\vec{S}_{p,n,\mathcal{N}}|J_{\mathcal{N}},s\rangle\exp(iq\cdot x). \tag{F29}$$

From Wigner-Eckart theorem, the rotational property of the above matrix element is well understood and it is identical to that of the matrix element of any vector operator. Explicitly, from the Wigner-Eckart theorem, we have

$$\begin{aligned}\langle J_{\mathcal{N}},s'|(\vec{S}_{p,n})_m|J_{\mathcal{N}},s\rangle &= \langle J_{\mathcal{N}}1;sm|J_{\mathcal{N}}1;J_{\mathcal{N}}s'\rangle\langle J_{\mathcal{N}}||S_{p,n}||J_{\mathcal{N}}\rangle, \\ \langle J_{\mathcal{N}},s'|(\vec{S}_{\mathcal{N}})_m|J_{\mathcal{N}},s\rangle &= \langle J_{\mathcal{N}}1;sm|J_{\mathcal{N}}1;J_{\mathcal{N}}s'\rangle\langle J_{\mathcal{N}}||S_{\mathcal{N}}||J_{\mathcal{N}}\rangle,\end{aligned} \tag{F30}$$

with $(\vec{S}_{p,n,\mathcal{N}})_{m=0,\pm1} = (\vec{S}_{p,n,\mathcal{N}})_z, \mp[(\vec{S}_{p,n,\mathcal{N}})_x \pm i(\vec{S}_{p,n,\mathcal{N}})_y]/\sqrt{2}$. Since the double line matrix elements are independent of s and s' (with $m = s'-s$), so does the ratio

$$\frac{\langle J_{\mathcal{N}},s'|(\vec{S}_{p,n})_m|J_{\mathcal{N}},s\rangle}{\langle J_{\mathcal{N}},s'|(\vec{S}_{\mathcal{N}})_m|J_{\mathcal{N}},s\rangle} = \frac{\langle J_{\mathcal{N}}||S_{p,n}||J_{\mathcal{N}}\rangle}{\langle J_{\mathcal{N}}||S_{\mathcal{N}}||J_{\mathcal{N}}\rangle} \equiv \lambda_{p,n}. \tag{F31}$$

Consequently, its value can be obtained by taking a convenient choice of s, s' as $s = s' = J_{\mathcal{N}}$ and $m = 0$. In other words, we have

$$\langle J_{\mathcal{N}},s'|\vec{S}_{p,n}|J_{\mathcal{N}},s\rangle = \lambda_{p,n}\langle J_{\mathcal{N}},s'|\vec{S}_{\mathcal{N}}|J_{\mathcal{N}},s\rangle, \tag{F32}$$

with

$$\lambda_{p,n} = \frac{\langle J_{\mathcal{N}},s=J_{\mathcal{N}}|(S_{p,n})_z|J_{\mathcal{N}},s=J_{\mathcal{N}}\rangle}{\langle J_{\mathcal{N}},s=J_{\mathcal{N}}|(S_{\mathcal{N}})_z|J_{\mathcal{N}},s=J_{\mathcal{N}}\rangle} \equiv \frac{\langle S_{p,n,z}\rangle}{J_{\mathcal{N}}}. \tag{F33}$$

When the contributions of the two-body current are included, one needs to change $\langle S_{p,n}\rangle$ in $\lambda_{p,n}$ into effective $\langle S_{p,n}\rangle_{\rm eff}$, where we have

$$\langle S_{p(n)}\rangle_{\rm eff} \equiv \langle S_{p(n)}\rangle \pm \delta a_1 \frac{\langle S_p\rangle - \langle S_n\rangle}{2}, \tag{F34}$$

and δa_1 is the fraction contributing to the isovector coupling [55]. We use the predicted spin expectation values in Refs. [20,55] for the calculation. Putting everything together in the $q=0$ limit and the $p^{(\prime)}$ rest frame, we obtain

$$\begin{aligned}
&\langle \mathcal{N}(m_\mathcal{N}, s')|j^i_{Aq}(0)|\mathcal{N}(m_\mathcal{N}, s)\rangle = 4m(\Delta^p_q\lambda_p + \Delta^n_q\lambda_n)\langle J_\mathcal{N}, s'|(\vec{S}_\mathcal{N})_i|J_\mathcal{N}, s\rangle,\\
&\langle \mathcal{N}(m_\mathcal{N}, s')|j^0_{Aq}(0)|\mathcal{N}(m_\mathcal{N}, s)\rangle = 0,
\end{aligned} \tag{F35}$$

where Eq. (F14) has been used. These results will be useful later.

Similarly, from Eq. (F12), we have

$$\begin{aligned}
&\langle \mathcal{N}(m_\mathcal{N}, s')|s_h(0)|\mathcal{N}(m_\mathcal{N}, s)\rangle = 2m_\mathcal{N} f_{s\mathcal{N}}\delta_{ss'},\\
&\langle \mathcal{N}(m_\mathcal{N}, s')|p_h(0)|\mathcal{N}(m_\mathcal{N}, s)\rangle = 0,
\end{aligned} \tag{F36}$$

where $s_h = a^q\bar{q}q$. For the scalar density matrix element, we make use of (no sum on q)

$$\langle p(p,s')|m_q\bar{q}q(0)|p(p,s)\rangle = 2E\delta_{ss'}m_q f_{sp,q} = 2E\delta_{ss'}\begin{cases} m_p f^{(p)}_{Tq}, & q=u,d,s,\\ \frac{2}{27}m_p\left(1-\sum\limits_{q=u,d,s} f^{(p)}_{Tq}\right), & q=c,b,t. \end{cases} \tag{F37}$$

In the above, the matrix elements of the light-quark currents in the proton or neutron are obtained in chiral perturbation theory from measurements of the pion-nucleon sigma term [61–63]. Heavy quarks contribute to the mass of the nucleon through triangle diagrams [64]. Consequently, we have

$$\begin{aligned}
&f_{s\mathcal{N}} = (Zf_{sp} + (A-Z)f_{sn}),\\
&f_{sp(n)} = a^q f_{sp,q} = \sum_{q=u,d,s} a^q \frac{m_{p(n)}}{m_q} f^{(p(n))}_{Tq} + \sum_{q=c,b,t} a^q \frac{2}{27}\frac{m_{p(n)}}{m_q}\left(1-\sum_{q'=u,d,s} f^{(p(n))}_{Tq'}\right).
\end{aligned} \tag{F38}$$

These matrix elements at $q=0$ are used in Eq. (50) in Sec. II C to obtain the DM-nucleus scattering differential cross section at $q^2=0$.

4. Total cross section σ and σ_0

Using the standard formula, we find that the differential cross section in the center-of-mass frame is given by

$$\frac{d\sigma(q^2=0)}{d\cos\theta} = \frac{1}{32\pi S}\frac{p'_\chi}{p_\chi}\overline{\sum}|M_{fi}(q^2=0)|^2 \simeq \frac{\mu^2_\mathcal{N}}{32\pi m^2_N m^2_\chi}\overline{\sum}|M_{fi}(q^2=0)|^2, \tag{F39}$$

where $\mu_\mathcal{N}$ is the reduced mass of m_χ and m_N. The explicit expression of M_{fi} is given in Eq. (58). It is useful to define σ_0 as [13]

$$\sigma_0 \equiv \left|\frac{d\sigma(q^2=0)}{d|\mathbf{q}|^2}\right| \int_0^{4\mu^2_\mathcal{N}v^2} d|\mathbf{q}|^2. \tag{F40}$$

Recall that we have $|\mathbf{q}|^2 = -q^2 = 2\mu_\mathcal{N}v^2(1-\cos\theta)$ and, consequently, the Jacobian $d|\mathbf{q}|^2/d\cos\theta = -2\mu^2_\mathcal{N}v^2$ is a constant. The quantity σ_0 can now be expressed as

$$\sigma_0 = \left|\frac{d\sigma(q^2=0)}{d\cos\theta}\right| \int_{-1}^{1} d\cos\theta \simeq \frac{\mu_{\mathcal{N}}^2}{16\pi m_N^2 m_\chi^2} \overline{\sum} |M_{fi}(q^2=0)|^2. \tag{F41}$$

The differential cross section $d\sigma/d|\mathbf{q}|^2$ with nonzero momentum transfer is parametrized as [13]

$$\frac{d\sigma(q^2)}{d|\mathbf{q}|^2} = \frac{d\sigma(q^2=0)}{d|\mathbf{q}|^2} F^2(|\mathbf{q}|^2) \tag{F42}$$

with $F^2(|\mathbf{q}|^2)$ a form factor, giving

$$\sigma = \int_0^{4\mu^2 v^2} d|\mathbf{q}|^2 \frac{d\sigma(q^2)}{d|\mathbf{q}|^2} = \int_0^{4\mu^2 v^2} d|\mathbf{q}|^2 F^2(|\mathbf{q}|) \frac{d\sigma(q=0)}{d|\mathbf{q}|^2} = \frac{\sigma_0}{4\mu^2 v^2} \int_0^{4\mu^2 v^2} d|\mathbf{q}|^2 F^2(|\mathbf{q}|). \tag{F43}$$

5. Normalizing σ

The generic form of SI cross section σ_0 of DM scattering off the nucleus A with the ith isotope induced by spin-independent interaction is

$$\sigma_{0,A_i}^{\mathrm{SI}} \simeq \frac{\mu_{\mathcal{N}}^2}{16\pi} \frac{\overline{\sum} |M_{fi}^{\mathrm{SI}}(q^2=0)|^2}{m_{\mathcal{N}}^2 m_\chi^2} = \frac{\mu_{A_i}^2}{16\pi} (Q_{VA_i}^2 + Q_{SA_i}^2) \equiv \frac{\mu_{A_i}^2}{16\pi} \sum_{X=V,S} C_X [f_{Xp} Z + f_{Xn}(A_i - Z)]^2, \tag{F44}$$

where

$$C_V = 16\kappa_\chi^2 \frac{v^2}{1-v^2} \quad \text{and} \quad C_S = 16\kappa_\chi^2. \tag{F45}$$

For proton ($A=1$, $Z=1$) and neutron ($A=1$, $Z=0$), the above formulas give

$$\begin{aligned} \sigma_{0,p}^{\mathrm{SI}} &= \sum_{X=V,S} \sigma_{0,p}^{\mathrm{SI}(X)} = \frac{\mu_p^2}{16\pi} (C_V f_{Vp}^2 + C_S f_{Sp}^2), \\ \sigma_{0,n}^{\mathrm{SI}} &= \sum_{X=V,S} \sigma_{0,n}^{\mathrm{SI}(X)} = \frac{\mu_n^2}{16\pi} (C_V f_{Vn}^2 + C_S f_{Sn}^2). \end{aligned} \tag{F46}$$

For the nucleus with atomic mass number A_i and isotope abundance η_i, we define a scaled cross section as

$$\sigma_N^Z \equiv \frac{\sum_i \eta_i \sigma_{A_i}^{\mathrm{SI}}}{\sum_j \eta_j A_j^2 \frac{\mu_{A_j}^2}{\mu_p^2}}, \tag{F47}$$

with the SI DM-nucleus cross section defined as

$$\sigma_{A_i}^{\mathrm{SI}} \equiv \int \frac{d|\mathbf{q}|^2}{4\mu_{A_i}^2 v^2} \sigma_{0,A_i}^{\mathrm{SI}} F_{\mathrm{SI}}^2(|\mathbf{q}|), \tag{F48}$$

so

$$\sigma_{0,N}^Z = \frac{\sum_{X=V,S} \sigma_{0,p}^{\mathrm{SI}(X)} \sum_i \eta_i \mu_{A_i}^2 [Z + (A_i - Z)\frac{f_{Xn}}{f_{Xp}}]^2}{\sum \eta_j \mu_{A_j}^2 A_j^2}. \tag{F49}$$

In the isospin limit,

$$\frac{f_{Xp}}{f_{Xn}} \to 1, \tag{F50}$$

we have

$$\sigma^Z_{0,N} \to \sigma^{\rm SI}_{0,p} = \sigma^{\rm SI}_{0,n}. \tag{F51}$$

Data obtained from different experiments can be compared using σ^Z_N defined in Eq. (F47). Note that even if the isospin limit is not satisfied, we can still normalize $\sigma^{\rm SI}_A$ to σ^Z_N as in Eq. (F47) and compare it to the experimental result by taking σ^Z_N as some sort of scaled cross section but losing the generality among different experiments.

For spin-dependent interaction, from Eq. (58), we obtain

$$\sigma^{\rm SD}_{0,A_i} \simeq \frac{\mu^2_{A_i}}{16\pi} 64\kappa^2_\chi d^q d^{q'} (\Delta^p_q \langle S_p\rangle_{\rm eff} + \Delta^n_q \langle S_n\rangle_{\rm eff})(\Delta^p_{q'} \langle S_p\rangle_{\rm eff} + \Delta^n_{q'} \langle S_n\rangle_{\rm eff}) \frac{J_{A_i}+1}{J_{A_i}}. \tag{F52}$$

When DM scatters off a proton (neutron) target, we have

$$\begin{aligned}\sigma^{\rm SD}_{0,p(n)} &\simeq \frac{\mu^2_{p(n)}}{16\pi} 64\kappa^2_\chi d^q d^{q'} \left(\Delta^{p(n)}_q \frac{1}{2}\right)\left(\Delta^{p(n)}_{q'} \frac{1}{2}\right) \frac{(1/2)+1}{1/2} \\ &\simeq \frac{\mu^2_{p(n)}}{16\pi} 64\kappa^2_\chi d^q d^{q'} (\Delta^{p(n)}_q)(\Delta^{p(n)}_{q'}) \frac{3}{4}.\end{aligned} \tag{F53}$$

Now, return to the generic case, but observe that in the case the proton (neutron) contribution dominates the interaction ($|d_q \Delta^q_{p(n)}| \gg |d_q \Delta^q_{n(p)}|$) we have

$$\sigma^{\rm SD}_{0,A_i} \to \frac{4\mu^2_{A_j} \langle S_{p,n}\rangle^2_{\rm eff} (J_{A_j}+1)}{3\mu^2_{p,n} J_{A_j}} \sigma^{\rm SD}_{0,p(n)}. \tag{F54}$$

Given the above result, it will be useful to define the normalized DM-nucleus cross section as [58,65,66]

$$\sigma^{\rm SD}_{p,n} \equiv \left(\sum_i \eta_i \sigma^{\rm SD}_{A_i}\right)\left(\sum\nolimits_j \eta_j \frac{4\mu^2_{A_j} \langle S_{p,n}\rangle^2_{\rm eff} (J_{A_j}+1)}{3\mu^2_{p,n} J_{A_j}}\right)^{-1}, \tag{F55}$$

with the DM-nucleus SD cross section

$$\sigma^{\rm SD}_{A_i} \equiv \int \frac{d|\mathbf{q}|^2}{4\mu^2_{A_i} v^2} \sigma^{\rm SD}_{0,A_i} F^2_{\rm SD}(|\mathbf{q}|). \tag{F56}$$

In the above, the form factor is related to the structure function by [20,67]

$$F^2_{\rm SD}(|\mathbf{q}|) = \frac{S_A(|\mathbf{q}|)}{S_A(0)} \quad \text{so that } F^2_{\rm SD}(0) = 1, \tag{F57}$$

where

$$S_A(0) = \frac{(2J+1)(J+1)}{\pi J}[a_p \langle S_p\rangle_{\rm eff} + a_n \langle S_n\rangle_{\rm eff}]. \tag{F58}$$

The axial-vector structure function $S_A(|\mathbf{q}|)$ can be written in terms of its isoscalar/isovector (0/1) structure factors $S_{00}(|\mathbf{q}|), S_{01}(|\mathbf{q}|)$, and $S_{11}(|\mathbf{q}|)$ as [55]

$$S_A(|\mathbf{q}|) = a_0^2 S_{00}(|\mathbf{q}|) + a_0 a_1 S_{01}(|\mathbf{q}|) + a_1^2 S_{11}(|\mathbf{q}|), \tag{F59}$$

where the isoscalar and isovector couplings in this model are given by

$$a_{0,1} = a_p \pm a_n = \frac{d^q}{G_F/\sqrt{2}}(\Delta_q^p \pm \Delta_q^n). \tag{F60}$$

In fact, the form factor can be defined as

$$\begin{aligned} F_{\rm SD}^2(|\mathbf{q}|) &\equiv \frac{(d^q\Delta_q^p)^2\langle S_p\rangle_{\rm eff}^2 F_{pp}^2(|\mathbf{q}|) + 2d^q d^{q'}\Delta_q^p\Delta_{q'}^n\langle S_p\rangle_{\rm eff}\langle S_n\rangle_{\rm eff}F_{pn}^2(|\mathbf{q}|) + (d^q\Delta_q^n)^2\langle S_n\rangle_{\rm eff}^2 F_{nn}^2(|\mathbf{q}|)}{(d^q\Delta_q^p)^2\langle S_p\rangle_{\rm eff}^2 F_{pp}^2(0) + 2d^q d^{q'}\Delta_q^p\Delta_{q'}^n\langle S_p\rangle_{\rm eff}\langle S_n\rangle_{\rm eff}F_{pn}^2(0) + (d^q\Delta_q^n)^2\langle S_n\rangle_{\rm eff}^2 F_{nn}^2(0)} \\ &= \frac{(d^q\Delta_q^p)^2\langle S_p\rangle_{\rm eff}^2 F_{pp}^2(|\mathbf{q}|) + 2d^q d^{q'}\Delta_q^p\Delta_{q'}^n\langle S_p\rangle_{\rm eff}\langle S_n\rangle_{\rm eff}F_{pn}^2(|\mathbf{q}|) + (d^q\Delta_q^n)^2\langle S_n\rangle_{\rm eff}^2 F_{nn}^2(|\mathbf{q}|)}{(d^q\Delta_q^p\langle S_p\rangle_{\rm eff} + d^q\Delta_q^n\langle S_n\rangle_{\rm eff})^2}, \end{aligned} \tag{F61}$$

where

$$F_{pp(nn)}^2(|\mathbf{q}|) \equiv \frac{S_{00}(|\mathbf{q}|) + S_{11}(|\mathbf{q}|) \pm S_{01}(|\mathbf{q}|)}{S_{00}(0) + S_{11}(0) \pm S_{01}(0)}, \qquad F_{pn}^2(|\mathbf{q}|) \equiv \frac{S_{00}(|\mathbf{q}|) - S_{11}(|\mathbf{q}|)}{S_{00}(0) - S_{11}(0)}. \tag{F62}$$

Using the relations

$$\begin{aligned} S_{00}(0) + S_{11}(0) \pm S_{01}(0) &= \frac{(2J_{A_i}+1)(J_{A_i}+1)}{\pi J_{A_i}}\langle S_{p,n}\rangle_{\rm eff}^2, \\ S_{00}(0) - S_{11}(0) &= \frac{(2J_{A_i}+1)(J_{A_i}+1)}{\pi J_{A_i}}\langle S_p\rangle_{\rm eff}\langle S_n\rangle_{\rm eff}, \end{aligned} \tag{F63}$$

the former of which is derived from Eq. (F58) and the latter of which is from Eq. (F59), we recover the usual expression,

$$F_{\rm SD}^2(|\mathbf{q}|) = \frac{a_0^2 S_{00}((|\mathbf{q}|) + a_1 a_0 S_{01}((|\mathbf{q}|) + a_1^2 S_{11}((|\mathbf{q}|)}{a_0^2 S_{00}(0) + a_1 a_0 S_{01}(0) + a_1^2 S_{11}(0)}, \qquad a_{0,1} = \frac{d^q}{G_F/\sqrt{2}}(\Delta_q^p \pm \Delta_q^n). \tag{F64}$$

One may define another normalized SD cross section $\sigma'^{\rm SD}$ by attempting to remove the q^2 dependence,

$$\sigma_{p,n}'^{\rm SD} \equiv \sum_i \eta_i \int \frac{d|\mathbf{q}|^2}{4\mu_{A_i}^2 v^2}\sigma_{0,A_i}^{\rm SD}F_{\rm SD}^2(|\mathbf{q}|)\left(\sum_j \eta_j \frac{4\mu_{A_j}^2\langle S_{p,n}\rangle_{\rm eff}^2 F_{pp(nn)}^2(|\mathbf{q}|)(J_{A_j}+1)}{3\mu_{p,n}^2 J_{A_j}}\right)^{-1}. \tag{F65}$$

Although $F_{\rm SD}(|\mathbf{q}|)$ gives a compact expression for the relation between $\sigma^{\rm SD}$ and $\sigma_0^{\rm SD}$, it is not universal as it depends on the coupling d^q; nevertheless, $F_{pp,nn,pn}^2(|\mathbf{q}|)$ do not depend on the coupling d^q. We will give another expression below.

In the case with both spin-independent and spin-dependent interactions, we have

$$\frac{d\sigma_{A_i}}{d|\mathbf{q}|^2} = \frac{1}{4\mu_{A_i}^2 v^2}(\sigma_0^{\rm SD}F_{\rm SI}^2(|\mathbf{q}|) + \sigma_{0,pp}^{\rm SD}F_{pp}^2(|\mathbf{q}|) + \sigma_{0,nn}^{\rm SD}F_{nn}^2(|\mathbf{q}|) + \sigma_{0,pn}^{\rm SD}F_{pn}^2(|\mathbf{q}|)), \tag{F66}$$

where

$$\sigma_0^{\rm SI} = \frac{\mu_{A_i}^2}{\pi}\kappa_\chi^2\left[\frac{v^2}{1-v^2}Q_{VA_i}^2 + f_{sA_i}^2\right],$$
$$\sigma_{0,pp(nn)}^{\rm SD} = \frac{\mu_{A_i}^2}{\pi}\kappa_\chi^2\left[\left(4+\frac{4v^2}{3(1-v^2)}\right)\left(\sum d^q\Delta_q^{p(n)}\right)^2\lambda_{p(n)}^2 J_{A_i}(J_{A_i}+1)\right],$$
$$\sigma_{0,pn}^{\rm SD} = \frac{\mu_{A_i}^2}{\pi}\kappa_\chi^2\left[\left(4+\frac{4v^2}{3(1-v^2)}\right)2\left(\sum d^q d^{q'}\Delta_q^p\Delta_{q'}^n\right)\lambda_p\lambda_n J_{A_i}(J_{A_i}+1)\right]. \tag{F67}$$

Consequently, we have

$$\sigma_{A_i} = \int d|\mathbf{q}|^2\frac{d\sigma}{d|\mathbf{q}|^2} = (\sigma_0^{\rm SI}r_{\rm SI} + \sigma_{0,pp}^{\rm SD}r_{pp} + \sigma_{0,nn}^{\rm SD}r_{nn} + \sigma_{0,pn}^{\rm SD}r_{pn}), \tag{F68}$$

where

$$r_j \equiv \int_0^{4\mu_{A_i}^2 v^2}\frac{d|\mathbf{q}|^2}{4\mu_{A_i}^2 v^2}F_j^2(|\mathbf{q}|), \tag{F69}$$

with $j = {\rm SI},\ pp,\ nn,\ pn$.

We defined scaled cross sections as

$$\sigma_N^Z \equiv \frac{\sum_i \eta_i\sigma_{A_i}}{\sum_j \eta_j A_j^2\frac{\mu_{A_j}^2}{\mu_p^2}} \tag{F70}$$

and

$$\sigma_{p,n}^{\rm SD} \equiv \left(\sum_i \eta_i\sigma_{A_i}\right)\left(\sum_j \eta_j\frac{4\mu_{A_j}^2\langle S_{p,n}\rangle^2(J_{A_j}+1)}{3\mu_{p,n}^2 J_{A_j}}\right)^{-1}, \tag{F71}$$

or

$$\sigma_{p,n}^{\prime\rm SD} \equiv \left(\sum_i \eta_i\sigma'_{A_i,p(n)}\right)\left(\sum_j \eta_j\frac{4\mu_{A_j}^2\langle S_{p,n}\rangle^2(J_{A_j}+1)}{3\mu_{p,n}^2 J_{A_j}}\right)^{-1}, \tag{F72}$$

with

$$\sigma'_{A_i,p(n)} = (\sigma_0^{\rm SI}r'_{{\rm SI},p(n)} + \sigma_{0,pp}^{\rm SD}r'_{pp,p(n)} + \sigma_{0,nn}^{\rm SD}r'_{nn,p(n)} + \sigma_{0,pn}^{\rm SD}r'_{pn,p(n)}),$$
$$r'_{j,p(n)} = \int_0^{4\mu_{A_i}^2 v^2}\frac{d|\mathbf{q}|^2}{4\mu_{A_i}^2 v^2}\frac{F_j^2(|\mathbf{q}|)}{F_{pp(nn)}^2(|\mathbf{q}|)}. \tag{F73}$$

Data obtained from different experiments can be compared using σ_N^Z and $\sigma_{p,n}^{\rm SD}$ or $\sigma_{p,n}^{\prime\rm SD}$.

APPENDIX G: COANNIHILATION FORMULATION

It has been mentioned [50] that coannihilation becomes significantly important if the mass splitting $\delta m \simeq T_f$ between the dark matter particle χ_1^0 and one of the other WIMPs in this generic model. Let χ_1 be the dark matter and $\chi_i (i = 1, 2, \ldots, N)$ be the WIMPs having the masses with $m_i < m_j$ for $i < j$ and the internal degree of freedom g_i. Let n_i denote the number density of χ_i. We only need to consider the total number density $n = \sum_{i=1}^N n_i$ since all WIMPs χ_i will eventually decay to the dark matter χ_1. With the assumption $n_i/n \approx n_i^{\rm eq}/n^{\rm eq}$ before and after freeze-out, we have the Boltzmann equation [50]

$$\frac{dn}{dt} + 3Hn = -\langle\sigma_{\rm eff}v_{\rm M\phi l}\rangle(n^2 - n_{\rm eq}^2), \tag{G1}$$

where $\langle\sigma_{\rm eff}v_{\rm M\phi l}\rangle = \sum_{i,j=1}^{N}\sigma_{ij}(\chi_i\chi_j \to XX')r_i r_j v_{ij}$. The X and X' denote the SM particles, and the r_i is the ratio of $n_i^{\rm eq}/n^{\rm eq}$. Let the mass fraction be $\Delta_i \equiv (m_i - m_1)/m_1$ so that r_i can be given by

$$r_i \equiv n_i^{\rm eq}/n^{\rm eq} = \frac{g_i(1+\Delta_i)^{3/2}\exp(-x\Delta_i)}{\sum_{i=1}^{N} g_i(1+\Delta_i)^{3/2}\exp(-x\Delta_i)} \equiv \frac{g_i(1+\Delta_i)^{3/2}\exp(-x\Delta_i)}{g_{\rm eff}}. \tag{G2}$$

Here, we only consider the leading effect; namely, we only consider the effect of the WIMPs, χ_2^0 and $\chi_{1,2}^{\pm}$, with two SM particles in the final states through the s-channel interaction. Similarly, we do not take the Taylor series expansion on v^2 in the s channel and put a step function for the allowed threshold energy for each interaction channel in the nonrelativistic thermal averaged cross section as follows:

$$\langle\sigma_{\rm eff}v_{\rm M\phi l}\rangle_{\rm n.r.} = \sum_{i,j}\frac{x_{ij}^{3/2}}{2\sqrt{\pi}}\sum_{A,B}\int_0^\infty dv v^2 e^{-x_{ij}v^2/4}[\sigma(\chi_i\bar{\chi}_j \to A+B)v]\theta\left[m_i^2+m_j^2+\frac{2m_im_j}{\sqrt{1-v^2}}-(m_A+m_B)^2\right]. \tag{G3}$$

In the above, $x_{ij} = \frac{\mu_{ij}}{\mu_{11}}x$ and μ_{ij} is the reduced mass of χ_i and χ_j. From the freeze-out condition, the new freeze-out temperature parameter x_f can be solved numerically by the following equation:

$$x_f = \ln\left[c(c+2)\sqrt{\frac{45}{8}}\frac{g_{\rm eff}m_\chi M_{\rm PL}\langle\sigma_{\rm eff}v\rangle_{x=x_f}}{2\pi^3\sqrt{g_*(m_\chi)}x_f^{1/2}}\right]. \tag{G4}$$

The relic density now becomes

$$\Omega_{\rm DM}h^2 \approx 1.04\times10^9\frac{\rm GeV^{-1}}{M_{\rm PL}\sqrt{g_*(m_\chi)}J(x_f)}, \tag{G5}$$

where

$$J(x_f) \equiv \int_{x_f}^\infty \frac{\langle\sigma_{\rm eff}v\rangle}{x^2}dx. \tag{G6}$$

Note that the $\sigma_{\rm eff}$ is not only the function of v but also a function of x in coannilation.

APPENDIX H: MATRIX ELEMENTS FOR WIMP COANNIHILATION

In this article, we only consider the leading effect of coannihilation with the first two lightest neutral as well as single charged WIMPs annihilating to SM fermions through the s channel.

1. $\chi_j^0\chi_k^+ \to \bar{q}'q$, $l^+\nu$

The neutral WIMP χ_j^0 and the single charged WIMP χ_k^+ can annihilate into SM fermions through the s-channel exchange of a W^+ boson corresponding to the matrix element

$$M(\chi_j^0\chi_k^+ \to \bar{q}'q) = -i\left(\frac{g}{\sqrt{2}}\right)^2 V_{qq'}\frac{1}{s-M_W^2+iM_W\Gamma_W}g_{\mu\nu}[\bar{v}_j(p_1)\gamma^\mu(O_{jk}^{L_{W^-}}P_L + O_{jk}^{R_{W^-}}P_R)u_k(p_2)][\bar{u}(p_4)\gamma^\nu P_L v(p_3)], \tag{H1}$$

and

$$M(\chi_j^0\chi_k^+ \to l^+\nu) = -i\left(\frac{g}{\sqrt{2}}\right)^2\frac{1}{s-M_W^2+iM_W\Gamma_W}g_{\mu\nu} \times [\bar{v}_j(p_1)\gamma^\mu(O_{jk}^{L_{W^-}}P_L + O_{jk}^{R_{W^-}}P_R)u_k(p_2)][\bar{u}(p_4)\gamma^\nu P_L v(p_3)]. \tag{H2}$$

2. $\chi_k^0\chi_j^- \to q'\bar{q}, l^-\bar{\nu}$

Similarly, the neutral WIMP χ_k^0 and the single charged WIMP χ_j^- can annihilate into SM fermions via the s-channel exchange of a W^- boson corresponding to the matrix element

$$M(\chi_k^0\chi_j^- \to q'\bar{q}) = -i\left(\frac{g}{\sqrt{2}}\right)^2 V_{qq'}^* \frac{1}{s - M_W^2 + iM_W\Gamma_W} g_{\mu\nu} \times [\bar{v}_j(p_2)\gamma^\mu(O_{jk}^{L_{W^+}}P_L + O_{jk}^{R_{W^+}}P_R)u_k(p_1)][\bar{u}(p_3)\gamma^\nu P_L v(p_4)], \tag{H3}$$

and

$$M(\chi_k^0\chi_j^- \to l^-\bar{\nu}) = -i\left(\frac{g}{\sqrt{2}}\right)^2 \frac{1}{s - M_W^2 + iM_W\Gamma_W} g_{\mu\nu} \times [\bar{v}_j(p_2)\gamma^\mu(O_{jk}^{L_{W^+}}P_L + O_{jk}^{R_{W^+}}P_R)u_k(p_1)][\bar{u}(p_3)\gamma^\nu P_L v(p_4)]. \tag{H4}$$

3. $\chi_j^0\chi_k^0 \to f\bar{f}$

The neutral WIMPs χ_j^0 and χ_k^0 can annihilate into $f\bar{f}$ through the s-channel exchange of a Z^0 boson or an H^0 scalar corresponding to the matrix element

$$M(\chi_j^0\chi_k^0 \to f\bar{f}) = M_{1a} + M_{1b} + 2M_{2a}, \tag{H5}$$

where

$$\begin{aligned}
M_{1a} &= -\frac{i}{2}\left(\frac{g}{\cos\theta_W}\right)^2 g_{\alpha\nu}\frac{1}{s - M_Z^2 + iM_Z\Gamma_Z} \\
&\quad \times [v_j(p_1)\gamma^\alpha[(O_{jk}^{L_Z}P_L + O_{jk}^{R_Z})P_R)u_k(p_2)][\bar{u}(p_3)\gamma^\nu(g_V^f + g_A^f\gamma^5)v(p_4)], \\
M_{1b} &= -\frac{i}{2}\left(\frac{g}{\cos\theta_W}\right)^2 g_{\alpha\nu}\frac{1}{s - M_Z^2 + iM_Z\Gamma_Z} \\
&\quad \times [v_k(p_1)\gamma^\alpha[(O_{kj}^{L_Z}P_L + O_{kj}^{R_Z})P_R)u_j(p_2)][\bar{u}(p_3)\gamma^\nu(g_V^f + g_A^f\gamma^5)v(p_4)], \\
M_{2a} &= i\frac{gm_f}{2M_W}\frac{1}{s - M_H^2 + iM_H\Gamma_H}[\bar{v}_j(p_1)(O_{jk}^{L_H}P_L + O_{jk}^{R_H}P_R)u_k(p_2)][\bar{u}(p_3)v(p-4)].
\end{aligned} \tag{H6}$$

4. $\chi_j^-\chi_k^+ \to f\bar{f}$

The single charged WIMPs χ_j^- and χ_k^+ can annihilate into $f\bar{f}$ through the s-channel exchange of a Z^0 boson, an A^0 boson, or a H^0 scalar corresponding to the matrix element

$$M(\chi_j^-\chi_k^+ \to f\bar{f}) = M_1 + M_2 + M_3, \tag{H7}$$

where

$$\begin{aligned}
M_1 &= i\left(\frac{g}{\cos\theta_w}\right)^2 \frac{1}{s - M_Z^2 + iM_Z\Gamma_Z} g_{\alpha\mu}[\bar{u}(p_3)\gamma^\alpha(g_V^f + g_A^f\gamma^5)v(p_4)][\bar{v}_j(p_2)\gamma^\mu(O_{jk}^{L_Z^+}P_L + O_{jk}^{R_Z^+}P_R)j_k(p_1), \\
M_2 &= -ie^2 g_{\alpha\mu}\frac{1}{s}\delta_{jk}[\bar{u}(p_3)\gamma\alpha v(p_4)][\bar{v}_j(p_2)\gamma^\mu u_k(p_1), \\
M_3 &= -i\frac{gm_f}{2M_W}\frac{1}{s - M_H^2 + iM_H\Gamma_H}[\bar{u}(p_3)v(p_4)][\bar{v}_j(p_2)(O_{jk}^{L_H^+}P_L + O_{jk}^{R_H^+}P_R)u_k(p_1)].
\end{aligned} \tag{H8}$$

[1] F. Zwicky, Helv. Phys. Acta **6**, 110 (1933).
[2] V. C. Rubin and W. K. Ford, Jr., Astrophys. J. **159**, 379 (1970).
[3] K. G. Begeman, A. H. Broeils, and R. H. Sanders, Mon. Not. R. Astron. Soc. **249**, 523 (1991).
[4] J. Beringer *et al.* (Particle Data Group Collaboration), Phys. Rev. D **86**, 010001 (2012).
[5] S. M. Carroll, Nat. Phys. **2**, 653 (2006).
[6] D. Clowe, M. Bradac, A. H. Gonzalez, M. Markevitch, S. W. Randall, C. Jones, and D. Zaritsky, Astrophys. J. **648**, L109 (2006).
[7] D. N. Spergel *et al.* (WMAP Collaboration), Astrophys. J. Suppl. Ser. **148**, 175 (2003).
[8] M. Tegmark *et al.* (SDSS Collaboration), Phys. Rev. D **69**, 103501 (2004).
[9] G. Hinshaw *et al.* (WMAP Collaboration), Astrophys. J. Suppl. Ser. **208**, 19 (2013).
[10] P. A. R. Ade *et al.* (Planck Collaboration), Astron. Astrophys. **571**, A16 (2014).
[11] B. W. Lee and S. Weinberg, Phys. Rev. Lett. **39**, 165 (1977).
[12] J. R. Ellis, J. S. Hagelin, D. V. Nanopoulos, K. A. Olive, and M. Srednicki, Nucl. Phys. **B238**, 453 (1984).
[13] G. Jungman, M. Kamionkowski, and K. Griest, Phys. Rep. **267**, 195 (1996).
[14] K. A. Olive *et al.* (Particle Data Group Collaboration), Chin. Phys. C **38**, 090001 (2014).
[15] M. Drees and G. Gerbier, arXiv:1204.2373.
[16] V. A. Mitsou, Int. J. Mod. Phys. A **28**, 1330052 (2013).
[17] J. Goodman, M. Ibe, A. Rajaraman, W. Shepherd, T. M. P. Tait, and H. B. Yu, Phys. Rev. D **82**, 116010 (2010).
[18] P. J. Fox, R. Harnik, J. Kopp, and Y. Tsai, Phys. Rev. D **85**, 056011 (2012).
[19] D. S. Akerib *et al.* (LUX Collaboration), Phys. Rev. Lett. **112**, 091303 (2014)].
[20] E. Aprile *et al.* (XENON100 Collaboration), Phys. Rev. Lett. **111**, 021301 (2013).
[21] C. Amole *et al.* (PICO Collaboration), Phys. Rev. D **93**, 061101 (2016).
[22] C. Amole *et al.* (PICO Collaboration), Phys. Rev. D **93**, 052014 (2016).
[23] M. Ackermann *et al.* (Fermi-LAT Collaboration), Phys. Rev. Lett. **115**, 231301 (2015).
[24] K. Freese, J. A. Frieman, and A. Gould, Phys. Rev. D **37**, 3388 (1988).
[25] S. P. Ahlen, F. T. Avignone, R. L. Brodzinski, A. K. Drukier, G. Gelmini, and D. N. Spergel, Phys. Lett. B **195**, 603 (1987).
[26] M. W. Goodman and E. Witten, Phys. Rev. D **31**, 3059 (1985).
[27] J. R. Ellis and R. A. Flores, Nucl. Phys. **B307**, 883 (1988).
[28] H. E. Haber and G. L. Kane, Phys. Rep. **117**, 75 (1985).
[29] L. Roszkowski, E. M. Sessolo, and A. J. Williams, J. High Energy Phys. 02 (2015) 014.
[30] A. Fowlie, K. Kowalska, L. Roszkowski, E. M. Sessolo, and Y. L. S. Tsai, Phys. Rev. D **88**, 055012 (2013).
[31] P. Agrawal, Z. Chacko, C. Kilic, and R. K. Mishra, arXiv:1003.1912.
[32] J. M. Zheng, Z. H. Yu, J. W. Shao, X. J. Bi, Z. Li, and H. H. Zhang, Nucl. Phys. **B854**, 350 (2012).
[33] K. Cheung, P. Y. Tseng, Y. L. S. Tsai, and T. C. Yuan, J. Cosmol. Astropart. Phys. 05 (2012) 001.
[34] R. E. Shrock and M. Suzuki, Phys. Lett. B **110**, 250 (1982).
[35] C. P. Burgess, M. Pospelov, and T. ter Veldhuis, Nucl. Phys. **B619**, 709 (2001).
[36] B. Patt and F. Wilczek, arXiv:hep-ph/0605188.
[37] X. G. He, T. Li, X. Q. Li, J. Tandean, and H. C. Tsai, Phys. Lett. B **688**, 332 (2010).
[38] M. Dutra, C. A. de S. Pires, and P. S. Rodrigues da Silva, J. High Energy Phys. 09 (2015) 147.
[39] Y. Bai, V. Barger, L. L. Everett, and G. Shaughnessy, Phys. Rev. D **88**, 015008 (2013).
[40] X. G. He and J. Tandean, Phys. Rev. D **88**, 013020 (2013).
[41] Y. Bai and J. Berger, J. High Energy Phys. 11 (2013) 171.
[42] A. Alves, S. Profumo, and F. S. Queiroz, J. High Energy Phys. 04 (2014) 063.
[43] E. M. Dolle and S. Su, Phys. Rev. D **77**, 075013 (2008).
[44] W. L. Guo, Y. L. Wu, and Y. F. Zhou, Phys. Rev. D **81**, 075014 (2010).
[45] C. K. Chua and R. C. Hsieh, Phys. Rev. D **88**, 036011 (2013).
[46] L. Calibbi, A. Mariotti, and P. Tziveloglou, J. High Energy Phys. 10 (2015) 116.
[47] E. W. Kolb and M. S. Turner, *The Early Universe* (Addison-Wesley Publishing Company, Reading, 1990).
[48] T. S. Coleman and M. Roos, Phys. Rev. D **68**, 027702 (2003).
[49] P. Gondolo and G. Gelmini, Nucl. Phys. **B360**, 145 (1991).
[50] K. Griest and D. Seckel, Phys. Rev. D **43**, 3191 (1991).
[51] M. Drees and M. M. Nojiri, Phys. Rev. D **47**, 376 (1993).
[52] M. Garny, A. Ibarra, and S. Vogl, Int. J. Mod. Phys. D **24**, 1530019 (2015).
[53] K. Inoue, A. Kakuto, H. Komatsu, and S. Takeshita, Prog. Theor. Phys. **68**, 927 (1982); **70**, 330 (1983).
[54] J. R. Ellis, A. Ferstl, and K. A. Olive, Phys. Lett. B **481**, 304 (2000).
[55] J. Menendez, D. Gazit, and A. Schwenk, Phys. Rev. D **86**, 103511 (2012).
[56] V. A. Bednyakov and F. Simkovic, Phys. Part. Nucl. **37**, S106 (2006).
[57] G. K. Mallot, Int. J. Mod. Phys. A **15**, 521 (2000); eConf C 990809, 521 (2000).
[58] F. Giuliani, Phys. Rev. Lett. **93**, 161301 (2004).
[59] C. S. Kochanek, Astrophys. J. **457**, 228 (1996).
[60] B. Kayser, Phys. Rev. D **30**, 1023 (1984).
[61] T. P. Cheng, Phys. Rev. D **38**, 2869 (1988).
[62] H. Y. Cheng, Phys. Lett. B **219**, 347 (1989).
[63] J. Gasser, H. Leutwyler, and M. E. Sainio, Phys. Lett. B **253**, 252 (1991).
[64] M. A. Shifman, A. I. Vainshtein, and V. I. Zakharov, Phys. Lett. **78B**, 443 (1978).
[65] D. R. Tovey, R. J. Gaitskell, P. Gondolo, Y. A. Ramachers, and L. Roszkowski, Phys. Lett. B **488**, 17 (2000).
[66] C. Savage, P. Gondolo, and K. Freese, Phys. Rev. D **70**, 123513 (2004).
[67] M. T. Ressell, M. B. Aufderheide, S. D. Bloom, K. Griest, G. J. Mathews, and D. A. Resler, Phys. Rev. D **48**, 5519 (1993).